Doctoral School in Environmental Engineering

1D Mobile-Bed Model for Uniform and Non-Uniform Sediment Transport in Free Surface Flows

Giulia Garegnani

UNIVERSITÀ DEGLI STUDI DI TRENTO
Dipartimento di Ingegneria Civile e Ambientale

2011

Doctoral thesis in **Environmental Engineering**, 23^{th} **cycle**

Faculty of Engineering, **University of Trento**

Academic year 2010/2011

Supervisor: **Prof. Giorgio Rosatti, University of Trento**

University of Trento

Trento, Italy

31^{st} January 2011

You have to be patient and go on experimenting until you find out that you can't find out (Mark Twain).

Acknowledgements

First and foremost, I offer my gratitude to my supervisor, Prof. Giorgio Rosatti, who has supported me with his knowledge and patience. Particular thanks and gratitude go to Dr. Luca Bonaventura for his uninterrupted support also after my master thesis.

In addition, I thank Prof. Aronne Armanini for passing on his valuable knowledge of the statistical moments formulation and for all the information and references on the non-uniform sediment transport in rivers. I want to thank the TUDelft University and Prof. Guus Stelling for their hospitality. I also greatly appreciate the revisions suggested me by Prof. Mustafa Altinakar. Besides, the contribution of Dr. Alberto Deponti to the initial development stages of the sediment transport model is kindly and friendly acknowledged.

Finally, in recognition of all your help and support, I would like to mention all the Doctoral School in Environmental Engineering and, in particular, the secretariat who has been very helpful throughout the three years.

Contents

List of Figures **xii**

List of Tables **xiii**

List of Symbol **xviii**

Summary **xix**

I Quasi Two-Phase and Essentially Mono-Phase Models for Water and Sediment Flows **1**

1 Governing Equations of Water and Sediment Two-Phase Flow **3**

1.1 Literature Review 3

1.2 The Equations of Motion for Water-Sediment Mixtures 4

1.2.1 The Two-Dimensional System of the Vertically Averaged Shallow Water Equations 7

1.2.2 The 1D Open Channel System for the Mixture 13

1.3 Closure Relations 15

1.3.1 Sediment Transport Relations 15

1.3.2 Bed Shear Stress 17

1.3.3 Formula for the Redistribution of the Solid Area 20

2 The Essentially Mono-Phase Model and its Range of Applicability **23**

2.1 Non-Dimensional Analysis of the Quasi Two-Phase Model 23

2.1.1 Derivation of the Essentially Mono-Phase Model 24

2.1.2 Eigenvalues Analysis 26

2.2 A Simplified Quasi Two-Phase Equation for the Bed Evolution . 30

2.3 Range of Validity of the Models 32

2.4 Analysis of the Existing Models 33

3 Development of an Efficient Numerical Scheme for the Two Models 37

3.1 Literature Review on the Existing Schemes 37
3.2 Discretization of the Model Equations 38
3.2.1 The Momentum Equation 40
3.2.2 The Continuity Equation for the Total Mass 43
3.2.3 The Continuity Equation for the Solid Mass 45
3.3 Solution Procedure 46
3.4 Stability and Efficiency of the Two Schemes 50

4 Test Cases 53

4.1 Comparison with the Solutions of the Simplified Equation 53
4.2 Impact of Model Simplifications 55
4.2.1 A Non Prismatic Channel 55
4.2.2 Depth Variation 57
4.2.3 Arbitrary Cross Section 59
4.3 Aggradation Test Case 61
4.4 Conclusions 64

II Non Uniform Sediment Transport 65

5 Mathematical Description of the Non-Uniform Sediment Transport 67

5.1 The Bed Material Fraction Approach 67
5.1.1 The Grain-Size Distribution Curve 67
5.1.2 Continuity Equations for Each Sediment Class 68
5.2 The Moments Approach 72
5.2.1 An Analytical Procedure for the Derivation of the Moments Equations 72
5.2.2 Sediment Transport Formulas with respect to the Statistical Moments 78
5.3 A Simplified Solution for the Evolution of the River-Bed and the Grain-Size Distribution 80

6 Extension of the Numerical Scheme to the Non-Uniform Sediment Transport 83

6.1 Equations of the Model 83
6.2 Continuity Equations for Each Sediment Class 84

6.3 Extension of the Solution Procedure 86

7 Test Cases **89**

7.1 Propagation of a Small Perturbation 89

7.2 Non Prismatic Channel 91

7.3 Effects on the Numerical Results of the Thickness of the Mixing Layer 93

7.4 Comparison with Experimental Data 94

7.5 Conclusions 97

Conclusions **99**

Bibliography **105**

List of Figures

1.1 Sketch of the main variables and control volume $dV = dx\,dy\,dz$. 5
1.2 Velocity and concentration profiles 9
1.3 Sketch of the main variables and control volume for the 1D open channel model. 13
1.4 The Shields diagram (1936) obtained through experimental data with uniform sediment. 16
1.5 Scheme for the Einstein-Horton method based on sub-areas with the same velocity. 18
1.6 Scheme for the redistribution of the sediment along the section. . 20

2.1 Control volume for determination of shallow water equations with mobile-bed, where h is the water depth, z_b the bed elevation, η the free surface elevation and B the channel width (for simplicity unitary). 24
2.2 Eigenvalues for the coupled system. Sediment concentration C_0 increasing from 0.000002 to 0.045. The lines are dashed for small values of the Froude numbers because high concentrations with small Froude number are not physically meaningful. 29
2.3 Comparison between the QTP and the EMP system eigenvalues with $C_0 = 0.03$. 29

3.1 Non-uniform distribution of the velocity along the y coordinate . 39
3.2 Staggered computational grid 40
3.3 Sketch of the discrete variables 46
3.4 Flow chart of the solution procedure 47

4.1 Comparison between the approximated and the numerical solutions. 54
4.2 Geometry of the non prismatic channel 56
4.3 Initial conditions. 56
4.4 Comparison between the QTP model and EMP model during the transient state ($t = 200\ s$). 57

4.5 Comparison between the QTP model and EMP model during the transient state ($t = 150\ s$). 58
4.6 Froude number and concentration at $t = 150\ s$. 58
4.7 Bathymetry at time $t = 0\ s$. 60
4.8 Computed free-surface elevation at the time $t = 20\ h$ in the 14^{th} section ($x = 130\ m$). 60
4.9 Bed evolution at the time $t = 200\ h$ calculated with the QTP model and the EMP model. 61
4.10 Section shape evolution ($x = 130\ m$) at the time $t = 200\ h$ calculated with the QTP model and the EMP model. 62
4.11 Computed bed and water surface profiles compared to data of Soni et al. [49] at the time $t = 40\ min$. The dashed lines are initial bed and water surface profiles. 63

5.1 Examples of frequency histogram reported by [56] for the Rio Grande, New Mexico. 68
5.2 Sketch of a generic cross section and of the main model variable in the case of non-uniform sediment 69
5.3 Sediment concentration of each grain-size fraction j 70
5.4 Sediment distribution curve. 73

6.1 Solution procedure for the non uniform model 86

7.1 Initial conditions. 90
7.2 Comparison between the simplified solution and the EMP model with non-uniform sediment. 91
7.3 Channel geometry 92
7.4 Time evolution of the bed level and the sediment fractions in a non prismatic channel. 92
7.5 Bed level calculated with different thickness δ of the mixing layer at time 1000 h. 94
7.6 Grain-size distribution at the 21^{th} section ($x = 200\ m$). 94
7.7 Sediment fraction p_j calculated with different thickness δ of the mixing layer at time 1000 h. 95
7.8 Evolution of the transport layer composition p_1. 96

List of Tables

2.1 Scaling factors used in the model. Here, quantity = scale × dimensionless quantity. 25

4.1 Initial and boundary conditions 54
4.2 Coordinates of the first section at $x = 0\ m$. 59
4.3 Upstream boundary conditions. 60
4.4 Experimental test [49] 62
4.5 Numerical simulation: initial and boundary conditions 63

7.1 Upstream and downstream boundary conditions. 93
7.2 Boundary conditions on the grain size distribution. 93
7.3 Upstream boundary conditions. 96

List of Symbol

A	Area of the cross section occupied by water and sediment over the bed level
A_δ	Area of the mixing layer
A_b	Area of the cross section occupied by water and sediment under the bed level
C	Depth-averaged sediment concentration
C_b	Bed depth-averaged concentration
C_c	Sediment transport capacity
C_w	Wetted contour
c	Local sediment concentration
c_b	Local sediment concentration under the bed level
d	Sediment diameter
d_{50}	Characteristic 50% diameter
d_{90}	Characteristic 90% diameter
F	Flux term
F_{μ^2}	Flux in the equation for the mean value μ
F_{σ^2}	Flux in the equation for the variance σ^2
Fr	Froude number
$\mathbf{f}$	Body force per unit volume
$\mathbf{G}$	Vector of the right-hand side terms
g	Gravitational acceleration

H	Maximum depth of the water-sediment mixture with respect to the bed level
h	Depth of the water column
$\mathbf{I}$	Unit tensor
i	Bed slope
i_c	Coupling parameter
i_e	Energy loss
j	Grain-size class
k_s	Strickler coefficient
$\mathbf{M}$	Symmetric tridiagonal matrix
m	Number of grain-size classes
p	Fraction of sediment in the mixing layer
p, p_a	Pressure, atmospheric pressure
p^{subst}	Fraction of sediment in the substrate
p_T	Sediment fraction transported by the flow
Q	Depth-averaged water-sediment discharge
Q_c	Sediment transport capacity
Q_s	Depth-averaged solid discharge
Q_w	Depth-averaged water discharge
R_h	Hydraulic radius
Re_*	Reynolds number
$\mathbf{T}_s$	Partial stress tensor of solid phase
$\mathbf{T}_w$	Partial stress tensor of liquid phase
$\widehat{\mathbf{T}}_s, \widehat{\mathbf{T}}_w$	Tensor of interaction surface forces
t	Temporal coordinate
t^*	Hydrodynamic time scale

U	Depth-averaged velocity in the x direction
$\mathbf{u_s} = (u_s, v_s, w_s)$	Local velocity of the solid phase
$\mathbf{u_w} = (u_w, v_w, w_w)$	Local velocity of the water phase
$\mathbf{u} = (u, v, w)$	Local velocity of the water sediment mixture
u^b, v^b, w_s^b, w_w^b	Velocity component at the bottom boundary
u^s, v^s, w^s	Velocity component at the free surface
u_{*c}	Bed shear velocity
V	Depth-averaged velocity in the y direction
V_t	Sediment-water volume
$\mathbf{V_t}$	Vector of the total volumes
x, y	Horizontal Cartesian coordinate
z	Vertical coordinate
z_b	Bed elevation
$\alpha_{cv}, \alpha_{cu}, \alpha_{cv^2}, \alpha_{cu^2}, \alpha_{cvuv}$	Corrective factors
α_h, α_{u^2}	Corrective factors
γ	Linearization od the friction term
Δ_s	Relative density of the sediment
δ	Mixing layer thickness
$\epsilon = \dfrac{\tau^*}{t^*} = \dfrac{C_0}{C_b}$	Scaling factor
η	Free surface elevation
θ'	Shields parameter
θ_c	Critical parameter
ϑ	Time-averaging parameter
$\lambda_1, \lambda_2, \lambda_2$	Eigenvalue of the hyperbolic system
μ	Mean value of the grain-size distribution curve

ν	Kinematic viscosity of the water
ϕ	Dummy variable
ρ	Mixture density
ρ_s	Sediment density
ρ_w	Water density
σ^2	Variance of the grain-size distribution curve
$\bar{\tau}_0$	Shear stress at the bed level
$\boldsymbol{\tau}$	Deviatoric stress tensor
τ^*	Morphodynamic time scale
τ^b	Bed shear stress
τ^s	Wind shear force per unit area
χ	Chezy friction coefficient

Summary

In the last fifty years, new engineering problems, connected with gravel extraction, installation of dams and disposal of mine waste into rivers, have risen to the extent that sediment transport modeling is assuming a key role in realistic river hydraulic simulations. Floods, meandering, sediment load computation, river bed aggradation or degradation, channel design and navigation are some of the problems concerning the sediment transport in rivers.

In literature, different models and numerical schemes have been proposed in order to describe the river dynamics. Mathematical modeling of river flow is usually based on the vertically averaged Saint-Venant equations, which express the conservation laws of mass and momentum for water flow, and the Exner equation for the conservation of the sediment mass. In this work several aspects on the river modeling have been considered. The first purpose is a clearer understanding of the coupling between water and sediment in order to better explain the limitations of models in which the conservation equations are simplified. The second objective is the implementation of an efficient solution procedure. The last aim is the development of a mathematical model for the non–uniform sediment transport and the extension of the algorithm to this case. Consequently, the thesis focuses on two main parts: the comparison between a quasi two-phase and a simplified model and the implementation of a non-uniform sediment transport model.

In the first part, existing methods for solving 1D morphodynamic system with uniform sediment transport are reviewed. In the river morphological models with low sediment concentration, it is often assumed that the rate of bed evolution is of a lower order of magnitude than flow changes (see e.g. [30, 47] and [13]). In this case, the spatial differences in sediment fluxes are the mainly responsible of topography changes [19] and the sediment storage in the water is negligible. Besides, in the momentum equation only the water phase is considered. Consequently, this simplified models is essentially mono-phase and, due to its simplicity, has been widely used [5, 22]. Different numerical schemes have

been proposed in order to numerically solve the problem. The limit of this approach is its applicability only for lower concentration and Froude numbers (see e.g. [13, 41]). For this reason a rather complete approach, a quasi two-phase model, is studied and compared with the simplified approach. The equations of the model are written for the sediment-water mixture as proposed by Rosatti and Fraccarollo [43] and Wu and Wang [54]) and, consequently, the sediment storage in the water column is considered in the continuity equation for the mass and in the momentum equation.

Firstly, the model equations for the sediment-water mixture are presented. Secondly, a non-dimensional analysis is carried out for the quasi two-phase model in order to derive a simplified (essentially mono-phase) model. The equations for these two approaches are presented and differences with the literature highlighted. The eigenstructure of the two systems are compared and a range of validity pointed out. In the third chapter, both the models are discretized as proposed by Rosatti et al. [45]. This solution procedure, herein explained, consider the effects of morphodynamics on the flow and vice versa. The schemes are validated with a reference solution and test cases for both the models performed. The comparison of the numerical results highlights the differences between the two systems and the importance of the coupling terms in the time evolution of the bed in rivers with high sediment concentration. Then, the model is suitable for mountain rivers where the concentration becomes relevant and with immediately adaptation of the sediment transport to the flow.

Another peculiarity of the mobile-bed models is the description of the non-uniformity of the sediment. In this second part, the study focuses only on the sediment gradation in alluvial rivers where, generally, the concentration are low and an essentially mono-phase model can be used. In conventional models, the concept of mixing layer is essential. Deeply buried grains have minimal probability of entrainment into motion and all the bed fluctuations are assumed to be concentrated in a mixed layer of finite thickness. Indeed, it is known in literature [4, 28, 52] that only in mixing layer grains can be eroded.

In particular, in the second part, a mathematical analysis and physical interpretation of mobile-bed model with non-uniform sediment is carried out (see e.g. [42]). In the standard models, the sediment transport capacity is computed for each class of the grain size distribution curve and the mass balance written for each grain size class into the mixing layer (see e.g. [4] and [55]). In Chapter 5 a new formulation based on the series expansion of sediment transport formulas is introduced (see e.g. [3] and [4]) and an analytical derivation of the model developed in the Section 5.2.1. The model equations describe the time variation

of the statistical moments of the sediment distribution curve. An approximate solution for the non-uniform sediment transport is proposed under the assumption that time variation of free surface elevation is negligible and the discharge of the mixture is constant on the whole domain (see e.g. [30] and [42]). A system of two equations with unknowns the bed mean diameter and the bed elevation has to be solved in order to get a simplified solution. This solution is compared with numerical results. In fact, the standard model based on the division of the sediment distribution curve is discretized in agreement with the solution procedure proposed in Chapter (3). In the last chapter, test cases for non-prismatic channels and unsteady condition are presented and the sensitivity of the model to the mixing layer thickness highlighted. Finally, in order to validate the model, numerical results are compared with the experimental data obtained by Ribberink [42].

Part I

Quasi Two-Phase and Essentially Mono-Phase Models for Water and Sediment Flows

Chapter 1

Governing Equations of Water and Sediment Two-Phase Flow

In order to simulate the sediment transport process, a variety of mathematical models have been proposed. In this chapter a briefly review of existing models is presented and the governing equations for a two-phase fluids explained.

1.1 Literature Review

Model equations for sediment transport processes are generally based on the conservation laws of mass and momentum, but they can differ in key aspects of the mathematical description, such as the use of simplified conservation equations versus equations for the sediment-liquid mixture, the definition and use of parameterized sediment transport functions, capacity or non capacity models and mobile-bed resistance.

Capacity models or equilibrium models are applied under the assumption of local equilibrium between the sediment transport rate and the sediment-carrying capacity of the flow. More specifically, the solid discharges is assumed to be computable on the basis of various parameters that characterize the flow and the transport regime. This concept is not always reliable because the sediment transport rate doesn't adapt immediately to the local flow condition, as proved by many authors [8, 56]. Besides, the sediment transport formula are usually derived for steady flow and are unable to consider the non-stationarity of the flow. Nevertheless, a definitive description of the adaptation time is not the argument of this work and the governing equations are derived under the assumptions of immediate adaptation.

A second main difference among models is between simplified equations for low sediment concentration and two-phase models for higher concentration. In

fact, in the case of strong interaction between flow and morphodynamics, the aggradation and degradation processes are strictly connected with the hydrodynamics. Consequently, the conservation equations for mass and momentum are written for the water-sediment mixture. In particular, in order to model mountain rivers, the effects of the sediment concentration on the bulk-fluid density and on the temporal variation of the bed elevation are considered. In these quasi two-phase models [14, 37, 43, 48, 54], the sediment transport immediately adapts to the flow. The model equations were analyzed in the case of a rectangular channel by Morris and Williams [41]. Besides, in order to close the problem, it is necessary to add two further relations: for the friction term in the momentum equation and for the sediment concentration. In literature, different closure relations have been proposed and are reported in Section 1.3.

On the other hand, in the most widely used models the inertia and concentration associated to the solid phase are assumed to be negligible, so that the momentum equation for the solid mass is disregarded. The conservation equations for the solid and liquid mass are simplified under the assumption of low sediment concentration. Consequently, the model is essentially mono-phase. This approach is widely used in modelling river flow, see e.g. Armanini [5] and Wu and Vieira [53]. The resulting equations were analyzed by de Vries [22], Lyn and Altinakar [37] and Sieben [47] in the simplified case of sediment transport in a rectangular channel.

The problem is that authors [1, 12, 23, 29, 31, 34, 51] propose different reductions under the same assumptions as shown in Chapter 2. Then, a deeper understanding of the quasi two-phase models is necessary in order to clarify some simplifications.

1.2 The Equations of Motion for Water-Sediment Mixtures

The fundamental equations of motion for a sediment-mixture system come from three considerations:

- conservation of mass,
- conservation of the momentum,
- material properties.

The two phases of the fluid are characterized by density ρ_s for the sediment phase and ρ_w for the water phase. The fraction occupied by the solid particle is

c and ,consequently, $1-c$ is the fraction of volume occupied by the water phase.

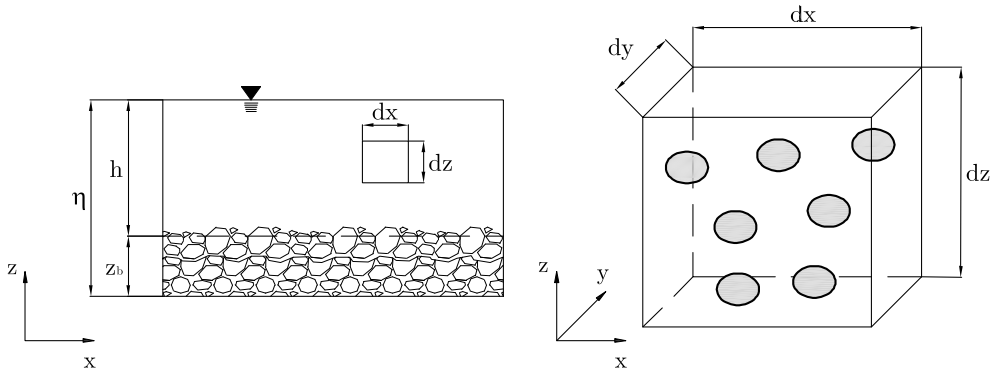

Figure 1.1: *Sketch of the main variables and control volume $dV = dx\,dy\,dz$*

An infinitesimal element of fluid with volume dV, located at position $\mathbf{x} = (x, y, z)$ at the time t, is considered as shown Figure (1.1). The motion of water and solid phase is regarded as the flow of an homogeneous medium and the mass and momentum equations are written separately for the solid and liquid components. The liquid and the solid particles are incompressible, the densities ρ_s and ρ_w are constant factors and the conservation equations for the liquid and solid phases written for the control volume dV are:

$$\frac{\partial}{\partial t}(1-c) + \nabla \cdot [(1-c)\,\mathbf{u_w}] = 0, \tag{1.1}$$

$$\frac{\partial c}{\partial t} + \nabla \cdot (c\mathbf{u_s}) = 0, \tag{1.2}$$

where $\mathbf{u_w} = (u_w, v_w, w_w)$ and $\mathbf{u_s} = (u_s, v_s, w_s)$ are respectively the velocity of the water phase and solid phase, u_s and u_w are the solid phase and water phase velocity components in the x-direction, v_s and v_w velocity components in the y-direction, w_s and w_w in the z-direction.

It is possible to derive the corresponding equations for the mixture as a whole. The notions of the density and velocity of the mixture for the elementary volume dV of space are introduced. The density of the mixture ρ can be determined by the water density ρ_w and the solid density ρ_s:

$$\rho(\mathbf{x}, t) = \rho_w [1 - c(\mathbf{x}, t)] + c(\mathbf{x}, t)\,\rho_s = 0. \tag{1.3}$$

The conservation equation of the total mass is:

$$\frac{\partial \rho}{\partial t} + \nabla \cdot (\rho \mathbf{u}), \tag{1.4}$$

with $\mathbf{u} = (u, v, w)$ velocity of the sediment-water mixture and density ρ not constant. The momentum equations for the incompressible solid and liquid phases can be respectively written as [10]:

$$\frac{\partial}{\partial t}\left(c\rho_s \mathbf{u}_s\right) + \nabla \cdot \left(c\rho_s \mathbf{u}_s \otimes \mathbf{u}_s\right) = c\rho_s \mathbf{f} + \nabla \cdot \mathbf{T}_s + c\nabla \cdot \widehat{\mathbf{T}}_s, \tag{1.5}$$

$$\begin{aligned}\frac{\partial}{\partial t}\left[\left(1-c\right)\rho_w \mathbf{u}_w\right] + \nabla \cdot \left[\left(1-c\right)\rho_w \mathbf{u}_w \otimes \mathbf{u}_w\right] = \\ = \left(1-c\right)\rho_w \mathbf{f} + \nabla \cdot \mathbf{T}_w - c\nabla \cdot \widehat{\mathbf{T}}_s\end{aligned} \tag{1.6}$$

where the first term on the right side of Equations (1.5) and (1.6) represents the rate of increase of momentum per unit volume in the control volume while $\nabla \cdot \left(c\rho_s \mathbf{u}_s \otimes \mathbf{u}_s\right)$ and $\nabla \cdot \left[\left(1-c\right)\rho_w \mathbf{u}_w \otimes \mathbf{u}_w\right]$ are the rate of momentum lost by convection through the volume surface, $\mathbf{f}$ is the body force per unit volume, $\mathbf{T}_w$ and $\mathbf{T}_s$ the stress tensor of liquid and solid phase and $c\nabla \cdot \widehat{\mathbf{T}}_s$ the reciprocal forces between the phases acting on the surface δV_s as explained by Armanini [7] and Meruane et al. [39].

The lag between local water velocities and sediment movement is usually assumed negligible, and nearly no relative motion exists except for the settling due to gravity. Thus, the velocity components in the x and y-directions of the liquid and solid phases are equal:

$$u^s = u^w = u; \tag{1.7}$$

$$v^s = v^w = v. \tag{1.8}$$

with u and v components of the water-sediment velocity vector $\mathbf{u}$.

Since the sediment velocities u_s and v_s are equal to the fluid velocities, the model is not properly two-phase but quasi two-phase (QTP). Under this assumption, adding Equation (1.5) and (1.6) gives the momentum equation for the mixture:

$$\frac{\partial}{\partial t}\left(\rho \mathbf{u}\right) + \nabla \cdot \left(\rho \mathbf{u} \otimes \mathbf{u}\right) = \nabla \cdot \mathbf{T} + \rho \mathbf{f}, \tag{1.9}$$

with $\mathbf{T} = \mathbf{T}_w + \mathbf{T}_s$. The tensor $\mathbf{T}$ has the same form as that for an homogeneous incompressible liquid:

$$\mathbf{T}_w = -p\mathbf{I} + \boldsymbol{\tau} \tag{1.10}$$

where p is the pressure, $\mathbf{I}$ is the unit tensor and τ is the deviatoric stress tensor.

$$\frac{\partial}{\partial t}\left(\rho \mathbf{u}\right) + \nabla \cdot \left(\rho \mathbf{u} \otimes \mathbf{u}\right) = -\nabla \mathbf{p} + \nabla \cdot \boldsymbol{\tau}\rho \mathbf{f}. \tag{1.11}$$

where $\mathbf{u} = (u, v, w)$ is the vector of the water-sediment mixture velocities. The component w in the z-direction is:

$$w = \frac{c\rho_s w_s + \rho_w w_w}{c\rho_s + (1-c)\,\rho_w} \tag{1.12}$$

Equations (1.2),(1.4) and (1.11) are the equations for instantaneous motions of flow and sediment. Assuming that each instantaneous quantity can be split into time-averaged and fluctuating components, one can obtained the Reynolds-averaged equations. In the Reynolds decomposition, the fluctuating part of the velocity and the concentration satisfy:

$$\overline{c'} = \frac{1}{T}\int_t^{t+T} c' d\tau = 0, \tag{1.13}$$

where $^-$ and $'$ respectively denote the mean and the fluctuating part, while T is the time period considered that should be longer than the fluctuation period of turbulence. The resulting time-averaged equation of conservation of the total mass, Equation (1.4), is:

$$\frac{\partial \rho}{\partial t} + \nabla \cdot (\rho \bar{\mathbf{u}})\,. \tag{1.14}$$

Secondly, the Reynolds-averaged momentum equation is

$$\frac{\partial}{\partial t}(\rho \bar{\mathbf{u}}) + \nabla \cdot (\rho \bar{\mathbf{u}} \otimes \bar{\mathbf{u}}) = \nabla \cdot \mathbf{T^t} + \rho \mathbf{f}, \tag{1.15}$$

where the terms concerning the Reynolds stress, $\nabla \cdot \left(\rho \overline{\mathbf{u}' \otimes \mathbf{u}'}\right)$, is included in the tensor $\mathbf{T^t}$. Finally the conservation equation for the solid mass, Equation (1.2), becomes:

$$\frac{\partial \bar{c}}{\partial t} + \nabla \cdot (\bar{c}\bar{\mathbf{u}}_\mathbf{s}) + \nabla \cdot \left(\overline{c'\mathbf{u}'_\mathbf{s}}\right) = 0, \tag{1.16}$$

where $\nabla \cdot (c'\mathbf{u}'_\mathbf{s})$ represents the turbulent sediment flux.

1.2.1 The Two-Dimensional System of the Vertically Averaged Shallow Water Equations

By dropping, for simplicity, the bar $^-$ of the time-averaged components, the Equation (1.15) is written explicitly in the z-direction, where the z direction is defined as positive from the bed level z_b to the free surface elevation η as shown in Figure 1.1. Under the assumption of gradually varied flows, the inertial and diffusion effects are neglected and the only external force is the gravity force ρg:

$$\frac{\partial p}{\partial z} = -\rho g, \tag{1.17}$$

where g is the gravitational acceleration. In order to derive the shallow water equations [9], ρ is assumed constant along the depth h. The analytic solution of the Equation (1.17) is:

$$p = p_a + \rho(\mathbf{x}, t)g\,(\eta - z) \tag{1.18}$$

where η is the free surface, Figure (1.1). The atmospheric pressure p_a is assumed to be zero, then, the derivatives of pressure p with respect the horizontal coordinate x and y are:

$$\frac{\partial p}{\partial x} = gh\frac{\partial \rho}{\partial x} + g\rho\frac{\partial \eta}{\partial x}, \tag{1.19}$$

$$\frac{\partial p}{\partial y} = gh\frac{\partial \rho}{\partial y} + g\rho\frac{\partial \eta}{\partial y}, \tag{1.20}$$

Writing explicitly the vector Equation (1.11) and substituting Equation (1.19) and (1.20) yields the momentum equations for gradually varied mixture flows in the x direction:

$$\rho\left(\frac{\partial u}{\partial t} + u\frac{\partial u}{\partial x} + v\frac{\partial u}{\partial y} + w\frac{\partial u}{\partial z}\right) = -gh\frac{\partial \rho}{\partial x} - g\rho\frac{\partial \eta}{\partial x} + \\ + \frac{\partial \tau^t_{xx}}{\partial x} + \frac{\partial \tau^t_{xy}}{\partial y} + \frac{\partial \tau^t_{xz}}{\partial z}. \tag{1.21}$$

and, similarly, in the y direction:

$$\rho\left(\frac{\partial v}{\partial t} + u\frac{\partial v}{\partial x} + v\frac{\partial v}{\partial y} + w\frac{\partial v}{\partial z}\right) = -gh\frac{\partial \rho}{\partial y} - g\rho\frac{\partial \eta}{\partial y} + \\ + \frac{\partial \tau^t_{yx}}{\partial x} + \frac{\partial \tau^t_{yy}}{\partial y} + \frac{\partial \tau^t_{yz}}{\partial z}. \tag{1.22}$$

By remembering that the velocity components in the x and y directions are the same for the liquid and solid phases, the three dimensional hydrostatic model system is:

$$\frac{\partial}{\partial t}\left[(1-c)\right] + \frac{\partial}{\partial x}\left[(1-c)\,u\right] + \frac{\partial}{\partial y}\left[(1-c)\,v\right] + \frac{\partial}{\partial z}\left[(1-c)\,w_s\right] \\ + \frac{\partial}{\partial x}\left[(1-c')\,u'\right] + \frac{\partial}{\partial y}\left[(1-c')\,v'\right] + \frac{\partial}{\partial z}\left[(1-c')\,w'_s\right] = 0, \tag{1.23}$$

$$\frac{\partial c}{\partial t} + \frac{\partial}{\partial x}\left(cu\right) + \frac{\partial}{\partial y}\left(cv\right) + \frac{\partial}{\partial z}\left(cw_s\right) + \frac{\partial}{\partial x}\left(c'u'\right) + \frac{\partial}{\partial y}\left(c'v'\right) + \frac{\partial}{\partial z}\left(c'w'_s\right) = 0 \tag{1.24}$$

$$\rho\left(\frac{\partial u}{\partial t}+u\frac{\partial u}{\partial x}+v\frac{\partial u}{\partial y}+w\frac{\partial u}{\partial z}\right)=-gh\frac{\partial \rho}{\partial x}-g\rho\frac{\partial \eta}{\partial x}+\frac{\partial \tau^t_{xx}}{\partial x}+\frac{\partial \tau^t_{xy}}{\partial y}+\frac{\partial \tau^t_{xz}}{\partial z}, \tag{1.25}$$

$$\rho\left(\frac{\partial v}{\partial t}+u\frac{\partial v}{\partial x}+v\frac{\partial v}{\partial y}+w\frac{\partial v}{\partial z}\right)=-gh\frac{\partial \rho}{\partial y}-g\rho\frac{\partial \eta}{\partial y}+\frac{\partial \tau^t_{yx}}{\partial x}+\frac{\partial \tau^t_{yy}}{\partial y}+\frac{\partial \tau^t_{yz}}{\partial z}. \tag{1.26}$$

The system of vertically averaged momentum equations can be determined by integrating Equations (1.23)-(1.26) over the interval $[0,\eta]$ where $z_b = 0$ is the reference level as shown in Figure 1.2. It should be notice that the bed level z_b is defined as the surface of discontinuity for the concentration $c = c(x,y,z)$ and the velocities $u = u(x,y,z)$ and $v = v(x,y,z)$. In fact, the concentration c is assumed constant and equal to the value c_b in $[0,z_b]$, while the velocities u and v are zero. Instead, in $[z_b,\eta]$ the velocities and the concentration c are not uniformly distributed as shown in Figure 1.2. Due to this discontinuity, for

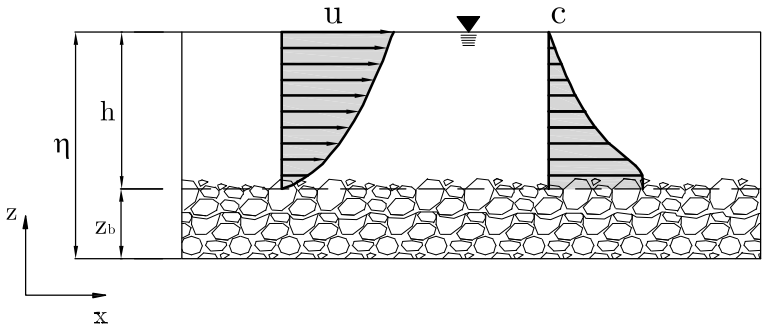

Figure 1.2: *Velocity and concentration profiles*

example the integral of the first term of Equation (1.23) becomes:

$$\int_0^{\eta(t)}\frac{\partial}{\partial t}\left[1-c\left(t,z\right)\right]dz=\int_0^{z_b(t)}\frac{\partial}{\partial t}\left[1-c\left(t,z\right)\right]dz+\int_{z_b(t)}^{\eta(t)}\frac{\partial}{\partial t}\left[1-c\left(t,z\right)\right]dz \tag{1.27}$$

In order to integrate the second term on the left side of the Equation (1.27) the Leibniz rule is applied:

$$\begin{aligned}\int_{z_b(t)}^{\eta(t)}\frac{\partial}{\partial t}\left[1-c\left(t,z\right)\right]dz=&\frac{\partial}{\partial t}\int_{z_b(t)}^{\eta(t)}\left[1-c\left(t,z\right)\right]dz+\\&-\frac{\partial \eta}{\partial t}\left[1-c\left(z=\eta\right)\right]+\frac{\partial z_b}{\partial t}\left[1-c\left(z=z_b\right)\right].\end{aligned} \tag{1.28}$$

Then, the value of the concentration c at the boundary of the interval $[z_b, \eta]$ should be defined. At the solid surface z_b and at the free surface boundary η, the local concentration c assumes the following values:

$$c\left(z = z_b\right) = c_b, \tag{1.29}$$

$$c\left(z = \eta\right) = 0. \tag{1.30}$$

The depth-averaged concentration C is defined as:

$$C(x, y, t) = \frac{1}{h\left(x, t\right)} \int_{z_b}^{\eta} c(x, z, t) dz. \tag{1.31}$$

Consequently, by applying the Leibniz rule and the previous definitions, the integral of Equation (1.27) is:

$$\begin{aligned} \int_0^{\eta(t)} \frac{\partial}{\partial t} \left[1 - c\left(t, z\right)\right] dz = \frac{\partial}{\partial t} \left[\left(1 - C\right) h\right] - \frac{\partial \eta}{\partial t} + \frac{\partial z_b}{\partial t} \left(1 - c_b\right) + \\ + \frac{\partial}{\partial t} \left[\left(1 - C_b\right) h\right] - \frac{\partial z_b}{\partial t} \left(1 - c_b\right) \end{aligned} \tag{1.32}$$

with

$$C_b(x, y, t) = \frac{1}{z_b\left(x, t\right)} \int_0^{z_b} c(x, z, t) dz. \tag{1.33}$$

Similarly, in order to integrate all the other terms in the Equations (1.23)-(1.26), the depth-average velocities are defined:

$$U(x, y, t) = \frac{1}{h\left(x, t\right)} \int_{z_b}^{\eta} u(x, z, t) dz, \tag{1.34}$$

$$V(x, y, t) = \frac{1}{h\left(x, t\right)} \int_{z_b}^{\eta} v(x, z, t) dz. \tag{1.35}$$

where z_b is the bed level and $h = \eta - z_b$ is the depth of the column water.

Besides, it should be notice that the concentration c and the velocities u and v are not uniformly distributed over the water column depth h. Consequently, the integral of the product between local variables is:

$$\int_{z_b}^{\eta} c(x, z, t) u(x, z, t) dz = \alpha_{cu} ChU. \tag{1.36}$$

where α_{cu} is a corrective coefficient. The other correction factors are:

$$\alpha_{cv} = \frac{1}{ChV} \int_{z_b}^{\eta} c(x, z, t) v(x, z, t) dz, \tag{1.37}$$

$$\alpha_{cu^2} = \frac{1}{ChU^2}\int_{z_b}^{\eta} c(x,z,t)u^2(x,z,t)dz, \tag{1.38}$$

$$\alpha_{cv^2} = \frac{1}{ChV^2}\int_{z_b}^{\eta} c(x,z,t)v^2(x,z,t)dz. \tag{1.39}$$

Finally, the conditions at the free surface η and at the bed boundary z_b are:

Kinematic condition of the free surface The water free surface η is a free moving boundary and can be expressed as a single valued function,

$$z = \eta\,(x,y,t)\,. \tag{1.40}$$

After differentiating Equation (1.40), the free surface equation is:

$$\frac{\partial \eta}{\partial t} + u^s\frac{\partial \eta}{\partial x} + v^s\frac{\partial \eta}{\partial y} = w^s, \tag{1.41}$$

where u^s, v^s and w^s are the velocity components at the free surface.

Velocity components at the bed boundary At the solid boundary a no-slip condition is assumed:

$$u^b = 0, \qquad v^b = 0. \tag{1.42}$$

where u^b, v^b are the velocity components at the bottom. The bed level z_b is defined as the surface where the vertical sediment velocity w_s^b and the water sediment velocity w_w^b are equal to zero:

$$w_w^b = 0, \qquad w_s^b = 0. \tag{1.43}$$

Shear stress boundary condition at the free surface They are usually specified by prescribing the wind stresses. Here, both the two components of the wind shear force per unit area are assumed equal to zero:

$$\tau_{xz}^{t\,s} + \tau_{xx}^{t\,s}\frac{\partial \eta}{\partial x} + \tau_{xy}^{t\,s}\frac{\partial \eta}{\partial y} = 0, \tag{1.44}$$

$$\tau_{yz}^{t\,s} + \tau_{yx}^{t\,s}\frac{\partial \eta}{\partial x} + \tau_{yy}^{t\,s}\frac{\partial \eta}{\partial y} = 0. \tag{1.45}$$

Shear stress boundary condition at the bed The $x-$component τ_{0x} and the $y-$component τ_{0y} of the bed shear stress per unit area are:

$$\tau_{0x} = \tau_{xz}^{t\,b} + \tau_{xx}^{t\,b}\frac{\partial z_b}{\partial x} + \tau_{xy}^{t\,b}\frac{\partial z_b}{\partial y}, \tag{1.46}$$

$$\tau_{0y} = \tau_{yz}^{t\,b} + \tau_{yx}^{t\,b}\frac{\partial z_b}{\partial x} + \tau_{yy}^{t\,b}\frac{\partial z_b}{\partial y}. \tag{1.47}$$

Vertical sediment flux across the free surface The vertical sediment flux across the water surface should be zero:

$$\left(w_s c + \overline{w_s' c'}\right)_{z_b=\eta} = 0. \tag{1.48}$$

Under all the previous assumptions, applying the Leibniz rule and by neglecting the turbulent diffusion fluxes and the dispersion terms [52], the equations for the conservation of solid and liquid phases, Equation (1.1) and Equation (1.2), become:

$$\begin{aligned}\frac{\partial}{\partial t}\left[(1-C)\,h\right] + \frac{\partial}{\partial t}\left[(1-C_b)\,z_b\right] + \frac{\partial}{\partial x}\left[(1-\alpha_{cu}C)\,Uh\right] \\ + \frac{\partial}{\partial y}\left[(1-\alpha_{cv}C)\,Vh\right] = 0,\end{aligned} \tag{1.49}$$

$$\frac{\partial}{\partial t}\left(Ch\right) + c_b\frac{\partial z_b}{\partial t} + \frac{\partial}{\partial x}\left(\alpha_{cu}CUh\right) + \frac{\partial}{\partial y}\left(\alpha_{cu}CVh\right) = 0, \tag{1.50}$$

while x and y momentum equations, Equations (1.21) and (1.22), are:

$$\begin{aligned}&\frac{\partial}{\partial t}\left[(1+\alpha_{cu}C\Delta_s)\,U\right] + \frac{\partial}{\partial x}\left(1+\alpha_{cu^2}C\Delta_s\right)U^2 + \frac{\partial}{\partial y}\left[(1+\alpha_{cuv}C\Delta_s)\,UV\right] = \\ &= -\frac{1}{\rho_w}g\left(1+C\Delta_s\right)\frac{\partial \eta}{\partial x}dz - \frac{1}{2\rho_w}gh^2\Delta_s\frac{\partial C}{\partial x} + \frac{1}{\rho_w}\frac{\partial T_{xx}}{\partial x} + \frac{1}{\rho_w}\frac{\partial T_{xy}}{\partial x} - \frac{1}{\rho_w}\tau_{0x},\end{aligned} \tag{1.51}$$

$$\begin{aligned}&\frac{\partial}{\partial t}\left[(1+\alpha_{cv}C\Delta_s)\,V\right] + \frac{\partial}{\partial y}\left(1+\alpha_{cuv}C\Delta_s\right)UV + \frac{\partial}{\partial y}\left[\left(1+\alpha_{cv^2}C\Delta_s\right)V^2\right] = \\ &= -\frac{1}{\rho_w}g\left(1+C\Delta_s\right)\frac{\partial \eta}{\partial y}dz - \frac{1}{2\rho_w}gh^2\Delta_s\frac{\partial C}{\partial y} + \frac{1}{\rho_w}\frac{\partial T_{xy}}{\partial y} + \frac{1}{\rho_w}\frac{\partial T_{yy}}{\partial y} - \frac{1}{\rho_w}\tau_{0y},\end{aligned} \tag{1.52}$$

where $T_{xx} = \int_{z_b}^{\eta}\tau_{xx}^t dz$, $T_{xy} = \int_{z_b}^{\eta}\tau_{xy}^t dz$ and $T_{yy} = \int_{z_b}^{\eta}\tau_{yy}^t dz$ are neglected under the shallow water assumptions [9, 38, 46] and $\Delta_s = (\rho_s - \rho_w)/\rho_w$ is the submerged relative density of the sediment.

Equations (1.49)-(1.52) constitute a two-dimensional system where the variables are U, V, h and z_b. All the other quantities should be expressed in function of the unknowns through closure relations.

1.2.2 The 1D Open Channel System for the Mixture

Finally, the one dimensional equations for unsteady flows in open channel can be derived by performing a laterally integration of the two dimensional model (1.49)-(1.52) or directly from the 3D equations by an average over the cross section. To this purpose $l(x, y, t)$ and $r(x, y, t)$ represent the left and the right walls while $B(x, y, t)$ is the width as shown in Figure 1.3.

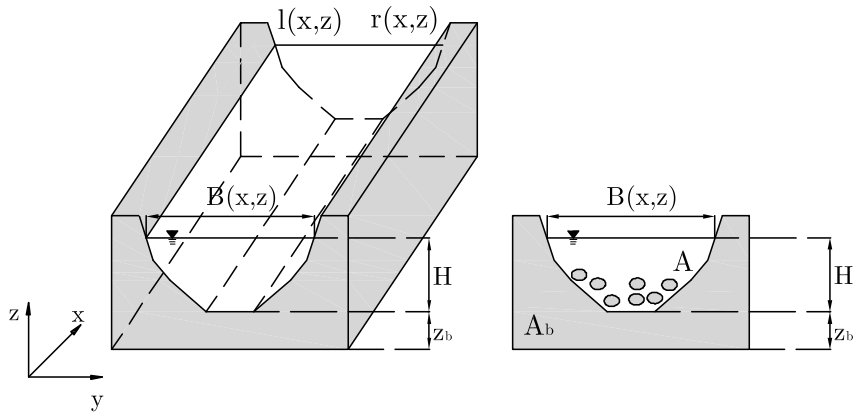

Figure 1.3: *Sketch of the main variables and control volume for the 1D open channel model.*

The resulting equations are given by:

$$\frac{\partial}{\partial t}\left[(1-C)\,A\right]+\frac{\partial}{\partial t}\left[(1-C)\,A_b\right]+\frac{\partial}{\partial x}\left[(1-\alpha_{cu}C)\,Q\right]=0, \tag{1.53}$$

$$\frac{\partial\,(CA)}{\partial t}+C_b\frac{\partial A_b}{\partial t}+\frac{\partial(\alpha_{cu}CQ)}{\partial x}=0, \tag{1.54}$$

$$\frac{\partial}{\partial t}\left[(1+\alpha_{cu}C\Delta_s)\,Q\right]+\frac{\partial}{\partial x}\left[\alpha_{cu^2}\,(1+C\Delta_s)\,\frac{Q^2}{A}\right]+g\,(1+C\Delta_s)\,A\frac{\partial\eta}{\partial x}+$$
$$+g\Delta_s\alpha_h\frac{AH}{2}\frac{\partial C}{\partial x}=-\frac{\bar{\tau}_0}{\rho_w}C_w, \tag{1.55}$$

with A area of the cross section occupied by water and sediment set by the bed level z_b and the free surface η, A_b area of the cross section occupied by water and sediment set by the reference level $z = 0$ and the free surface elevation η, Q total discharge, C_w is the wetted contour and α_h a corrective coefficient defined as following:

$$\alpha_h=\frac{1}{AH}\int_y h^2dy. \tag{1.56}$$

where H is the maximum depth of the water-sediment mixture with respect to the bed level, Figure 1.3. The coefficient α_{cu} and α_{cu^2}, Equation (1.36) and (1.38), are redefined as:

$$\alpha_{cu} = \frac{\int_A c(x,z,t)u(x,z,t)dz}{CAU}, \tag{1.57}$$

$$\alpha_{cu^2} = \frac{\int_A c(x,z,t)u^2(x,z,t)dz}{CAU^2}. \tag{1.58}$$

In most of the existing models [14, 43], the values of the coefficients α_{cu} and α_{cu^2} are approximated to the unit.

In the system (1.53)-(1.54), the total discharge Q is the volume rate of the water-sediment flow, including any suspended solids which is transported through the cross-sectional area A and, then, it results:

$$Q = UA, \tag{1.59}$$

while the depth-averaged solid and liquid discharges are defined as:

$$Q_s = \alpha_{cu} CUA, \tag{1.60}$$

$$Q_w = (1 - \alpha_{cu} C)\, UA. \tag{1.61}$$

By summing the two conservation equations, Equation (1.53) and (1.54), the following continuity equation is derived:

$$\frac{\partial A}{\partial t} + \frac{\partial A_b}{\partial t} + \frac{\partial Q}{\partial x} = 0. \tag{1.62}$$

It is possible to consider the Equation (1.62) in the final system rather than Equation (1.53) and the quasi two-phase (QTP) model equations are:

$$\frac{\partial A}{\partial t} + \frac{\partial A_b}{\partial t} + \frac{\partial Q}{\partial x} = 0, \tag{1.63}$$

$$\frac{\partial}{\partial t}\left[(1 + \alpha_{cu} C\Delta_s)\, Q\right] + \frac{\partial}{\partial x}\left[(1 + \alpha_{cu^2} C\Delta_s)\, \frac{Q^2}{A}\right] + g\,(1 + C\Delta_s)\, A\frac{\partial \eta}{\partial x} + \\ + g\Delta_s \alpha_h \frac{AH}{2}\frac{\partial C}{\partial x} = -\frac{\bar{\tau}_0}{\rho} C_w, \tag{1.64}$$

$$\frac{\partial (CA)}{\partial t} + C_b \frac{\partial A_b}{\partial t} + \frac{\partial (CQ)}{\partial x} = 0. \tag{1.65}$$

where the unknowns are the free surface elevation η, the area A_b and the total discharge Q. The friction term $\frac{\bar{\tau}_0}{\rho}C_w$ and the concentration C are expressed through closure formulas reported in the Section (1.3). Generally, the solid discharge Q_s is estimated from sediment transport formulas and the concentration C can be calculated from Equation (1.60) as:

$$C = \frac{Q_s}{\alpha_{cu} U h}. \tag{1.66}$$

Instead, the friction term is expressed through the following relation [15]:

$$\frac{\bar{\tau}_0}{\rho} C_w = \gamma Q, \tag{1.67}$$

which represents a linearization of a closure formula as reported in the Section 1.3.2.

1.3 Closure Relations

Closure relations for the friction term and for the solid concentration are needed for the solution of Equations (1.63)-(1.65) and herein reported.

1.3.1 Sediment Transport Relations

In order to express the sediment concentration C in terms of the unknowns U, h and z_b different sediment transport formulas can be used. A sediment transport formula relates the sediment-carrying capacity of the flow to the hydrodynamics and the sediment features. These formulas estimate the solid capacity of the flow Q_c that, if the availability of sediments is limited, can be different from the real solid discharge Q_s. However, many models [29, 30, 31, 32, 36] assume the solid discharge Q_s equal to the sediment-carrying capacity Q_c.

In this section, only two sediment transport relations are reported: the Meyer-Peter Müller formula and a monomial relation.

Empirical sediment transport formulas are mainly based on a critical value of incipient motion of bed particles. Usually, the critical condition for incipient motion is referred to the critical Shields parameter θ_c. In particular, the Shields diagram, Figure 1.4, establishes the relationship between this critical parameter θ_c and the shear Reynolds number Re_*:

$$\theta_c = \frac{u_{*c}^2}{g \Delta_s d} \qquad \text{and} \qquad Re_* = \frac{d u_*}{\nu}, \tag{1.68}$$

with Δ_s the relative density of the sediment, d sediment diameter, u_* bed shear

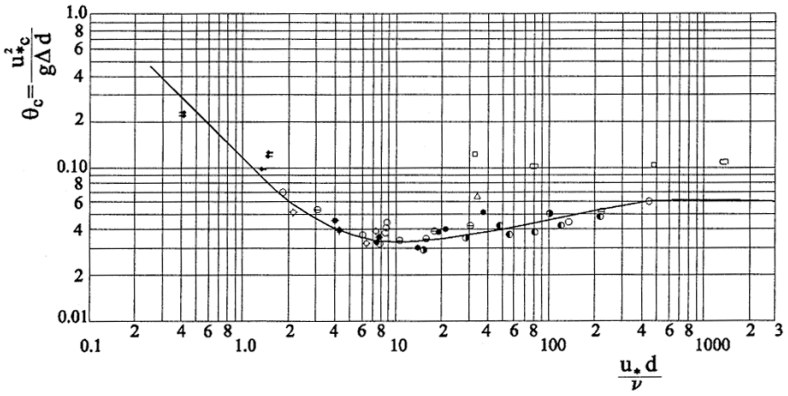

Figure 1.4: *The Shields diagram (1936) obtained through experimental data with uniform sediment.*

velocity and ν kinematic viscosity of the water. The bed shear velocity u_* is usually calculated through the Chézy law, Equation (1.78). Since both the non-dimensional parameter θ_c and Re_* depend on the shear stress velocity, the incipient condition can be recast in terms of the explicit particle Reynold's number D_* [57]:

$$D_* = d\left(\frac{g\Delta_s}{\nu^2}\right)^{1/3}.$$

The relation between the critical parameter θ_c and the explicit particle Reynold's number D_* can be approximated as following [11]:

$$\theta_c = 0.22D_*^{-1} + 0.06\exp\left(-17.77D_*^{-1}\right). \tag{1.69}$$

Although the Shields theory presents limits, many sediment transport formulas are still based on the critical Shields parameter θ_c. One of the most widely used is the Meyer-Peter Müller formula [40], a power law of the difference between the Shields parameter θ' and the critical parameter θ_c:

$$\frac{Q_s}{d\sqrt{g\Delta_s d}} = 8(\theta' - \theta_c)^{1.5} \tag{1.70}$$

where $\theta' = u_{*c}^2/\left(g\Delta_s d\right)$ is the Shields parameter due to the grain resistance. If the global resistance is considered, the Shields parameter can be corrected as following:

$$\theta' = \left(\frac{k_s'}{k_s}\right)^{-1.5}\frac{u_*^2}{g\Delta_s d} \tag{1.71}$$

where k_s' is the Strickler coefficient due to the resistance of the grain.

Starting from the Meyer-Peter Müller relation, the solid capacity can now be rewritten as a function of the Froude number $Fr = \sqrt{gh}/U$ [43]. After substituting $Q_s = \alpha_{cu} CUh$ into the Equation (1.70), the solid concentration can be obtained:

$$C = Fr^2 \frac{8}{\alpha_{cu} \Delta_s U^3} \left(u_*^2 - g\Delta_s d\theta_c\right)^{3/2} \tag{1.72}$$

The shear velocity for the uniform flow is expressed through the Gauckler-Strickler formula:

$$u_*^2 = \frac{gU^2}{k_s^2 R_h^{1/3}} \tag{1.73}$$

where k_s is the Strickler coefficient $\left[m^{1/3}s^{-1}\right]$ and R_h the hydraulic radius, defined as the rate between the area of the water column A and the wetted perimeter C_w. In conclusion, the following algebraic expression is derived:

$$C = Fr^2 \beta, \tag{1.74}$$

where

$$\beta = \frac{8}{\Delta_s \alpha_{cu}} \left(\frac{g}{k_s^2 R_h^{1/3}} - \frac{g\Delta_s d}{U^2} \theta_c \right)^{3/2}. \tag{1.75}$$

If the sediment mobility is high, the critical parameter can be neglected and the coefficient β is:

$$\beta = \frac{8}{\Delta_s \alpha_{cu}} \left(\frac{g}{k_s^2 R_h^{1/3}} \right)^{3/2}. \tag{1.76}$$

Finally, thanks to its simplicity the relation proposed by Grass [27] can be used in many test cases herein reported. This formula doesn't refer to a critical parameter and the solid discharge is a function of the velocity U and an empirical coefficient δ depending on the grain dimensions and calculated on the basis of experimental data:

$$Q_s = \delta U \left|U\right|^{m-1} \tag{1.77}$$

with $1 < m < 4$.

1.3.2 Bed Shear Stress

The friction relation is obtained in uniform flow conditions (gravitational forces exactly balanced by the frictional resistance forces) under the hypothesis that the concentration of the particles is enough small and, consequently, the direct interaction between particles can be ignored. In particular, the bottom shear stress $\bar{\tau}_0$ is expressed in function of the unknowns through the Chézy-Tadini law

[5]:

$$\frac{\bar{\tau}_0}{\rho} = u_*^2 = U^2 \frac{g}{\chi^2} \tag{1.78}$$

with χ the Chézy friction coefficient and u_* the bed shear velocity.

Besides, the Chézy friction coefficient can be substituted by the Strickler coefficient k_s:

$$\chi = k_s R_h^{\frac{1}{6}}. \tag{1.79}$$

The advantage of using the Strickler coefficient k_s is the lower dependency on the hydraulic radius and, then, the greater dependency on the bed roughness.

If a cross section of area A is considered, the roughness along the coordinate y is usually not constant as shown in Figure 1.5. The section shown in Figure

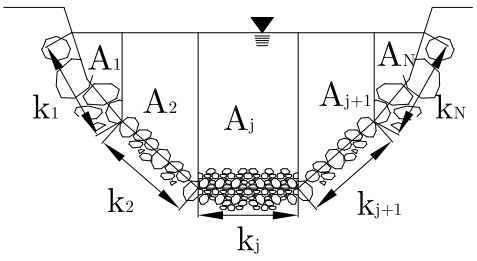

Figure 1.5: *Scheme for the Einstein-Horton method based on sub-areas with the same velocity.*

1.5 is dived in N sub-areas A_j and wet contours $(C_w)_j$ with different friction coefficients k_j. In order to calculated the equivalent friction coefficient k_s starting from the coefficients k_j, two methods are herein reported.

Method of Einstein-Horton

In this method, proposed by Einstein [24], the area A is subdivided in N sub-areas A_j characterized by the same mean velocity U as shown in Figure 1.5. Starting from the Gauckler-Strickler relation and assuming the rate between the velocity U and the energy slope $\sqrt{i_E}$ constant along the section, the averaged friction coefficient k_s is:

$$k_s = \frac{U}{\sqrt{i_E}} (R_h)^{-2/3} \tag{1.80}$$

where the hydraulic radius R_h is:

$$R_h = \frac{C_w}{\sum_{j=1}^{N} (C_w)_j (R_h)_j}. \tag{1.81}$$

Similarly, the hydraulic radius $(R_h)_j$ for the subsection A_j is calculated through

the Gauckler-Strickler relation:

$$(R_h)_j = k_j^{-3/2}\left(\frac{U}{\sqrt{i_E}}\right)^{3/2}. \tag{1.82}$$

After substitution of Equation (1.82) into Equation (1.80), the following equation is obtained:

$$k_s = \frac{(C_w)_j^{2/3}}{\left(\sum_{j=1}^{N}(C_w)_j k_j^{-3/2}\right)^{2/3}}. \tag{1.83}$$

By remembering that:

$$U_j = \chi\sqrt{(R_h)_j i_E}.$$

is possible to calculate an equivalent Chézy coefficient:

$$\chi = \sqrt{\frac{C_w}{\left(\sum_{j=1}^{N}(C_w)_j \chi_j^2\right)}}. \tag{1.84}$$

This criterion is based on the assumption that each sub-area is characterized by the same mean velocity U but it is evident that a lower velocity corresponds to the area with more vegetation. Then, this method is applied when the roughness doesn't strongly change along the section. Instead, the method proposed by Lotter can be applied in the case of larger roughness variation along the section.

Method of Lotter

The assumptions on the base of this criterion are:

1. the discharge Q is equal to the sum of the local discharge Q_j related to the area A_j in which the section is divided:

$$UA = \sum_j U_j A_j; \tag{1.85}$$

2. the energy loss i_E is constant along the section A:

$$i_E = (i_E)_j. \tag{1.86}$$

The local velocity U_j is calculated through the Chézy law:

$$U_j = \chi_j\sqrt{(R_h)_j i_E},$$

and substituted in Equation (1.85):

$$k_s A R_h^{2/3} i_E^{1/2} = \sum K_j A_j (R_h)_j^{2/3} (i_E)_j^{1/2}, \tag{1.87}$$

By using the second assumption, Equation 1.86, the equivalent Strickler coefficient becomes:

$$k_s = \frac{\sum k_j A_j^{5/3} (C_w)_j^{-2/3}}{A^{5/3} C_w^{-2/3}}. \tag{1.88}$$

Similarly to the method of Einsten-Horton, the equivalent Chézy coefficient χ can be derived starting from the previous equation:

$$\chi = \frac{\sum \chi_j A_j^{3/2} (C_w)_j^{-1/2}}{A^{3/2} C_w^{-1/2}}. \tag{1.89}$$

1.3.3 Formula for the Redistribution of the Solid Area

The solid area A_b is computed by solving the system of Equations (1.63)-(1.65), but, in order to study the evolution of the section shape, the local variation of the bed level z_b should be determined, Figure 1.6.

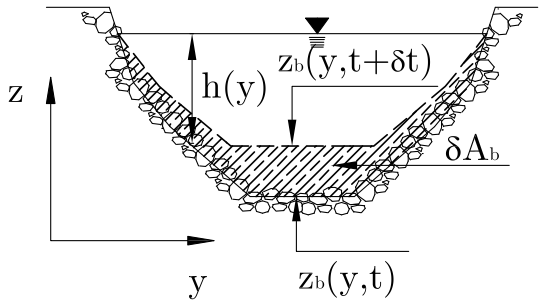

Figure 1.6: *Scheme for the redistribution of the sediment along the section.*

The temporal variation of the bed level is a function of the bed shear velocity:

$$\frac{\partial}{\partial t} \left[z_b (y) \right] = f \left(u_* \right), \tag{1.90}$$

and, then, of the shear stress at the bottom:

$$\frac{\partial}{\partial t} \left[z_b (y) \right] = f \left(\sqrt{\frac{\bar{\tau}_0}{\rho_w}} \right). \tag{1.91}$$

Under the hypothesis of energy loss i_E constant in the section and hydraulic

radius R_h equal to the depth h, the stress $\bar{\tau}_0$ is:

$$\bar{\tau}_0 = g\rho_w i_E h. \tag{1.92}$$

If the temporal derivatives of the bed level ∂z_b depends on the depth h [20] as following:

$$\frac{\partial}{\partial t}\left[z_b\left(y\right)\right] = k\left[h\left(y\right)\right]^m, \tag{1.93}$$

and the Equation (1.93) corresponds to the Equation (1.91), the coefficient m should be equal to 1/2.

Instead, k is the redistribution coefficient and can determined by integrating the bed level variation over the interval $[l, r]$:

$$\frac{\partial A_b}{\partial t} = \int_l^r \frac{\partial}{\partial t} k h^{1/2} dy, \tag{1.94}$$

and, then:

$$k = \frac{\dfrac{\partial A_b}{\partial t}}{\displaystyle\int_l^r \frac{\partial}{\partial t} h^{1/2} dy}. \tag{1.95}$$

Chapter 2

The Essentially Mono-Phase Model and its Range of Applicability

A non-dimensional analysis was carried out in order to investigate the applicability of some reductions of the quasi two-phase (QTP) model. The equations were scaled with respect to the uniform flow and the equilibrium concentration. In this analysis two parameters emerge: the Froude number of the basic flow and the ratio ϵ between the sediment concentration in the water column C_0 at the equilibrium and the solid concentration under the bed level C_b. The solid concentration C_b is usually considered constant in time, while the sediment concentration in the water column C is a function of the hydrodynamic variables and sediment features as shown in the Section 1.3. The aim of this chapter is to clarify the importance of each term with respect to the variation of the solid concentration in the water column and to the coupling between hydrodynamics and morphodynamics. Finally, the eigenvalues of the two systems for the rectangular section were analyzed and a simplified solution proposed.

2.1 Non-Dimensional Analysis of the Quasi Two-Phase Model

For simplicity, a rectangular channel with unit width was considered as shown in Figure 2.1. In this case the hydrodynamics and the morphodynamics of a water-sediment mixture are described by the following QTP system:

$$\frac{\partial}{\partial t}\left(h + z_b\right) + \frac{\partial}{\partial x}\left(Uh\right) = 0, \tag{2.1}$$

$$\frac{\partial}{\partial t}\left[\left(1+\alpha_{cu}C\Delta_s\right)Uh\right]+\frac{\partial}{\partial x}\left[\left(1+\alpha_{cu^2}C\Delta_s\right)U^2h\right]+g\frac{\partial}{\partial x}\left[\left(1+C\Delta_s\right)\frac{h^2}{2}\right]+$$
$$+gh\left(1+C\Delta_s\right)\frac{\partial z_b}{\partial x}=\gamma Uh, \tag{2.2}$$

$$\frac{\partial}{\partial t}\left(Ch\right)+C_b\frac{\partial z_b}{\partial t}+\frac{\partial}{\partial x}(\alpha_{cu}CUh)=0. \tag{2.3}$$

where Equations (2.1) and (2.3) are respectively the conservation of the total mass of the mixture and the solid mass. Instead, Equation (2.2) is the conservation of the momentum for the mixture as show in the Chapter 1. The corrective coefficient α_{cu} and α_{cu^2}, Equation (1.36) and Equation (1.38), are considered unitary and neglected [9]. In literature [26, 56], experimental data asset the value to $0.4 \div 1$.

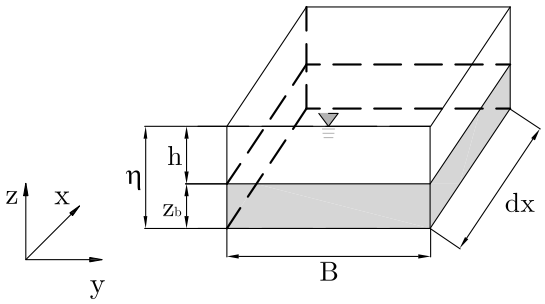

Figure 2.1: *Control volume for determination of shallow water equations with mobile-bed, where h is the water depth, z_b the bed elevation, η the free surface elevation and B the channel width (for simplicity unitary).*

2.1.1 Derivation of the Essentially Mono-Phase Model

A non-dimensional analysis of the Equations (2.1)-(2.3) was carried out in order to clarify the importance of each term with respect to the variation of the solid concentration C in the water column and the coupling between the hydrodynamics and the bed evolution. The scaling factors are reported in Table 2.1 where

$$\epsilon=\frac{t^*}{\tau^*} \tag{2.4}$$

denotes the ratio between the morphodynamic τ^* and the hydrodynamic t^* time scales. In facet, it should be remarked that two different time scales are employed for the hydrodynamics and bed evolution variables since, for low concentration, bed variations occur on a time scale significantly longer than that of typical hydrodynamical phenomena [33]. The scale for the axial coordinate x is the same for both the hydrodynamics and morphodynamics quantities, in

Quantity	Scale	Comments
U	U_0	U_0 uniform flow velocity
x	l_0	l_0 length of the hydrodynamic wave
t	$\frac{l_0}{U_0}$	for the hydrodynamic quantities
t	$\frac{l_0}{\epsilon U_0}$	for the bed evolution, τ^* is the non-dimensional time
h, z_b	h_0	uniform flow depth
C	C_0	C_0 concentration at the equilibrium (stationary flow)
γ	$\frac{U_0}{l_0}$	with $\gamma U h = \frac{\overline{\tau}_0}{\rho} C_w$

Table 2.1: *Scaling factors used in the model. Here, quantity = scale × dimensionless quantity.*

fact the length of morphodynamic waves has the same magnitude of the hydrodynamic wave.

After rescaling the Equations (2.1)-(2.3) and performing some standard algebraic manipulations, the following equations are obtained:

$$\frac{\partial h^*}{\partial t^*} + \epsilon \frac{\partial z_b^*}{\partial \tau^*} + \frac{\partial}{\partial x^*}\left(U^* h^*\right) = 0, \tag{2.5}$$

$$\frac{\partial}{\partial t^*}\left[\left(1 + C_0 C^* \Delta_s\right) U^* h^*\right] + \frac{\partial}{\partial x^*}\left[\left(1 + C_0 C^* \Delta_s\right) h^* U^{*2}\right] + \tag{2.6}$$
$$+ \frac{1}{Fr_0^2} \frac{\partial}{\partial x^*}\left[\left(1 + C_0 C^* \Delta_s\right) \frac{h^{*2}}{2}\right] + \frac{1}{Fr_0^2} h^* \left(1 + C_0 C^* \Delta_s\right) \frac{\partial z_b^*}{\partial x} = -\gamma^* U^* h^*,$$

$$\epsilon C_0 \frac{\partial}{\partial \tau^*}\left(C^* h^*\right) + \epsilon C_b \frac{\partial z_b^*}{\partial \tau^*} + C_0 \frac{\partial}{\partial x^*}(C^* U^* h^*) = 0. \tag{2.7}$$

where $*$ denotes the non-dimensional quantity and $Fr_0 = U_0/\sqrt{g h_0}$ is the Froude number of the base flow.

Empirical evidence [19] suggests that, for low concentration, topography changes are mainly due to the spatial variation in the sediment flux. Consequently, the second and third term of the solid mass continuity equation should have the same magnitude and the parameter ϵ should be:

$$\epsilon = \frac{C_0}{C_b} \tag{2.8}$$

with $C_0 = C\left(U_0, h_0\right)$ equilibrium concentration for the base flow.

Since in general the typical concentration C_0 of the sediment in the water column h is much smaller than the sediment concentration C_b in the river bed, the morphodynamic time scale is much longer then the hydrodynamic time scale

but, if the concentration C_0 increases, the two time scales become comparable. Using this definition, Equation (2.8), the non-dimensional model equations are finally rewritten as:

$$\frac{\partial h^*}{\partial t^*} + \epsilon \frac{\partial z_b^*}{\partial \tau^*} + \frac{\partial}{\partial x^*}\left(U^* h^*\right) = 0, \tag{2.9}$$

$$\frac{\partial}{\partial t^*}\left[\left(1+\epsilon C_b \Delta_s C^*\right) U^* h^*\right] + \frac{\partial}{\partial x^*}\left[\left(1+\epsilon C_b \Delta_s C^*\right) h^* U^{*2}\right] + \tag{2.10}$$
$$+\frac{1}{Fr_0^2}\frac{\partial}{\partial x^*}\left[\left(1+\epsilon C_b \Delta_s C^*\right)\frac{h^{*2}}{2}\right] + \frac{1}{Fr_0^2} h^* \left(1+\epsilon C_b \Delta_s C^*\right)\frac{\partial z_b^*}{\partial x} = -\gamma^* U^* h^*,$$

$$\epsilon \frac{\partial}{\partial \tau^*}\left(C^* h^*\right) + \frac{\partial z_b^*}{\partial \tau^*} + \frac{\partial}{\partial x^*}(C^* U^* h^*) = 0. \tag{2.11}$$

If all the terms multiplied by ϵ are simplified, an essentially mono-phase (EMP) model is consistently derived:

$$\frac{\partial h^*}{\partial t^*} + \frac{\partial}{\partial x^*}\left(U^* h^*\right) = 0, \tag{2.12}$$

$$\frac{\partial}{\partial t^*}\left(U^* h^*\right) + \frac{\partial}{\partial x^*}\left(h^* U^{*2}\right) + \tag{2.13}$$
$$+\frac{1}{Fr_0^2} h^* \frac{\partial h^*}{\partial x^*} + \frac{1}{Fr_0^2} h^* \frac{\partial z_b^*}{\partial x} = -\gamma^* U^* h^*,$$

$$\frac{\partial z_b^*}{\partial \tau^*} + \frac{\partial}{\partial x^*}(C^* U^* h^*) = 0. \tag{2.14}$$

It is important to underlined that the EMP was obtained starting from the QTP model. In literature, many simplified models are presented and in the Section 2.4 and they will be introduced and compared with the results of the non-dimensional analysis. In the following sections the two non-dimensional systems are studied and a simplified solution derived.

2.1.2 Eigenvalues Analysis

The behavior of the eigenvalues of the hyperbolic part of the System (2.9)-(2.11) were discussed by Morris and Williams [41]. The eigenvalue analysis will be extended here to the non-dimensional fully coupled system. For simplicity the symbol $*$ is dropped.

Neglecting friction, the non-dimensional model equations can be rewritten in compact form as:

$$\frac{\partial \mathbf{U}}{\partial t} + \frac{\partial \mathbf{F}}{\partial x} + \mathbf{H}\frac{\partial z}{\partial x} = 0, \tag{2.15}$$

where

$$\mathbf{U} = \begin{bmatrix} h + z_b \\ UH\left(1 + C_b\epsilon\Delta_s C\right) \\ Ch + \epsilon^{-1} z_b \end{bmatrix}, \mathbf{F} = \begin{bmatrix} Uh \\ \left(1 + \epsilon C_b \Delta_s C\right)\left(U^2 h + \dfrac{h^2}{2Fr_0^2}\right) \\ CUh \end{bmatrix},$$

$$\mathbf{H} = \begin{bmatrix} 0 \\ \dfrac{h}{Fr_0^2}\left(1 + C_b\epsilon\Delta_s C\right) \\ 0 \end{bmatrix}. \tag{2.16}$$

Also the bed evolution is expressed in terms of the free surface time variable t. The system (2.15) can then be rewritten in quasi-linear form as

$$\mathbf{B}\left(\mathbf{W}\right)\frac{\partial \mathbf{W}}{\partial t} + \mathbf{A}\left(\mathbf{W}\right)\frac{\partial \mathbf{W}}{\partial x} = 0, \tag{2.17}$$

where

$$\mathbf{W} = \begin{bmatrix} h \\ U \\ z_b \end{bmatrix}, \quad \mathbf{B} = \begin{bmatrix} 1 & 0 & 1 \\ U\left(\alpha + \xi h\dfrac{\partial C}{\partial h}\right) & h\left(\alpha + \xi U\dfrac{\partial C}{\partial U}\right) & Uh\xi\dfrac{\partial C}{\partial z} \\ \epsilon\left(C + h\dfrac{\partial C}{\partial h}\right) & \epsilon h\dfrac{\partial C}{\partial U} & 1 + \epsilon h\dfrac{\partial C}{\partial z} \end{bmatrix}$$

$$\mathbf{A} = \begin{bmatrix} U & h & 0 \\ \alpha\left(U^2 + \dfrac{h}{Fr_0^2}\right) + \xi hr\dfrac{\partial C}{\partial h} & 2Uh\alpha + \xi hr\dfrac{\partial C}{\partial U} & \alpha\dfrac{h}{Fr_0^2} + \xi hr\dfrac{\partial C}{\partial z} \\ \epsilon U\left(C + h\dfrac{\partial C}{\partial h}\right) & \epsilon h\left(C + U\dfrac{\partial C}{\partial U}\right) & \epsilon hu\dfrac{\partial C}{\partial z} \end{bmatrix} \tag{2.18}$$

whit

$$\xi = \epsilon C_b \Delta_s, \quad \alpha = 1 + \xi C, \quad r = U^2 + \frac{h}{2Fr_0^2}.$$

The eigenvalues of System (5.43) can be computed by imposing the condition $\det\left(\mathbf{A} - \lambda\mathbf{B}\right) = 0$, which yields the characteristic polynomial

$$\alpha_3\lambda^3 + \alpha_2\lambda^2 + \alpha_1\lambda + \alpha_0 = 0, \tag{2.19}$$

where

$$\alpha_0 = \epsilon hU\alpha b_1, \tag{2.20}$$

$$\alpha_1 = \alpha\left(-U^2 + \frac{h}{Fr_0^2}\right) + \epsilon\alpha b_2 + \xi r b_3\left(1 - \epsilon C\right), \tag{2.21}$$

$$\alpha_2 = U\alpha\left(2 + \epsilon b_4\right) + \xi b_5\left(1 - \epsilon C\right), \tag{2.22}$$

$$\alpha_3 = -\alpha\left(1-\epsilon b_6\right) - \xi U\frac{\partial C}{\partial U}\left(1-\epsilon C\right), \tag{2.23}$$

with

$$b_1 = \frac{h}{Fr_0^2}\left(h\frac{\partial C}{\partial h} - U\frac{\partial C}{\partial U} - h\frac{\partial C}{\partial z}\right) + U^2\frac{\partial C}{\partial z}, \tag{2.24}$$

$$\begin{aligned} b_2 = &-\frac{h}{Fr_0^2}\left(C + h\frac{\partial C}{\partial h} - U\frac{\partial C}{\partial U} - h\frac{\partial C}{\partial z}\right) + \\ &+U^2\left(C + 2h\frac{\partial C}{\partial h} - U\frac{\partial C}{\partial U} - 3h\frac{\partial C}{\partial z}\right), \end{aligned} \tag{2.25}$$

$$b_3 = h\frac{\partial C}{\partial h} - U\frac{\partial C}{\partial U}, \tag{2.26}$$

$$b_4 = -2C - 3h\frac{\partial C}{\partial h} + 2U\frac{\partial C}{\partial U} + 3h\frac{\partial C}{\partial z}, \tag{2.27}$$

$$b_5 = \left(r + U^2\right)\frac{\partial C}{\partial U} - hU\frac{\partial C}{\partial h}, \tag{2.28}$$

$$b_6 = C + h\frac{\partial C}{\partial h} - U\frac{\partial C}{\partial U} - h\frac{\partial C}{\partial z}. \tag{2.29}$$

In the case of fixed bed, Equation (2.19) reduces to:

$$\widehat{\alpha}_3\lambda^3 + \widehat{\alpha}_2\lambda^2 + \widehat{\alpha}_1\lambda = 0, \tag{2.30}$$

with

$$\widehat{\alpha}_1 = \left(-U^2 + \frac{h}{Fr_0^2}\right), \tag{2.31}$$

$$\widehat{\alpha}_2 = 2U, \tag{2.32}$$

$$\widehat{\alpha}_3 = -1. \tag{2.33}$$

The solutions of Equation (2.30) are the two well-known relative celerities of the free-water surface:

$$\lambda_1 = U + \frac{\sqrt{h}}{Fr_0}, \tag{2.34}$$

$$\lambda_2 = U - \frac{\sqrt{h}}{Fr_0}, \tag{2.35}$$

while the eigenvalue λ_3, associated with the propagation of bed disturbance, is equal to zero.

Instead, in the case of mobile-bed, the three solutions, Figure (2.2), depend on the choice of the closure relation. In fact, the solid concentration C should be expressed as a function of the other unknowns by a closure formula. In this case, following e.g. Rosatti and Fraccarollo [43], the closure formula proposed

in Section 1.3 is chosen:

$$C = \beta Fr^2. \tag{2.36}$$

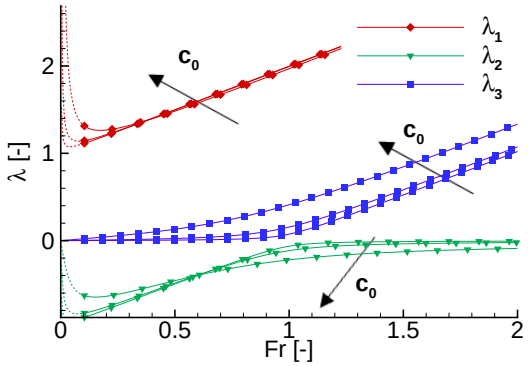

Figure 2.2: *Eigenvalues for the coupled system. Sediment concentration C_0 increasing from 0.000002 to 0.045. The lines are dashed for small values of the Froude numbers because high concentrations with small Froude number are not physically meaningful.*

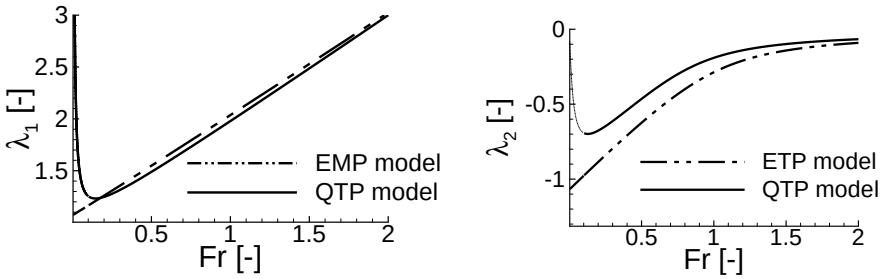

(a) (b)

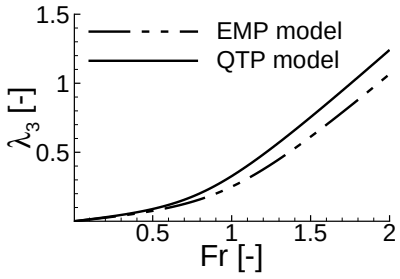

(c)

Figure 2.3: *Comparison between the QTP and the EMP system eigenvalues with* $C_0 = 0.03$.

The eigenvalues of the QTP system are compared with the eigenvalues of the EMP system derived e.g. by de Vries [22]. In the case of the EMP model, the quasi-linear system (5.43) has the form:

$$\mathbf{W} = \begin{bmatrix} h \\ U \\ z_b \end{bmatrix}, \quad \mathbf{B} = \begin{bmatrix} 1 & 0 & 0 \\ U & h & 0 \\ 0 & 0 & 1 \end{bmatrix}$$

$$\mathbf{A} = \begin{bmatrix} U & h & 0 \\ \left(U^2 + \dfrac{h}{Fr_0^2}\right) & 2Uh & \dfrac{h}{Fr_0^2} \\ \epsilon U \left(C + h\dfrac{\partial C}{\partial h}\right) & \epsilon h \left(C + U\dfrac{\partial C}{\partial U}\right) & \epsilon h U \dfrac{\partial C}{\partial z} \end{bmatrix} \tag{2.37}$$

and the coefficients of the characteristic polynomial are

$$\alpha_0 = \epsilon h U b_1, \tag{2.38}$$

$$\alpha_1 = \left(\frac{h}{Fr_0^2} - U^2\right) + \epsilon h \left[\frac{1}{Fr_0^2}\left(C + U\frac{\partial C}{\partial U}\right) - 2U^2\frac{\partial C}{\partial z}\right], \tag{2.39}$$

$$\alpha_2 = 2U\left(1 + \epsilon\frac{h}{2}\frac{\partial C}{\partial z}\right), \tag{2.40}$$

$$\alpha_3 = -1. \tag{2.41}$$

It can be seen that the differences between the respective eigenvalues become significant for non negligible values of the sediment concentration.

2.2 A Simplified Quasi Two-Phase Equation for the Bed Evolution

In this section, an evolution equation for the unknown z_b describing bed evolution will be derived under the hypothesis of low Froude number and of approximately steady free surface and discharge profiles. In order to derive a simplified equation, the friction term is considered equal to zero. Similar equations were proposed also by Hudson and Sweby [29] for the low sediment concentration case. Instead, this derivation holds independently of the mixture-bed concentration ratio and provides a much more interesting and severe benchmark for numerical methods. Besides, this approximated solution can be useful to understand the importance of the coupling terms.

The non-dimensional Equations (2.9)-(2.11), where the stars are dropped again for simplicity, are considered and the hydrodynamic time scale is used in

the continuity equation for the total mass:

$$\frac{\partial h}{\partial t} + \frac{\partial z_b}{\partial t} + \frac{\partial}{\partial x}(Uh) = 0, \tag{2.42}$$

$$Fr_0^2 \frac{\partial}{\partial t}\left[(1+\epsilon C_b \Delta_s C)\, Uh\right] + Fr_0^2 \frac{\partial}{\partial x}\left[(1+\epsilon C_b \Delta_s C)\, hU^2\right] \tag{2.43}$$
$$+ \frac{\partial}{\partial x}\left[(1+\epsilon C_b \Delta_s C)\, \frac{h^2}{2}\right] + h\,(1+\epsilon C_b \Delta_s C)\, \frac{\partial z_b}{\partial x} = 0,$$

$$\epsilon \frac{\partial}{\partial \tau}(Ch) + \frac{\partial z_b}{\partial \tau} + \frac{\partial}{\partial x}(Cuh) = 0. \tag{2.44}$$

Furthermore, a quasi steady flow is considered and the following solutions are imposed:

$$\eta = \bar{\eta} + \delta \eta'(x,t), \tag{2.45}$$

$$Q = \bar{Q} + \delta Q'(x,t). \tag{2.46}$$

where now δ is a small parameter that is independent from $\epsilon = C_0/C_b$, which is not required to be small. A first obvious consequence of these assumptions is that:

$$\frac{\partial Q}{\partial x} = O(\delta), \quad \frac{\partial Q}{\partial t} = O(\delta),$$
$$\frac{\partial \eta}{\partial x} = O(\delta), \quad \frac{\partial \eta}{\partial \tau} = \frac{1}{\epsilon} O(\delta).$$

Besides, without losing any generality, it can be assumed that the sediment concentration formula is a function $C = C(\eta, z_b, Q)$. This implies that the derivative of C with respect to space and time has to be computed by the chain rule as

$$\frac{\partial C}{\partial x} = \frac{\partial C}{\partial \eta}\frac{\partial \eta}{\partial x} + \frac{\partial C}{\partial z_b}\frac{\partial z_b}{\partial x} + \frac{\partial C}{\partial Q}\frac{\partial Q}{\partial x}, \tag{2.47}$$

$$\frac{\partial C}{\partial \tau} = \frac{\partial C}{\partial \eta}\frac{\partial \eta}{\partial \tau} + \frac{\partial C}{\partial z_b}\frac{\partial z_b}{\partial \tau} + \frac{\partial C}{\partial Q}\frac{\partial Q}{\partial \tau}. \tag{2.48}$$

Neglecting all the terms of order δ yields:

$$\frac{\partial C}{\partial x} = \frac{\partial C}{\partial z_b}\frac{\partial z_b}{\partial x}, \tag{2.49}$$

$$\frac{\partial C}{\partial \tau} = \frac{\partial C}{\partial z_b}\frac{\partial z_b}{\partial \tau}. \tag{2.50}$$

By rewriting now Equation (2.44) in terms of η and z_b:

$$\epsilon \frac{\partial (C\eta)}{\partial \tau} - \epsilon \frac{\partial (Cz_b)}{\partial \tau} + C_b \frac{\partial z_b}{\partial \tau} + \frac{\partial (CQ)}{\partial x} = 0 \tag{2.51}$$

neglecting terms of order δ and expressing the free surface gradients in terms of z_b, one obtains:

$$\epsilon h C_z \frac{\partial z_b}{\partial \tau} - \epsilon C \frac{\partial z_b}{\partial \tau} + \frac{\partial z_b}{\partial \tau} + \bar{Q} C_z \frac{\partial z_b}{\partial x} = 0 \tag{2.52}$$

where $C = C(\bar{\eta}, z_b, \bar{Q})$ and $C_z = \dfrac{\partial C}{\partial z_b}$. Rearranging the previous equations yields the approximate evolution equation for the bed profile:

$$\frac{\partial z_b}{\partial \tau} + \frac{\bar{Q} C_z}{1 + \epsilon h C_z - \epsilon C} \frac{\partial z_b}{\partial x} = 0. \tag{2.53}$$

This nonlinear equation can be solved very accurately by the method of characteristics and an appropriate solution $z_b(x, \tau)$ can be obtained:

$$\frac{D z_b}{D x} = \frac{\partial z_b}{\partial \tau} + \frac{\bar{Q} C_z}{1 + \epsilon h C_z - \epsilon C} \frac{\partial z_b}{\partial x} = 0. \tag{2.54}$$

Consequently, the solution is constant and $z_b(x, \tau)$ is equal to $z_b(x_0, 0)$ along the characteristic line (x, t):

$$x = x_0 + \frac{\bar{Q} C_z}{1 + \epsilon C_z - \epsilon C} (\tau - \tau_0) \tag{2.55}$$

2.3 Range of Validity of the Models

The magnitude of the ϵ rate is an important parameter in order to know the importance of the coupling terms. It is not immediate to understand the effect of the concentration on the bed evolution but the parameter ϵ can be used as an estimation of the magnitude of the negligible terms. Consequently, can be acceptable to neglect terms with order of magnitude inferior to the 1% and, instead, consider them when the parameter ϵ becomes more relevant. If the range of validity of the EMP model is fixed for values of ϵ inferior then 0.01 and the concentration under the bed level is usually 0.65, the limit of concentration C is 0.0065. In the numerical test cases, in fact, the differences between the two models, EMP and QTP, are observed for concentration higher then 6.5 ‰.

Besides, in the case of quasi-steady flow, the Equation (2.53) indicates the migration rate of a finite bed perturbation. Since the whole derivation of Equation (2.53) is independent of ϵ ratio, this equation can be considered to yield a good first approximation for the bed evolution also in regimes of quasi-steady flow with high sediment concentration.

A second information from the analysis of the equations is the difference in the stationary state. If the boundary conditions are constant in time, the steady

state, in case of QTP model, is:

$$\frac{\partial z_b}{\partial x} = -Fr_0^2 \frac{\gamma u}{1 + \epsilon c_b \Delta_s c}. \tag{2.56}$$

Starting from the consistent derivation of the EMP model and the definition of its range of validity, in the next section the existing models are analyzed.

2.4 Analysis of the Existing Models

In Cao et al. [13], the effects of simplifications on the numerical results are studied and the importance of these assumptions underlined. In this section, some of these models are consistently reviewed with respect the non-dimensional analysis.

Simplified models has been proposed [1, 12, 23, 29, 31, 34, 51] and, in the major part of them, the momentum Equation (2.2) is reduced to the equation of the clear water in the case of fixed bed, Equation (2.13), that in the dimensional case is:

$$\frac{\partial}{\partial t}(Uh) + \frac{\partial}{\partial x}\left(U^2 h + g\frac{h^2}{2}\right) + gh\frac{\partial z_b}{\partial x} = -\frac{\bar{\tau}_0}{\rho}, \tag{2.57}$$

Some authors [13] justify this choice also in the QTP models because the terms regarding the coupling between solid and liquid phase are incorporated in the uncertainty of the friction term. Otherwise, authors [1, 12, 23, 29, 31, 34, 51] propose different kinds of simplifications for the conservation of the solid and liquid mass.

In the following models the momentum equation is written for the clear water, instead, the conservation equations of mass are:

Model A While the continuity equation are written for the full system [1]:

$$\frac{\partial h}{\partial t} + \frac{\partial z_b}{\partial t} + \frac{\partial}{\partial x}(Uh) = 0, \tag{2.58}$$

$$\frac{\partial (Ch)}{\partial t} + C_b\frac{\partial z_b}{\partial t} + \frac{\partial(\alpha_{cu} CUh)}{\partial x} = 0, \tag{2.59}$$

the momentum equation is simplified, Equation (2.57). Consequently, terms with the same order of magnitude are not considered in all the Equations (2.9)-(2.11) as shown in Section 2.1.

Model B In the continuity equation of the total mass, the bed variation is not considered [23]:

$$\frac{\partial h}{\partial t} + \frac{\partial}{\partial x}(Uh) = 0, \tag{2.60}$$

$$C_b \frac{\partial z_b}{\partial t} + \frac{\partial (Ch)}{\partial t} + \frac{\partial (\alpha_{cu} CUh)}{\partial x} = 0; \tag{2.61}$$

In this case the system is simplified except for the temporal variation of the sediment storage in the water column in Equation (2.11).

Model C Cui et al. [21], remembering that the flux of the sediment-water mixture Q is the sum of the liquid discharge Q_l and the solid discharge Q_s and they rewrite the conservation equation for the total mass, Equation (2.1), as:

$$\frac{\partial h}{\partial t} + \frac{\partial z_b}{\partial t} + \frac{\partial Q_w}{\partial x} + \frac{\partial Q_s}{\partial x} = 0, \tag{2.62}$$

where Q_w and Q_s are respectively the liquid and solid discharges for unit length. The authors assume that the liquid discharge $Q_w = (1 - C)\, Uh$ is equal to the discharge of the sediment-water mixture $Q = Uh$ and the following equations for the conservation of the mass are obtained:

$$\frac{\partial h}{\partial t} + \frac{\partial z_b}{\partial t} + \frac{\partial}{\partial x}(Uh) + \frac{\partial}{\partial x}(\alpha_{cu} CUh) = 0, \tag{2.63}$$

$$C_b \frac{\partial z_b}{\partial t} + \frac{\partial (Ch)}{\partial t} + \frac{\partial (CUh)}{\partial x} = 0. \tag{2.64}$$

The incoherence of this formulation is that if the liquid discharge Q_w is equal to Uh, the solid concentration C should be zero and consistently also the solid discharge $Q_s = CUh$ should be negligible in Equation (2.62) and, then, in Equation (2.63).

Model D Both the time variation of the bed level and the sediment storage in the water column are neglected. This is the most used model [12, 29, 31, 34, 51] and the simplified system is:

$$\frac{\partial h}{\partial t} + \frac{\partial}{\partial x}(Uh) = 0, \tag{2.65}$$

$$C_b \frac{\partial z_b}{\partial t} + \frac{\partial (\alpha_{cu} CUh)}{\partial x} = 0. \tag{2.66}$$

The model coincides with the EMP model, Equations (2.12)-(2.14), consistently derived with the non dimensional analysis.

Cao et al. [13] observe that the solutions of these simplified systems can be substantially different above all for aggradation processes and the inaccuracy due to the neglect of the coupling terms can be accumulative, but they not justify the choice of these models. However, a consistent analysis and derivation of the EMP system is now present. The model D coincides with the EMP model and can be used under the assumption of low concentration C. The models B and C

consider only some of the terms multiplied by ϵ in the non-dimensional system, Equations (2.5)-(2.7), while the conservation equations of mass in the model A are complete but the momentum equation is written for the clear water.

Finally, the choice of a model for fixed or mobile bed in one-dimensional river models can lead to lose some information connected to the topography of the river and to the non-uniform distribution of the velocity along the cross section. These models present substantial differences with the model presented in Section 1.2.2 or Wu [52] where the 2D information is considered. For example, in the case of an arbitrary shape of the cross section it is necessary to define a corrective coefficient in the momentum equation because of the non-uniformity of the velocity along the cross section as shown in the Chapter 1. Some algorithms, such as in Stelling and Verwey [50], assumed the corrective coefficient unitary while HEC-RAS [12] divides the cross section in two parts, thalweg and banks, and calculates the rate of discharge for both the two sub-areas. This solution procedure leads to an increasing of the computational cost with respect to consider a corrective coefficient.

In the following chapter the QTP and EMP models for a general cross section are discretized and an efficient solution procedure is proposed.

Chapter 3

Development of an Efficient Numerical Scheme for the Two Models

In this chapter the solution procedure proposed by Rosatti et al. [45] is extended to the case of a mobile bed for both the models. The advantages of this scheme are the high efficiency and the low computational cost, the reconstruction of hydrodynamic and morphodynamic 2D information and the possibility of solving the full system without the assumption of quasi-steady state. In fact, this solution procedure considers the effects of morphodynamics on the flow and vice versa. In the first section a briefly review on the existing method and their features is proposed.

3.1 Literature Review on the Existing Schemes

The main feature of numerical methods is the computational efficiency. Different schemes were proposed for the EMP model. There are several methods to solve numerically the equations for 1D open channel. Standard explicit numerical methods present a time step limitation due to the stability restriction imposed by the Courant-Friedrichs-Lewy (CFL) condition. Some recent numerical schemes, for example Stelling and Verwey [50] and Casulli [15] or the solution procedure of the software HEC-RAS [12], are based on a semi-implicit discretization. The more efficient methods are based on a semi-Lagrangian discretization of the momentum equation while the continuity equation for the mass is discretized with a finite volume method as proposed by Rosatti et al. [45]. Thus scheme is capable of accurate solutions in all regimes, except in presence of strong unsteady shocks as in dam-break cases. Instead, by using a suitable upwind Eulerian

discretization for the same equations, a scheme able of describing accurately also unsteady shocks can be obtained, although this scheme requires a more restrictive stability condition. In conclusion, this solution procedure makes the method appealing for computationally intensive simulations and it can be used for sediment transport simulations and river morphology studies. Two methods are herein proposed and extended to the mobile bed case: the upwind Eulerian discretization [15, 43] and a semi-Lagrangian formulation [17, 18, 45] for section averaged free surface flow modeling.

Finally, in Cao et al. [13], the difference between algorithms with synchronous and asynchronous solution procedure is highlighted. If all the equations are solved simultaneously the scheme is defined as synchronous. Instead, the asynchronous procedure is based on the fixed bed or quasi-steady flow assumption. In fact, the river bed is assumed to be fixed when the de Saint-Venant equations are solved. On the other hand, the flow is assumed to be steady when the evolution of the river bed is computed. Thus, the Exner equation is solved by using the hydrodynamic variables at the previous time step. Besides, in the quasi-synchronous procedure, as shown by Kassem and Chaudry [31], the de Saint-Venant equations are solved separately, but the bed variables are used to adjust the flow variable through an iterative procedure. Cao et al. [13] and Kassem and Chaudry [31] suggests that it is possible to decouple the solution procedure only when the sediment concentrations are negligible and the time scale of the bed evolution is less then the time scale concerning the hydrodynamic variables.

In the solution procedure described in the following section no assumption of quasi-steady flow or fixed bed are done when the equations are numerically solved. In fact, the three conservation equations are discretized without simplification of the temporal derivative as in the case of asynchronous solution. Then, the morphodynamic effects on the flow and viceversa are considered and the solution is fully synchronous.

3.2 Discretization of the Model Equations

In order to obtain an efficient numerical discretization, the EMP and QTP systems are reformulated by using an appropriate change of variables. The resulting QTP system in function of the free surface η, the bed elevation z_b and the discharge Q is:

$$\frac{\partial A_t ot\,(\eta)}{\partial t} + \frac{\partial Q}{\partial x} = 0, \tag{3.1}$$

$$\frac{\partial}{\partial t}\left[\left(1+C\Delta_s\right)Q\right]+\frac{\partial F}{\partial x}+gA\left(1+C\Delta_s\right)\frac{\partial \eta}{\partial x}+ \\ +g\Delta_s\alpha_h\frac{HA}{2}\frac{\partial C}{\partial x}+\alpha Q=0, \tag{3.2}$$

$$\frac{\partial (CA)}{\partial t}+C_b\frac{\partial A_b}{\partial t}+\frac{\partial \left(CQ\right)}{\partial x}=0, \tag{3.3}$$

with

$$A_{tot}=A+A_b, \tag{3.4}$$

$$F=\left(1+C\Delta_s\right)\frac{\alpha_{u^2}Q^2}{A}, \tag{3.5}$$

$$\alpha=\gamma+\frac{\partial}{\partial x}\left[\left(1+C\Delta_s\right)U\right]. \tag{3.6}$$

The local concentration c, see Chapter 1, is considered constant and, consequently, the corrective coefficient α_{cu} is unitary. Instead, the coefficient α_{u^2} is introduced instead of α_{cu^2} to consider only the non uniform distribution, Figure 3.1, of the local velocity u along the y coordinate:

$$\alpha_{u^2}=\frac{\int_A u^2(x,y,z,t)dz}{AU^2}. \tag{3.7}$$

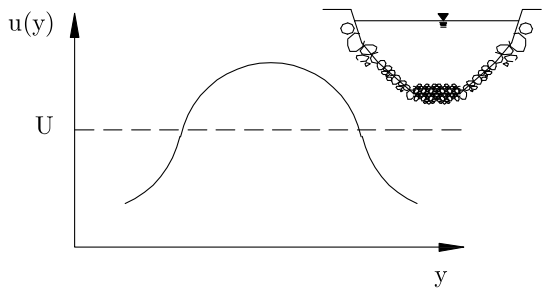

Figure 3.1: *Non-uniform distribution of the velocity along the y coordinate*

Similarly, the resulting EMP system consistently derived from the QTP system (3.1)-(3.3) is:

$$\frac{\partial \eta}{\partial t}+\frac{\partial Q}{\partial x}=0, \tag{3.8}$$

$$\frac{\partial Q}{\partial t}+\frac{\partial F}{\partial x}+gA\frac{\partial \eta}{\partial x}+\alpha Q=0, \tag{3.9}$$

$$C_b\frac{\partial A_b}{\partial t}+\frac{\partial \left(CQ\right)}{\partial x}=0, \tag{3.10}$$

with

$$F = \frac{\alpha_{u^2} Q^2}{A}, \tag{3.11}$$

$$\alpha = \gamma. \tag{3.12}$$

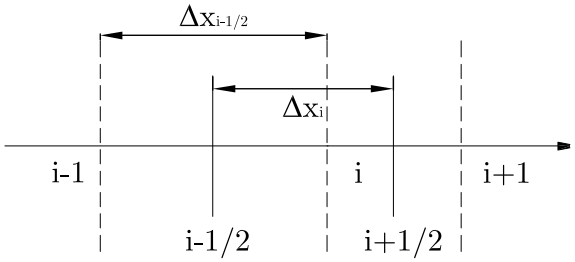

Figure 3.2: *Staggered computational grid*

The solution procedures for both the two systems, Equations (3.1)-(3.3) and Equations (3.8)-(3.10), are similar. The computational domain is discretized by a staggered computational grid, Figure 3.2, where the wet area A and the free surface elevation η are defined at the integer nodes x_i, $i = 1, \ldots, N$, while the discharge Q is defined at the half integer nodes $x_{i+1/2} = (x_i + x_{i+1})/2$. The node distribution is arbitrary and the node spacings are defined as $\Delta x_i = x_{i+1/2} - x_{i-1/2}$ and $\Delta x_{i+1/2} = x_{i+1} - x_i$, respectively.

3.2.1 The Momentum Equation

The two schemes already proposed by Rosatti et al. [45] for the fixed bed case depend on the formulation of the momentum equation.

Upwind Eulerian Discretization

The Equations (3.2) and (3.9) are integrated over the control volume $[x_i, x_{i+1}]$:

$$\int_{x_i}^{x_{i+1}} \left(\frac{\partial}{\partial t} \left[(1 + i_c C \Delta_s) Q \right] + \frac{\partial F}{\partial x} + gA \left(1 + i_c C \Delta_s \right) \frac{\partial \eta}{\partial x} + \right.$$
$$\left. + i_c g \Delta_s \alpha_h \frac{HA}{2} \frac{\partial C}{\partial x} + \alpha Q \right) dx = 0 \tag{3.13}$$

$$\tag{3.14}$$

where

$$i_c = \begin{cases} 0 & \text{decoupled model,} \\ 1 & \text{coupled model.} \end{cases} \tag{3.15}$$

and

$$F = (1 + i_c C \Delta_s) \frac{\alpha_{u^2} Q^2}{A}, \tag{3.16}$$

$$\alpha = \gamma. \tag{3.17}$$

Applying the mean value theorem to all the terms except the flux F yields:

$$\frac{\partial}{\partial t} \left[(1 + i_c C \Delta_s) Q \right] \Big|_{i+1/2} + \frac{F_{i+1} - F_i}{\Delta x_{i+1/2}} + g A_{i+1/2} (1 + i_c C \Delta_s) \frac{\partial \eta}{\partial x} \Big|_{i+1/2} + \\ + i_c g \Delta_s \alpha_h \frac{AH}{2} \frac{\partial C}{\partial x} \Big|_{i+1/2} + \alpha_{i+1/2} Q_{i+1/2} = 0. \tag{3.18}$$

The free-surface gradient and the total discharge Q are discretized in space by a centred finite difference and in time by a semi-implicit time average. The advective term is discretized by an explicit upwind scheme where F_i denotes the upwind-based discretization of the momentum flux [2]. The area A, the concentration C and the friction term α are linearized in time, while the other terms are function of η or Q and still contain all the information regarding the time evolution of hydrodynamics and morphodynamics:

$$\left(1 + i_c C^n_{1+1/2} \Delta_s\right) \frac{Q^{n+1}_{i+1/2} - Q^n_{i+1/2}}{\Delta t} + \frac{F^n_{i+1} - F^n_i}{\Delta x_{i+1/2}} + \\ + g A^n_{i+1/2} \left(1 + i_c C^n_{i+1/2} \Delta_s\right) \left[\vartheta \frac{\eta^{n+1}_{i+1} - \eta^{n+1}_i}{\Delta x_{i+1/2}} + (1 - \vartheta) \frac{\eta^n_{i+1} - \eta^n_i}{\Delta x_{i+1/2}} \right] + \\ + i_c g \Delta_s \alpha^n_{h_{i+1/2}} \frac{A^n_{i+1/2} H^n_{i+1/2}}{2} \frac{C^n_{i+1} - C^n_i}{\Delta x_{i+1/2}} + \\ + \alpha^n_{i+1/2} \left[\vartheta Q^{n+1}_{i+1/2} + (1 - \vartheta) Q^n_{i+1/2} \right] = 0. \tag{3.19}$$

with

$$F^n_i = \begin{cases} \left[\alpha_{u^2} (1 + i_c C \Delta_s) \frac{Q^2}{A} \right]^n_{i-1/2} & U \geq 0 \\ \left[\alpha_{u^2} (1 + i_c C \Delta_s) \frac{Q^2}{A} \right]^n_{i+1/2} & U < 0. \end{cases} \tag{3.20}$$

Rearranging the terms and solving for Q, the discrete formulation for the momentum equation becomes:

$$Q^{n+1}_{i+1/2} = \frac{\mathcal{F}^E_{i+1/2}(Q^n)}{1 + i_c C^n_{i+1/2} \Delta_s + \vartheta \Delta t \alpha^n_{i+1/2}} + \\ - \frac{\vartheta \Delta t}{\Delta x_{i+1/2}} \frac{g A^n_{i+1/2} \left(1 + i_c C^n_{i+1/2} \Delta_s\right)}{1 + i_c C^n_{i+1/2} \Delta_s + \vartheta \Delta t \alpha^n_{i+1/2}} \left(\eta^{n+1}_{i+1} - \eta^{n+1}_i \right), \tag{3.21}$$

where $\mathcal{F}^E_{i+1/2}$ denotes the sum of all the explicit terms:

$$\begin{aligned}\mathcal{F}^E_{i+1/2} &= (1+i_c C\Delta_s)^n_{1+1/2}\, Q^n_{i+1/2} + \\ -\Delta t\frac{F^n_{i+1}-F^n_i}{\Delta x_{i+1/2}} &- \Delta t(1-\vartheta) g(A)^n_{i+1/2}\left(1+i_c C^n_{i+1/2}\Delta_s\right)\frac{\eta^n_{i+1}-\eta^n_i}{\Delta x_{i+1/2}} \\ -i_c\Delta t g\alpha^n_{h_{i+1/2}}&\frac{A^n_{i+1/2}H^n_{i+1/2}}{2}\frac{C^n_{i+1}-C^n_i}{\Delta x_{i+1/2}} - (1-\vartheta)\Delta t\alpha^n_{i+1/2}Q^n_{i+1/2}.\end{aligned} \tag{3.22}$$

Since the values of the area A at the nodes $i+1/2$ are not defined, they are computed by a quadratic interpolation on an upwind-biased stencil or, alternatively, by an upwind-weighted interpolation of the form $A_{i+1/2} = pA_i + (1-p)A_{i+1}$, where p is an upwind weight.

Semi-Lagrangian Approach

For the section-averaged equations with arbitrary cross-section shape, unlike in the constant rectangular section and 2D cases, it is not possible to obtain a purely advective formulation of the momentum Equations (3.2)-(3.9). However, a quasi-Lagrangian formulation [18, 45] can be derived by expanding the momentum flux and canceling some of the resulting terms by use the mass-conservation equation:

$$\begin{aligned}\frac{\partial}{\partial t}[(1+i_c C\Delta_s)Q] + \alpha_{u^2}U\frac{\partial}{\partial x}[(1+i_c C\Delta_s)Q] + gA[(1+i_c C\Delta_s)Q]\frac{\partial\eta}{\partial x} = \\ = -i_c g\Delta_s\frac{AH}{2}\frac{\partial C}{\partial x} - Q\frac{\partial(\alpha_{u^2}U)}{\partial x} - \gamma Q.\end{aligned} \tag{3.23}$$

Then, the momentum equation in a quasi-Lagrangian formulation is:

$$\frac{D}{Dt}[(1+i_c C\Delta_s)Q] + gA\,(1+i_c C\Delta_s)\,\frac{\partial\eta}{\partial x} = -\alpha Q - i_c g\Delta_s\alpha_h\frac{AH}{2}\frac{\partial C}{\partial x} \tag{3.24}$$

with

$$\alpha = \frac{gQC_w}{\chi^2A^2} + (1+i_c C\Delta_s)\frac{\partial(\alpha_{u^2}U)}{\partial x}. \tag{3.25}$$

The material derivative is approximated in a semi-Lagrangian fashion (see e.g. [45]) for the coupled model as:

$$\left.\frac{D}{Dt}[(1+i_c C\Delta_s)Q]\right|_{i+1/2} = \frac{\left(1+i_c C^n_{i+1/2}\Delta_s\right)Q^{n+1}_{i+1/2} - (1+i_c C^n_*\Delta_s)\,Q^n_*}{\Delta t} \tag{3.26}$$

where $*$ denotes the quantities interpolated at the foot of the trajectory. The position of the quantities is define by:

$$x^*_{i+1/2} = x_{i+1/2} - \int_0^{\Delta t} \alpha_{u^2}\left(x\left(t\right)\right) U\left(x\left(t\right)\right) dt. \tag{3.27}$$

The integral is evaluated by sub-stepping technique as shown by Rosatti et al. [44] and the quantities at the foot of the trajectory are computed by a cubic interpolation of the four nodes nearest to the position $x^*_{i+1/2}$ as in the fixed bed case [45].

The resulting numerical discretization for the momentum Equation (3.2) is equal to Equation (3.21):

$$\begin{aligned} Q^{n+1}_{i+1/2} = \frac{\mathcal{F}^{SL}_{i+1/2}}{(1 + i_c C^n_{i+1/2}\Delta_s + \vartheta \Delta t \alpha^n_{i+1/2})} + \\ -\frac{\vartheta \Delta t}{\Delta x_{i+1/2}} \frac{g A^n_{i+1/2}\left(1 + i_c C^n_{i+1/2}\Delta_s\right)}{(1 + C^n_{i+1/2}\Delta_s + \vartheta \Delta t \alpha^n_{i+1/2})} \left(\eta^{n+1}_{i+1} - \eta^{n+1}_i\right), \end{aligned} \tag{3.28}$$

but the explicit terms $\mathcal{F}^{SL}_{i+1/2}$ are:

$$\begin{aligned} \mathcal{F}^{SL}_{i+1/2} = \left[\left(1 + i_c C \Delta_s\right) Q + \right. \\ -(1-\vartheta)\Delta t g A \left(1 + i_c C \Delta_s\right) \frac{\partial \eta}{\partial x} + \\ \left. -i_c \frac{g \Delta_s \left(\alpha_h\right)^n_1 1 + 1/2 A H}{2} \frac{\partial C}{\partial x} - (1-\vartheta)\Delta t \alpha Q \right]_* \end{aligned} \tag{3.29}$$

and $*$ denotes quantities interpolated at the foot of the trajectory. Defining the explicit terms as $\mathcal{F}^{E,SL}_{i+1/2}$ in a different way yields the same discretization for the discharge $Q^{n+1}_{i+1/2}$. Consequently, the same solution procedure shown in the Section 3.3 can be used for both the two formulation.

3.2.2 The Continuity Equation for the Total Mass

The conservation equation for the total mass is integrated by a finite-volume method over the control volume $\left[x_{i-1/2}, x_{i+1/2}\right]$:

$$\int_{x_{i-1/2}}^{x_{i+1/2}} \left(\frac{\partial A_{tot}}{\partial t} + \frac{\partial Q}{\partial x}\right) dx = 0. \tag{3.30}$$

Side fluxes are discretized in time in a semi-implicit fashion, by taking them equal to the weighted average of the corresponding values at time levels $n+1$ and n. The resulting discrete equation is:

$$\begin{aligned}(V_t)_i^{n+1} - (V_t)_i^n + \vartheta\Delta t\left(Q_{i+1/2}^{n+1} - Q_{i-1/2}^{n+1}\right) + \\ +(1-\vartheta)\Delta t\left(Q_{i+1/2}^{n} - Q_{i-1/2}^{n}\right) = 0\end{aligned} \tag{3.31}$$

where $(V_t)_i$ denotes the sediment-water volume between the section $i-1/2$ and $i+1/2$. If the section shape is arbitrary, the volume V_t is a non-linear function of the free surface η. Substituting Equation (3.21) or Equation (3.28) into Equation (3.31) yields:

$$\begin{aligned}(V_t)_i^{n+1} - \frac{\vartheta^2\Delta t^2}{\Delta x_{i+1/2}}\frac{gA_{i+1/2}^n\left(1+C_{i+1/2}^n\Delta_s\right)}{1+C_{i+1/2}^n\Delta_s+\vartheta\Delta t\alpha_{i+1/2}^n}\left(\eta_{i+1}^{n+1}-\eta_i^{n+1}\right) + \\ +\frac{\vartheta^2\Delta t^2}{\Delta x_{i-1/2}}\frac{gA_{i-1/2}^n\left(1+C_{i-1/2}^n\Delta\right)}{i+C_{1-1/2}^n\Delta_s+\vartheta\Delta t\alpha_{i-1/2}^n}\left(\eta_i^{n+1}-\eta_{i-1}^{n+1}\right) = \mathcal{G}_i^n\end{aligned} \tag{3.32}$$

where

$$\begin{aligned}\mathcal{G}_i^n = (V_t)_i^n - (1-\vartheta)\Delta t\left(Q_{i+1/2}^n - Q_{i-1/2}^n\right) + \\ -\vartheta\Delta t\left(\frac{\mathcal{F}_{i+1/2}}{1+C_{i+1/2}^n\Delta_s+\alpha_{i+1/2}^n\vartheta\Delta t} - \frac{\mathcal{F}_{i-1/2}}{i+C_{1-1/2}^n\Delta_s+\alpha_{i-1/2}^n\vartheta\Delta t}\right).\end{aligned} \tag{3.33}$$

The final system is:

$$(V_t)_i^{n+1} + \mathcal{K}_{i-1}^n\eta_{i-1}^{n+1} + \mathcal{K}_i^n\eta_i^{n+1} + \mathcal{K}_{i+1}^n\eta_{i+1}^{n+1} = \mathcal{G}_i^n, \tag{3.34}$$

with

$$\mathcal{K}_{i\mp1}^n = -\frac{\vartheta^2\Delta t^2 gA_{i\mp1/2}^n\left(1+i_cC_{i\mp1/2}^n\Delta_s\right)}{\Delta x_{i\mp1/2}\left(1+i_cC_{i\mp1/2}^n\Delta_s+\vartheta\Delta t\alpha_{i\mp1/2}^n\right)}, \tag{3.35}$$

$$\mathcal{K}_i^n = -\left(\mathcal{K}_{i-1}^n + \mathcal{K}_{i+1}^n\right). \tag{3.36}$$

The set of Equations (3.34) for all cells i of the computational domain constitutes a weakly nonlinear system that can be written in vector notation as:

$$\mathbf{V_t}(\boldsymbol{\eta}) + \mathbf{M}\boldsymbol{\eta} = \mathbf{G} \tag{3.37}$$

Here, $\boldsymbol{\eta}$ denotes the vector of the unknowns η_i^{n+1}, $\mathbf{V_t}(\boldsymbol{\eta})$ denotes the vector of the unknown V_i^{n+1} , $\mathbf{M}$ a symmetric tridiagonal matrix and $\mathbf{G}$ is the vector of the right-hand side terms $\mathcal{G}_i^n$. In order to guarantee full mass conservation in cross-sections of arbitrary geometry, a nonlinear relationship between η and $V_t(\eta)$ must be assumed. Thus, it is necessary to solve a scalar nonlinear equation for each cell to recover the new free-surface values from the new section volumes, even for explicit time discretizations. The system can be solved after assigned the right initial and boundary conditions as reported in the Section 3.3.

3.2.3 The Continuity Equation for the Solid Mass

The conservation equations of the solid mass, Equations (3.3) and (3.10) are integrated over the control volume i:

$$\int_{x_{i-1/2}}^{x_{i+1/2}} \left(\frac{\partial}{\partial t} \left(i_c C A \right) + C_b \frac{\partial A_b}{\partial x} + \frac{\partial}{\partial x} \left(CQ \right) \right) dx = 0 \tag{3.38}$$

The area A is substituted with the difference between the total area A_t and the bed area A_b:

$$\int_{x_{i-1/2}}^{x_{i+1/2}} \left(\frac{\partial}{\partial t} \left(i_c C A_t \right) - \frac{\partial}{\partial t} \left(i_c C A_b \right) + C_b \frac{\partial A_b}{\partial t} + \frac{\partial}{\partial x} \left(CQ \right) \right) dx = 0. \tag{3.39}$$

The fluxes are discretized in time in a semi-implicit fashion, while the concentration C is explicit in agreement with the discretization of the momentum equation:

$$\begin{aligned} & i_c \left[C_i^n (V_t)_i^{n+1} - C_i^{n-1} (V_t)_i^n - C_i^n (V_b)_i^{n+1} + C_i^{n-1} (V_b)_i^n \right] + \\ & + C_b (V_b)_i^{n+1} - C_b (V_b)_i^n + \vartheta \Delta t \left(C_{i+1/2}^n Q_{i+1/2}^{n+1} - C_{i-1/2}^n Q_{i-1/2}^{n+1} \right) + \\ & + (1-\vartheta) \Delta t \left(C_{i+1/2}^n Q_{i+1/2}^n - C_{i-1/2}^n Q_{i-1/2}^n \right) = 0 \,, \end{aligned} \tag{3.40}$$

From Equation (3.40) the variation of the solid volume $(\Delta V_b)_i^{n+1} = (V_b)_i^{n+1} - (V_b)_i^n$ for all the cells of the domain is, then, calculated:

$$\begin{aligned} (V_b)_i^{n+1} = & \frac{(1-\vartheta)\,\Delta t}{i_c C_i^n - C_b} \left(C_{i+1/2}^n Q_{i+1/2}^n - C_{i-1/2}^n Q_{i-1/2}^n \right) - \frac{i_c C_i^{n-1}}{i_c C_i^n - C_b} (V_t)_i^n + \\ & + \frac{i_c C_i^{n-1} - C_b}{i_c C_i^n - C_b} (V_b)_i^n + \frac{\vartheta \Delta t}{i_c C_i^n - C_b} \left(C_{i+1/2}^n Q_{i+1/2}^{n+1} - C_{i-1/2}^n Q_{i-1/2}^{n+1} \right) + \\ & + \frac{i_c C_i^n}{i_c C_i^n - C_b} (V_t)_i^{n+1} \end{aligned} \tag{3.41}$$

Since the values of the solid concentration C at the integer nodes i are not defined, they are computed, similarly to the area $A_{i+1/2}$, through a quadratic interpolation on an upwind-biased stencil or an upwind-weighted interpolation of the form $C_i = pC_{i-1/2} + (1-p)C_{i+1/2}$.

Finally, the volume $(\Delta V_b)_i^{n+1}$ is redistributed through the redistribution formula explained in the Section 1.3.3. The solution procedure is fully explained in the following section.

3.3 Solution Procedure

The aim is to calculate the following vectors of the unknowns in each node, as shown in Figure 3.3, at the time $n+1$:

- the free surface elevation $\boldsymbol{\eta}^{n+1}$,
- the discharge $\mathbf{Q}^{n+1}$,
- the bed volume variation $\Delta\mathbf{V_b}^{n+1}$.

The initial conditions are:

- the free surface elevation $\boldsymbol{\eta}^0$
- the discharge $\mathbf{Q}^0$,
- the sediment concentration $\mathbf{C}^0$,
- the matrix $\mathbf{z_b}^0$ of the unknown $(z_b)_{i,j}^0$ as shown in Figure 3.3.

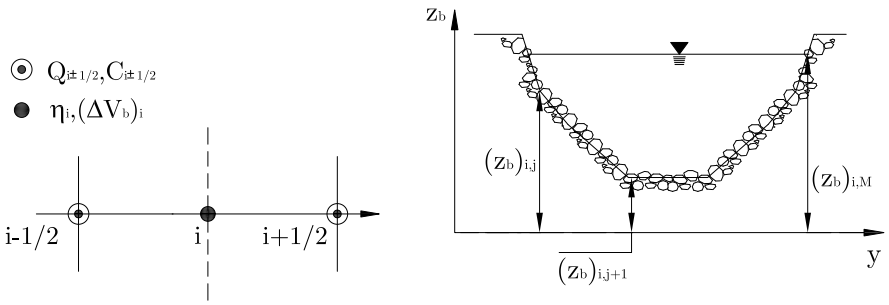

(a) Position of the unknowns on the computational Grid

(b) Discretization of the bathymetry

Figure 3.3: *Sketch of the discrete variables*

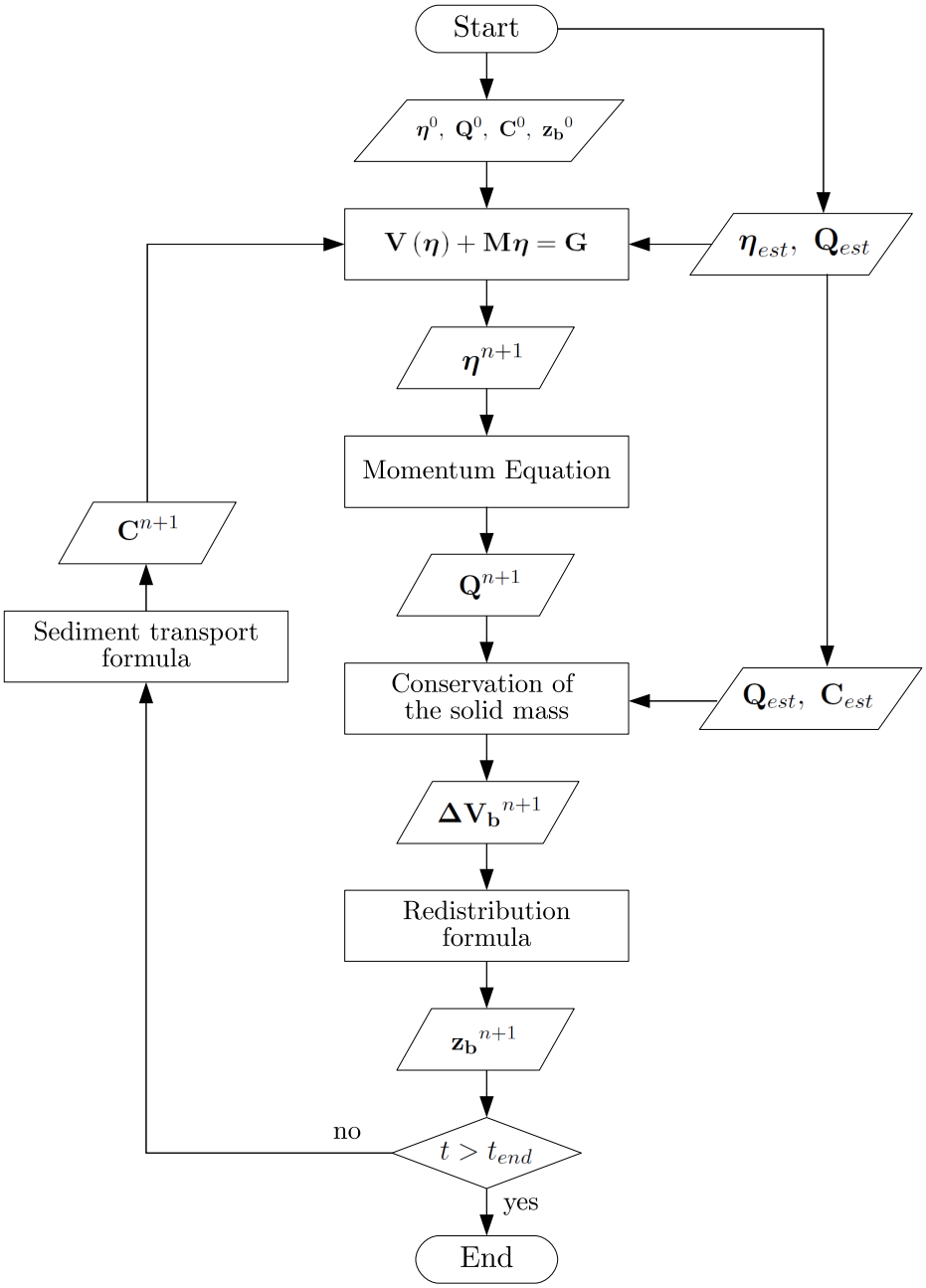

Figure 3.4: *Flow chart of the solution procedure*

If no values of sediment concentration is known, the initial condition $\mathbf{C}^0$ is calculated through one of the sediment transport formula reported in the Section 1.3 in function of the initial wetted area $A^0_{i+1/2}$, the total discharge $Q^0_{1+1/2}$ and

the sediment properties. Since the sediment concentration C^0 is defined at the node $i+1/2$, the area $A^0_{i+1/2}$ has to be calculated starting from the initial free surface η^0_i and the bed elevation $(z_b)^0_{i,j}$ through a cubic o linear interpolation.

After assigning initial and boundary conditions, the System (3.37) can be solved with appropriate boundary conditions as shown in the flow chart, Figure 3.4. The upstream boundary conditions affect the first computational cell, while the downstream boundary conditions the last cell N:

Upstream subcritical condition In the case of fixed bed the characteristic analysis shows that one boundary condition is necessary. In the case of mobile-mod another condition should be specified, but in the Equation (3.31) only the total discharge $Q_{1/2} = Q_{est}$ is imposed and the flux $Q_{3/2}$ is expressed by the momentum equation, Equation (3.21) or Equation (3.28):

$$(V_t)^{n+1}_1 - \mathcal{K}^n_2 \eta^{n+1}_1 + \mathcal{K}^n_2 \eta^{n+1}_2 = \widehat{\mathcal{G}}^n_1, \tag{3.42}$$

with

$$\begin{aligned} \widehat{\mathcal{G}}^n_1 = (V_t)^n_1 - (1-\vartheta)\Delta t \left(Q^n_{3/2} - Q^n_{ext}\right) + \\ -\vartheta \Delta t \left(\frac{\mathcal{F}^{E,SL}_{3/2}}{1 + C^n_{1+1/2}\Delta_s + \alpha^n_{1+1/2}\vartheta\Delta t} - Q^{n+1}_{est} \right). \end{aligned} \tag{3.43}$$

In the semi-Lagrangian approach, if the foot of the semi-Lagrangian trajectory is located outside the computational domain, the explicit terms $\mathcal{F}^{SL}$ are evaluated by setting all the quantities upstream the boundary equal to the values in the first computational cell. It can be noticed that the solid concentration C is not herein imposed as boundary condition, but the hydrograph of the sediment-water discharge Q_{est} is the only information required. In fact, the concentration C_{est} is required in the conservation equation of the solid mass as boundary condition.

Downstream subcritical conditions Similarly one boundary condition is required and the free surface elevation η is assigned. In this case the Equation (3.34) for the last cell N becomes:

$$(V_t)^{n+1}_N + \mathcal{K}^n_{N-1} \eta^{n+1}_{N-1} + \mathcal{K}^n_N \eta^{n+1}_N = \widehat{\mathcal{G}}^n_N, \tag{3.44}$$

with

$$\widehat{\mathcal{G}}_N^n = -\mathcal{K}_{N+1}^n \eta_{ext}^{n+1} + (V_t)_N^n - (1-\vartheta)\Delta t \left(Q_{N+1/2}^n - Q_{N-1/2}^n\right) + \\ -\vartheta\Delta t \left(\frac{\mathcal{F}_{N+1/2}^{E,SL}}{1 + C_{N+1/2}^n \Delta_s + \alpha_{N+1/2}^n \vartheta \Delta t} - \frac{\mathcal{F}_{N-1/2}^{E,SL}}{1 + C_{N-1/2}^n \Delta_s + \alpha_{N-1/2}^n \vartheta \Delta t} \right). \tag{3.45}$$

After solving the System (3.37), the vector $\mathbf{Q}^{n+1}$ of the unknowns $Q_{i+1/2}^{n+1}$ for $i = 1, \ldots, N$ is calculated using Equation (3.21) or Equation (3.28) and the vector $\mathbf{\Delta V_b}^{n+1}$ of the unknowns $(\Delta V_b)_i^{n+1}$ is updated through Equation (3.41). At the upstream boundary, two conditions are necessary: the total discharge Q_{est} and the sediment concentration C_{est}. If no values of the solid concentration at the upstream boundary are known, the solid concentration at the equilibrium can be calculated and imposed as boundary condition.

Then, the evolution of the section shape is calculated as shown in the flow chapter (Figure 3.4). In fact, the bed elevation $(z_b)_{i,j}^{n+1}$ depends on the volume $(V_b)_i^{n+1}$ through a redistribution formula as shown in the Section 1.3.3. Firstly, the coefficient k is determined by integrating Equation (1.95) between $\left[x_{i-1/2}, x_{i+1/2}\right]$:

$$k = \frac{\displaystyle\int_{x_{i-1/2}}^{x_{i+1/2}} \frac{\partial A_b}{\partial t} dx}{\displaystyle\int_{x_{i-1/2}}^{x_{i+1/2}} \int_l^r \frac{\partial}{\partial t} h^{1/2} dy dx}. \tag{3.46}$$

To calculate the denominator, the composite trapezoidal rule is used and the redistribution coefficient k_i for the section i results:

$$k_i^{n+1} = \frac{2\left(\Delta V_b\right)_i^{n+1}}{\sum_{j=1}^{M-1}\left(y_{j+1} - y_j\right)\left(\sqrt{\hat{h}_{i,j+1}^{n+1}} + \sqrt{\hat{h}_{i,j}^{n+1}}\right)\Delta x_i}, \tag{3.47}$$

with

$$\hat{h}_{i,j}^{n+1} = \eta_i^{n+1} - (z_b)_{i,j}^n. \tag{3.48}$$

The initial bed level $(z_b)_{i,j}^0$ is assigned. Since k_i^{n+1} is known, the bed elevation $(z_b)_i^{n+1}$ is:

$$(z_b)_i^{n+1} = k_i^{n+1}\sqrt{\hat{h}_{i,j}^{n+1}} + (z_b)_i^n \,. \tag{3.49}$$

Finally, the sediment concentration $C_{i-1/2}^{n+1}$ is calculated in function of $Q_{i-1/2}^{n+1}$ and $A_{i-1/2}^{n+1}$ through a sediment transport formula and the loop is executed until the final time t_{end}.

3.4 Stability and Efficiency of the Two Schemes

The computational cost of a scheme is a critical point in realistic applications. For example, fast simulations are mandatory for hazard management and very long-term simulations are needed to perform erosion/deposition simulations. Last, but not least, simulation of real river flows are very often performed by engineers who only have access to limited computational power. The efficiency of the two schemes are well described by Rosatti et al. [45].

The advantage of this solution procedure is, firstly, the higher efficiency with respect standard explicit schemes [35]. These schemes should respect the CFL condition and their stability depend on the Courant number:

$$C = \frac{max\left(\lambda\right)\Delta t}{\Delta x} \tag{3.50}$$

where λ is the generic eigenvalue of the hyperbolic system.

Two different Courant number are introduced in this work in order to evidence the efficiency of the schemes: the Courant number based on the celerity $C_{cel} = \left(|\alpha_{u^2} U| + \sqrt{gh}\right)\Delta t/\Delta x$ and the Courant number based on the velocity $C_{vel} = |\alpha_{u^2} U|\,\Delta t/\Delta x$.

The Eulerian upwind-based scheme for momentum advection was found to be stable under the condition $C_{vel} < 1$ in applications with smooth solutions, steady and quasi-steady shocks. For the simulation of dam-break waves, also a CFL condition $C_{cel} < 1$ must be guaranteed as shown by Rosatti et al. [45].

Instead, in the linear case, the semi-Lagrangian formulation is unconditionally stable [16]. In the non-linear case, as reported by Rosatti et al. [45], the stability can only be checked empirically. In test cases, no restriction seems to limit the time step and the semi-Lagrangian discretization was shown to be stable and accurate over a wide range of velocity and celerity Courant numbers, but to produce inaccurate results in presence of strong unsteady shocks.

Since, as shown in the Section 3.3, the solution of a nonlinear system at each time step is required, some consideration on this computational cost can be done. It should be remarked that, in order to guarantee mass conservation, the solution of a scalar nonlinear equation per node is necessary also for an explicit time discretization because the volume V_t is a non-linear function of the free surface elevation η. Thus, the only extra cost with respect to an explicit scheme solving the same equations is the solution of a tridiagonal linear system, Equation (3.34), multiplied by the number of fixed point iterations. The number of iteration is usually low and was found to be 6 on average in all tests with complex sections. Finally the cost to solve the tridiagonal system is similar to

an explicit scheme of comparable accuracy as shown by Rosatti et al. [45]. In conclusion, a minor computational cost is expected also for Courant number not much larger then one.

Chapter 4

Test Cases

Since a complete set of tests in various regimes of fixed bed flows are presented in [45], only test cases on mobile bed are herein presented. The numerical solutions of two models, EMP and QTP, are successively compared in order to highlight the significant differences arising in the case of high sediment concentration. In all the following test cases the θ parameter is set to 0.6 and the time discretization step Δt it is chosen so as to yield an assigned value of the maximum Courant number based on the velocity $C_{vel} = max\,|U|\,\Delta t/\Delta x$ and the maximum value of the Courant number based on the celerity $C_{cel} = max(|U| + \sqrt{gh})\Delta t/\Delta x$ is evaluated. Courant numbers larger than one show, as expected, a major efficient of this solution procedure with respect to the explicit scheme. The concentration under the bed level C_b is generally equal to 0.65. Both the two scheme, the semi-Lagrangian and the upwind Eulerian discretization, were tested but only the numerical results of the semi-Lagrangian scheme are reported.

4.1 Comparison with the Solutions of the Simplified Equation

In this test, the numerical solution of both the QTP and EMP systems are compared with the solution of the simplified equation, Equation (2.53), reported in the Section 2.2 and Section 2.3. A channel with rectangular cross section and unit width is considered. The friction term is, for simplicity, set to zero. The initial bathymetry is given by:

$$z_b\,(x,0) = \begin{cases} 0.2\sin^2\left(\dfrac{x-200}{400}\pi\right) & \text{if } 220\ m < x < 400\ m \\ 0 & \text{otherwise} \end{cases}$$

The channel is 5000 m long and discretized with 2000 cells. Thanks to

the semi-Lagrangian scheme a large time step ($\Delta t = 32\ s$) that corresponds to Courant number C_{vel} = equal to 1.3 can be used. The maximum Courant number based on the celerity C_{cel} is equal to 288. The solid concentration is written as a function of the Froude number $Fr = \sqrt{gh}/U$ as $C = \beta Fr^2$. The coefficient for the closure formula, the initial and boundary conditions are reported in Table 4.1.

Test case	η $[m]$	Q $[m^3 s^{-1}]$	Fr $[-]$	β $[-]$	ϵ $[-]$
a)	50	5	0.0045	200	0.006
b)	50	5	0.0045	2000	0.06

Table 4.1: *Initial and boundary conditions*

The flow can be considered quasi-steady. If the Froude number tends to zero, the simplified model for the bed evolution is valid. Indeed, if ϵ is negligible, test case (a) in Table 4.1, Equation (2.53) reduces to the simplified equation proposed by Hudson and Sweby [29]. The numerical solution of both the models, QTP and EMP, strictly agree, as shown in Figure 4.1 (a), with the simplified solution, Equation (2.53), for the ϵ rate negligible.

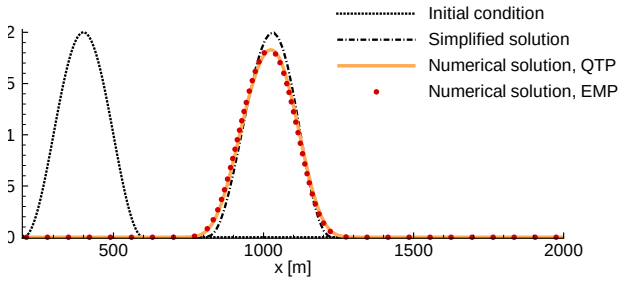

(a) $\epsilon = 0.006$, at time $t = 300000\ s$

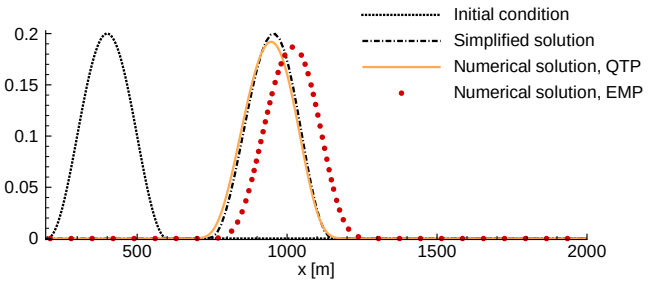

(b) $\epsilon = 0.06$, at time $t = 30000\ s$

Figure 4.1: *Comparison between the approximated and the numerical solutions.*

In the case (b), the solution of the simplified equation for the ϵ rate not neg-

ligible agree with the numerical solution of the QTP model, but not with the numerical solution of the EMP, Figure 4.1 (b). The parameter ϵ has increased ($\epsilon = 0.062$) and, if the two numerical solutions, QTP system and EMP system, are compared, the difference in the propagation velocity of the bed perturbation is evident. The shape of the numerical solution is slightly different from the solution of the simplified model because of the assumptions in Equation (2.15). Nevertheless, the numerical solution of the QTP system shows a lower propagation velocity of the finite perturbation of the bed with respect the model with ϵ set to zero. In conclusion, if the parameter ϵ is not negligible a fully coupled model has to be considered because differences due to the neglect of the terms multiplied by epsilon can be accumulative. These differences become evident for values of concentration C higher then 6.5 ‰.

4.2 Impact of Model Simplifications

In order to asses the performance of the proposed method in the case of bathymetry changes and underline the effect of the simplifications in the model equations during the transient state and with high concentration, three different test cases are presented: a channel with a width variation of the cross section, a local depth variation and a sediment wave in a channel with an arbitrary cross section.

4.2.1 A Non Prismatic Channel

The scheme has already tested in the case of non prismatic channel, fixed bed and supercritical condition by Rosatti et al. [45]. In the case of mobile bed, experimental data are not available. However, a non prismatic channel of 2000 m with roughness coefficient k_s constant, is herein considered. The channel is discretized with 201 cells and the space step is 14 m when the width is 50 m and 10 m otherwise. The flow becomes supercritical in correspondence to the channel constriction. Firstly, the steady-state in the case of fixed bed is calculated, the upstream discharge Q is 473 $m^3 s^{-1}$ and the free surface elevation at the downstream boundary is 10m. The geometry of the channel and the initial condition are shown in Figure 4.2 and Figure 4.3 while the bed slope is 1.2 ‰. In this case the time step should be reduced and the semi-implicit discretization used due to the high values of concentration and Froude number during the transient state where the width decreases. The Courant number based on the velocity is set equal to 0.4, but the maximum Courant number based on the celerity is still greater then one ($C_{cel} = 1.2$).

The sediment concentration is calculated by means of Meyer-Peter Müller relation with $d = 1$ cm. During the transient state and when the concentration

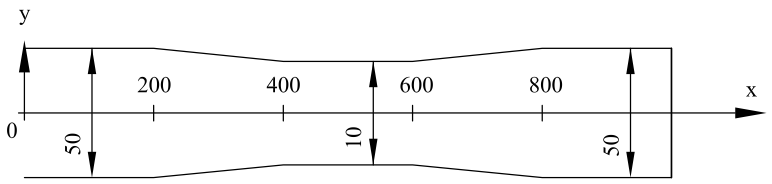

Figure 4.2: *Geometry of the non prismatic channel*

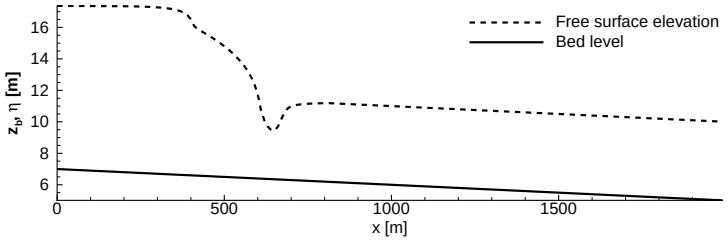

(a) Bed and water elevation

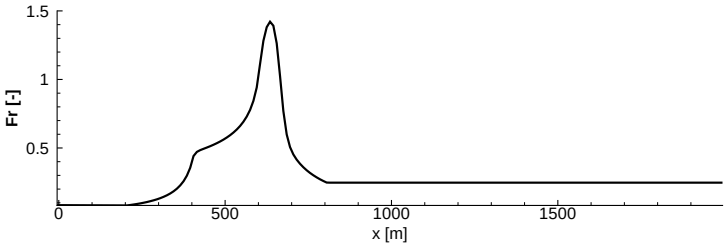

(b) Froude number

Figure 4.3: *Initial conditions.*

are higher, the differences between the QTP model and EMP model are evident as shown in Figure 4.4. The stationary state of the two systems is generally different with respect the same initial and boundary conditions and the difference is mainly due to the term $(1 + C\Delta)$ in Equation(3.2):

$$gA\,(1 + C\Delta)\,\frac{\partial z_b}{\partial x} = -\alpha Q. \tag{4.1}$$

In this test case the concentration is close to zero where the section is constant and differences in the steady state are not relevant. Instead of the difference due to EMP model can transiently be significant where the section changes and

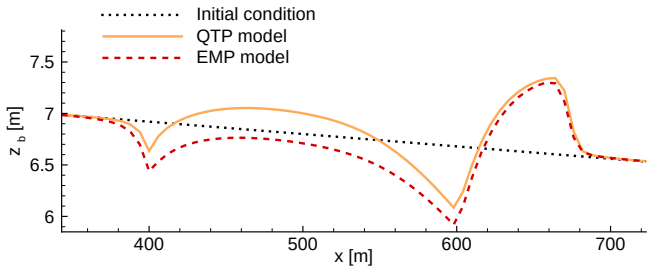

(a) Bed elevation

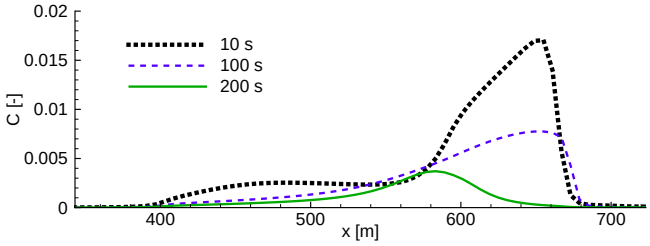

(b) Concentration

Figure 4.4: *Comparison between the QTP model and EMP model during the transient state* ($t = 200\ s$).

the concentration C increases.

4.2.2 Depth Variation

The channel is $2000\,m$ long and $3\,m$ width, the initial water depth is $3\,m$ and the discharge $27.6\,m^3s^{-1}$. The Strickler coefficient k_s is $30\,m^{1/3}s^{-1}$. The channel is discretized with 201 cells with Δx equal to $10\,m$. The regime is subcritical and the concentration is higher then 6 ‰ as shown in Figure 4.5. The bed slope i changes between $1000\,m$ and $1150\,m$ as:

$$z_b\,(x,0) = \begin{cases} 10\% & \text{if } 1000\ m < x < 1020\,m \text{ and } 1130\,m < x < 1150\,m \\ 1\% & \text{otherwise} \end{cases}$$

The initial condition is the steady state for the fixed bed case. As in the previous case, it is possible to observe, as during the transient state where the concentration are about 1% (Figure 4.6), the river bed evolves in a different way (Figure 4.5) depending on the model's choice. The closure relation is the Meyer-Peter Müller formula and the diameter d is equal to $0.4\,mm$.

The Courant number based on the velocity is 1.2 and based on the celerity

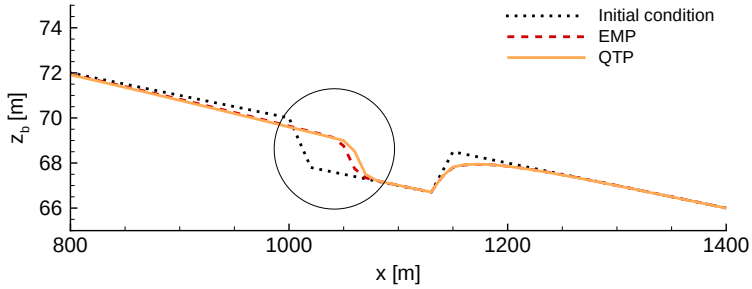

(a) Bed elevation

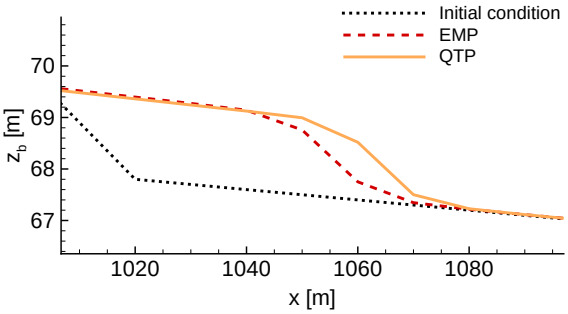

(b) Zoom of the bed elevation

Figure 4.5: *Comparison between the QTP model and EMP model during the transient state* ($t = 150\ s$).

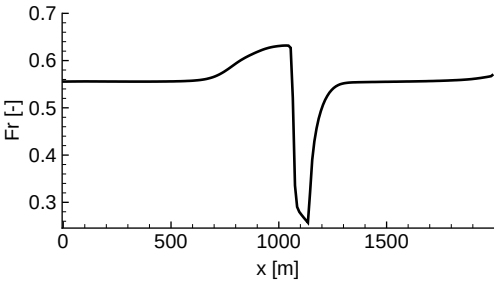

(a) Froude

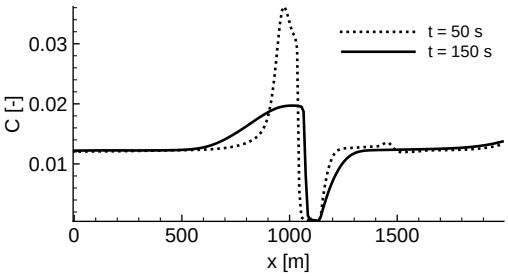

(b) Concentration

Figure 4.6: *Froude number and concentration at* $t = 150\ s$.

is 3.1.

4.2.3 Arbitrary Cross Section

A channel with an arbitrary section is considered. A flood and sediment wave propagating in the channel are considered in order to test the non-linear relation between the free-surface elevation and the area of the section. The importance of considering this relation is already demonstrated in Rosatti et al. [45].

The coordinates of the first section are reported in Table 4.2, while the bed slope is 0.1 ‰at the time $t = 0\ s$ as shown in Figure 4.8. The channel is 1500 m long and discretized with 151 cells ($\Delta x = 10\ m$). The Chézy coefficient is 20 $m^{1/2}s^{-1}$ in the flood areas and 30 $m^{1/2}s^{-1}$.

y $[m]$	z_b $[m]$	y $[m]$	z_b $[m]$
0.000	60.199	23.000	49.999
0.250	59.699	24.000	50.249
0.500	59.199	25.000	50.749
0.750	58.699	26.000	51.749
1.000	58.199	27.000	53.749
2.000	57.199	28.000	54.749
3.000	56.699	29.000	55.249
7.000	56.299	30.000	55.499
8.000	56.199	31.000	55.599
9.000	56.099	32.000	55.699
10.000	55.999	33.000	55.799
11.000	55.899	34.000	55.899
12.000	55.799	35.000	55.999
13.000	55.699	36.000	56.099
14.000	55.599	37.000	56.199
15.000	55.499	38.000	56.299
16.000	55.249	42.000	56.699
17.000	54.749	43.000	57.199
18.000	53.749	44.000	58.199
19.000	51.749	44.250	58.699
20.000	50.749	44.500	59.199
21.000	50.249	44.750	59.699
22.000	49.999	45.000	60.199

Table 4.2: *Coordinates of the first section at $x = 0\ m$.*

The initial discharge is Q equal to 6.95 m^3s^{-1} and the initial depth h is 3 m. The Meyer-Peter Müller relation is used with diameter of 0.4 mm . Initially, the concentration C along the channel is at the equilibrium with the hydrodynamic and is equal to 10^{-6}. Firstly, the solid concentration increases until the 1% in 1 h during the flood and, after, decreases to the initial value. In the meanwhile, the flood wave imposed at the upper boundary lasts 200 hours and the peak discharge is 120 m^3s^{-1}. The sediment concentration C at the upstream boundary and the water elevation η at the downstream change during the simulation as shown in Table 4.3.

During the simulation the maximum Courant number based on the velocity

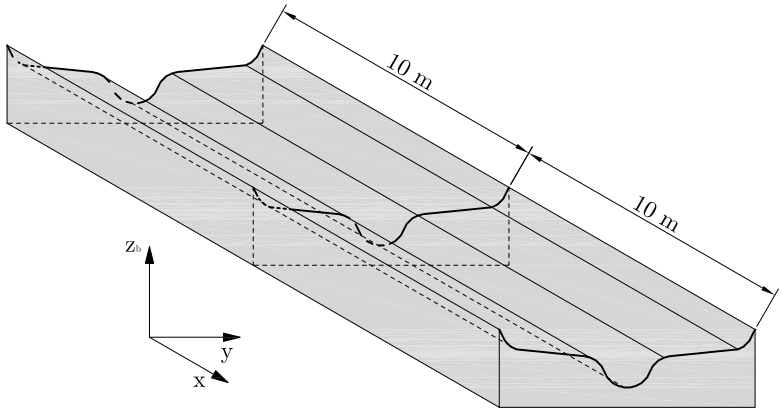

Figure 4.7: *Bathymetry at time $t = 0$ s.*

time $[s]$	Q $[m^3/s]$	time $[-]$	C $[m]$	time $[-]$	η $[m]$
0	6.950	0	10^{-6}	300	51.999
36000	120.000	360	10^{-2}	45000	56.999
72000	6.950	720	10^{-5}	150000	51.999
∞	6.950	∞	10^{-6}	∞	51.999

Table 4.3: *Upstream boundary conditions.*

is set equal to 2.2 ($C_{cel} = 17.4$). The scheme used is the semi-Lagrangian formulation. The flooding of the 14^{th} section ($x = 130$ m) is presented in Figure 4.8.

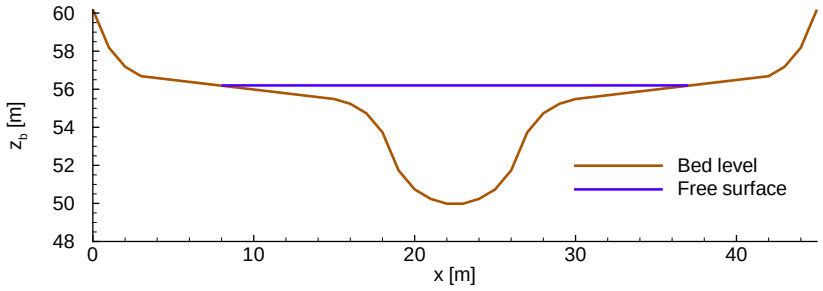

Figure 4.8: *Computed free-surface elevation at the time $t = 20$ h in the 14^{th} section ($x = 130$ m).*

Due to the increasing of solid concentration not only differences in the bed

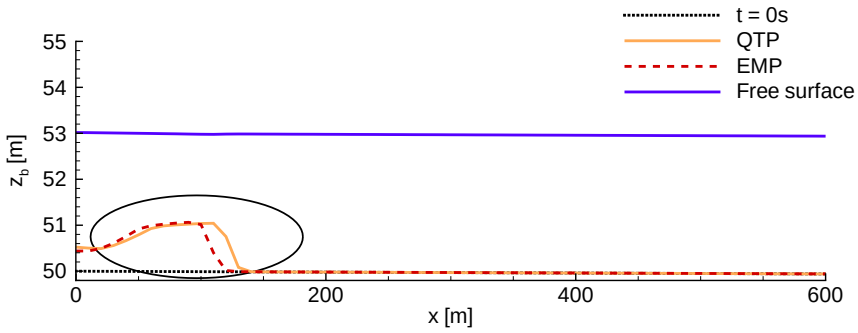

(a) Bed elevation and Free surface

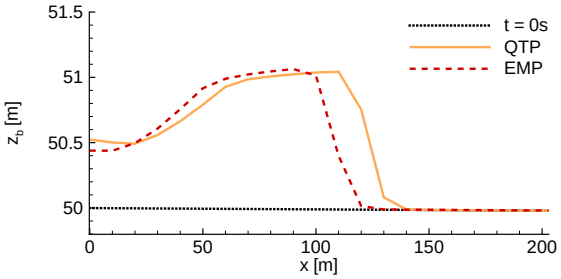

(b) Zoom of the bed elevation

Figure 4.9: *Bed evolution at the time $t = 200\ h$ calculated with the QTP model and the EMP model.*

level can be observed between the two models (Figure 4.9), but also the section shape differently evolves during the transient state (Figure 4.10). The formula used in order to redistribute the sediment is a function of the depth h as reported in the Section 1.3.3. Consequently, in the same section $x = 50\ m$ (Figure 4.10) the aggrading sediment process corresponding to the EMP numerical solution disagrees from the QTP model. As in the previous test cases, the bed evolution is different and depends on the model's choice and the front of sediment travels with different velocities depending on the model's choice. In Figures 4.9 and 4.10, the bed levels are plotted at the time $t = 200\ h$.

4.3 Aggradation Test Case

The model is applied to the flume experiment of Soni et al. [49] extensively studied by Cao et al. [13] and Kassem and Chaudry [31] in order to verify the model. The experimental flume was $0.2\ m$ wide and $30\ m$ long. The closure

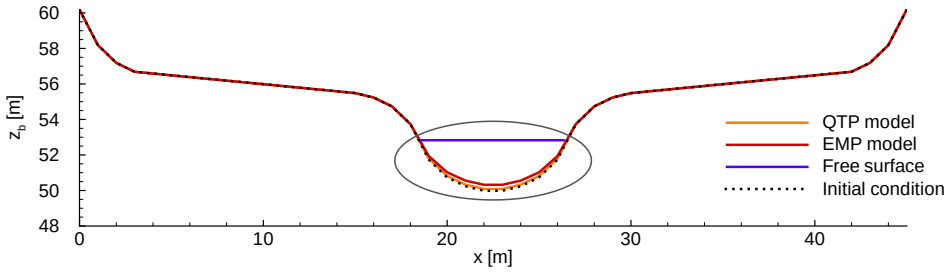

(a) Bed elevation and Free surface

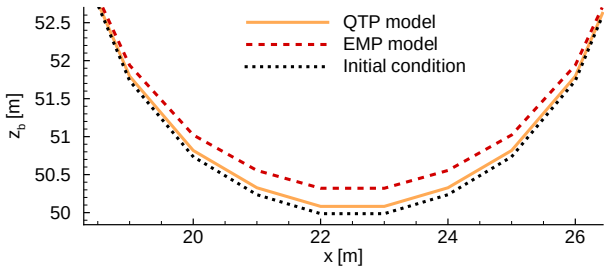

(b) Zoom of the bed elevation

Figure 4.10: *Section shape evolution ($x = 130\ m$) at the time $t = 200\ h$ calculated with the QTP model and the EMP model.*

formula is a monomial relation:

$$Q_s = \delta U^m, \tag{4.2}$$

with δ and α empirical coefficients, Table 4.4. The numerical solution herein implemented required the solid concentration C that is simply the rate between the solid discharge Q_s and discharge of the mixture Q. The values of δ and m for the sediment size used in the study [31] are respectively $1.45\ 10^{-03}$ and 5. The Chèzy coefficient χ is equal to $29.69\ m^{1/2}s^{-1}$ and the concentration of the sediment under the bed level C_b is 0.6. The values of the water depth h, the liquid discharges Q_l, the bed slope i and the increment of solid discharge are reported in Table 4.4.

h $[m]$	Q_l $[m^2 s]$	m $[-]$	δ $[s^4 m^{-2}]$	i $[-]$	χ $[m^{1/2} s^{-1}]$
0.05	$4.000\ 10^{-03}$	5	$1.45\ 10^{-03}$	$3.56\ 10^{-03}$	$29.69\ m^{1/2}s{-}1$

Table 4.4: *Experimental test [49]*

The initial data and the boundary conditions are reported in Table 4.5. For the numerical model two boundary conditions are specified at the upstream and one at the downstream. The total discharge at the upstream boundary is calculated as the sum of the liquid discharge Q_l and the solid discharge Q_s. At the downstream the free surface η is assigned constant.

Initial Condition		Upper Condition		Lower Condition
h	Q	Q	C	η
$[m]$	$[m^2 s]$	$[m^2 s]$	$[-]$	$[m]$
0.05	$4.003\,10^{-03}$	$4.0148\,10^{-03}$	$3.6983\,10^{-03}$	0.05

Table 4.5: *Numerical simulation: initial and boundary conditions*

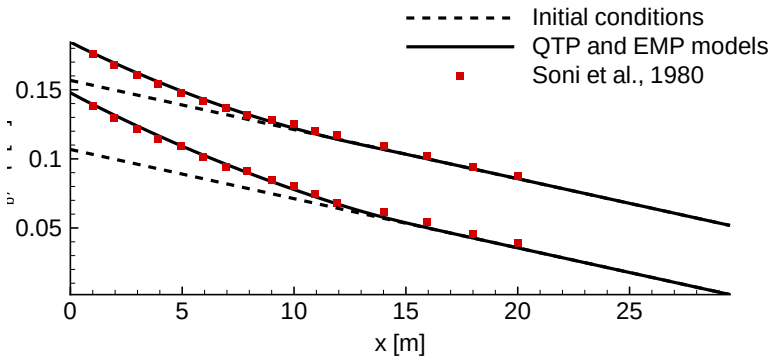

Figure 4.11: *Computed bed and water surface profiles compared to data of Soni et al. [49] at the time $t = 40\,min$. The dashed lines are initial bed and water surface profiles.*

The channel is discretized with 60 cells. The efficiency of the semi-Lagrangian scheme let to use a larger time step with respect [13] ($\Delta t = 0.6\,s$) and [31] where the Courant number is set to 0.65. In this scheme the time step is chosen equal to 1.6 s that corresponds to Courant number $C_{vel} = \left(|U| + \sqrt{gh}\right)/\Delta x$ equal to 3.5. In fact, the scheme is stable as shown in [16, 25] and no restrictions significantly limit the time step.

Finally, the calculated profiles strongly agree with the experimental data as shown in Figure 4.11. The QTP model gives the same results of the EMP model because the solid concentration are low as it is expected from the non-dimensional analysis. No experimental data are available in order to validate the models for higher concentration.

4.4 Conclusions

In natural river, discharge and geometry changes can be relevant. Consequently, the simplification of the mathematical model can lead to inaccuracy that could be cumulative with the increasing of the simulation time. The numerical tests clearly demonstrate as, for concentration C higher then C_{QTP}, $6.5‰ \div 1\%$, the solutions of the two models disagree. Otherwise, for lower concentration, the two solution are equivalent consistently with the non-dimensional analysis. The value of ϵ suggested in Section 2.3 is, then, confirmed by the numerical results. The solid concentration becomes usually higher in correspondence of transient flows and the use of the QTP model become essential. Besides, the model was tested for non prismatic channel, width and bed elevation changes and irregular section. The numerical results were compared with an analytical solution and with experimental data. Finally, with the proposed numerical method, the quasi two-phase models can be used without any loss in efficiency with respect to the essentially mono-phase or fixed bed case. In the following part only the EMP model is considered and the non-uniform sediment transport is analyzed only in the case of concentration lower then the C_{QTP} value.

Part II

Non Uniform Sediment Transport

Chapter 5

Mathematical Description of the Non-Uniform Sediment Transport

River-beds are usually composed of non-uniform sediment mixtures and the prediction of natural river processes is, consequently, complex. In the second part of this work, the shallow water equations are integrated with the description of the sediment transport with non-uniform grain-size. Only the EMP model is considered (Chapter 2) and, consequently, the range of validity of this model should be respected.

5.1 The Bed Material Fraction Approach

Firstly, a briefly review on the transport of sediment mixture is undertaken to highlight the mechanism of grain sorting. In particular, a model based on the division of the grain size distribution curve in a discrete number of classes is herein explained. Even though the literature has pointed out the limits of using this approach, this is the most commonly used method in numerical models [12, 34, 55, 56, 58].

5.1.1 The Grain-Size Distribution Curve

In a mixture of water and sediment with non-uniform grain-size, the particle size gradation of the bed surface is described by using a discrete number of classes. To assess the distribution of the granular material on the bed surface, sieve analysis is generally used. The availability factor of each class p_j is the percentage of the grain-size class j. The particle diameter is usually log-normally

distributed, but can be converted in a symmetrical Gaussian distribution by a logarithmic transformation. Wu et al. [56] plotted the particle diameters on a logarithmic scale against the availability factor of each grain class. These curves, Figure 7.3 (b) and (d), result bell-shaped with respect to the frequency distribution displayed in Figure 7.3 (a) and (c). The mass balance is, then, written for each class in which the grain-size distribution curve is divided.

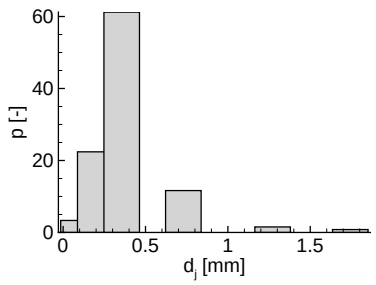

(a) Percentage of grain size class j against diameters

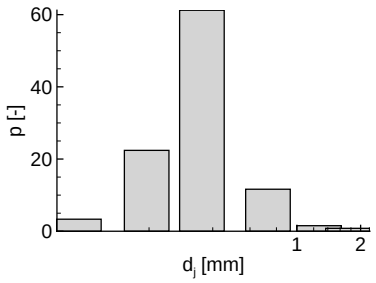

(b) Log-normal distribution

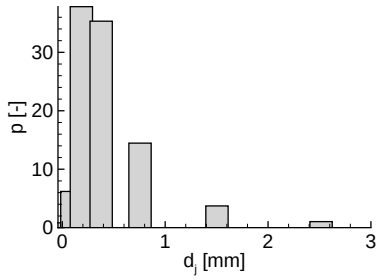

(c) Percentage of grain size class j against diameters

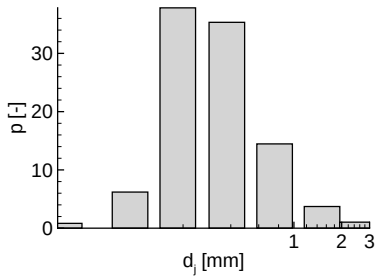

(d) Log-normal distribution

Figure 5.1: *Examples of frequency histogram reported by [56] for the Rio Grande, New Mexico.*

5.1.2 Continuity Equations for Each Sediment Class

In these models, the concept of mixing layer is essential [28]. Deeply buried grains have minimal probability of entrainment into motion and only grains in the mixing layer can be eroded. The sediment transport capacity and the mass balances are calculated for each class of the grain size distribution curve by considering the mixing layer thickness as shown in Figure 7.3. In particular, the curve is divided in m classes.

Under the hypothesis of EMP model and in agreement with the derivation

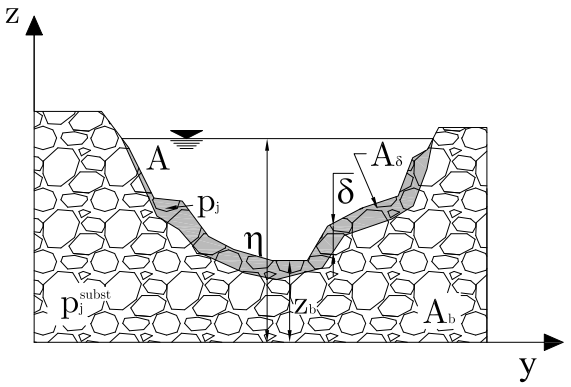

Figure 5.2: *Sketch of a generic cross section and of the main model variable in the case of non-uniform sediment*

in the Chapter 2, two systems of m equations of mass conservation, for both the mixing layer and the substrate, are written:

$$C_b \frac{\partial}{\partial t}\left(p_j A_\delta\right) + \frac{\partial \left(Q_s\right)_j}{\partial x} + C_b \bar{p}_j \frac{\partial}{\partial t}\left(A_b - A_\delta\right) = 0 \qquad j = 1...m, \tag{5.1}$$

$$C_b \frac{\partial}{\partial t}\left[p_j^{subst}\left(A_b - A_\delta\right)\right] = C_b \bar{p}_j \frac{\partial}{\partial t}\left(A_b - A_\delta\right) \qquad j = 1...m, \tag{5.2}$$

where the unknowns are the availability factors p_j and p_j^{subst}, while A_δ, the area of the mixing layer, is calculated through a closure formula. The availability factors $\bar{p}_j$ are equal to the value p_j in the mixing layer in the case of bed aggradations and to the value of the availability factor p_j^{subst} of the substrate in the case of bed degradations. The mixing layer thickness is usually related to the sand dunes height as [5, 52]:

$$\delta = \max(0.5\Delta_D, 2d_m), \tag{5.3}$$

where

$$\frac{\Delta_D}{h} = 0.11\left(\frac{d_{50}}{h}\right)^{0.3}\left(1 - e^{-0.5T}\right)(25 - T) \tag{5.4}$$

and

$$T = \frac{u_*^2 - u_{*c}^2}{u_{*c}^2}, \tag{5.5}$$

$$u_* = U\frac{\sqrt{g}}{\chi}. \tag{5.6}$$

Alternatively, the thickness δ can be related to the specific diameter d_{90} [8] as:

$$\delta \simeq 2 \div 3 d_{90}. \tag{5.7}$$

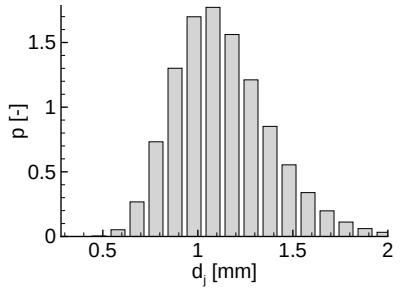

(a) Availability factor of each sediment class in the mixing layer

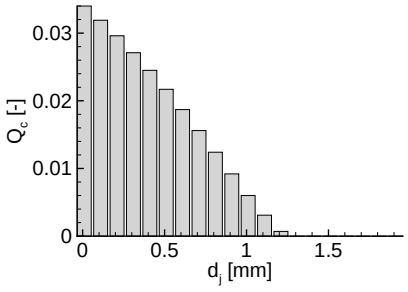

(b) Sediment transport capacity calculated through a transport formula

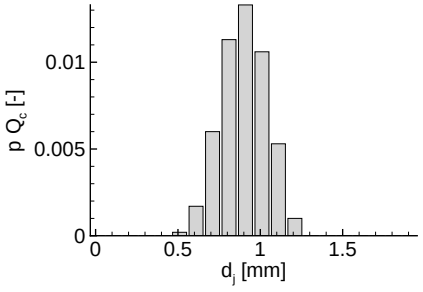

(c) Solid concentration for each class of sediment that is equal to the product between the availability factor p_j and the transport capacity $(Q_c)_j$

Figure 5.3: *Sediment concentration of each grain-size fraction j*

In order to calculate the solid discharge $(Q_s)_j$ or, equivalently, the sediment concentration C_j the Einstein theory is usually used. The solid discharge of each grain-size fraction j is assumed dependent on the number of grains present in the bed river as shown in Figure 5.3:

$$(Q_s)_j = p_j \, (Q_c)_j \tag{5.8}$$

where $(Q_c)_j$ is the sediment capacity, i.e.the solid discharge in the case of steady flow and uniform grain size material equal to d_j. The basic assumption of classical non-uniform models is that interactions among the moving sediment particles

are negligible. Each size class of the moving sediment mixture is assumed to have the same transport behavior as if there were uniform sediment and the sediment capacity $(Q_c)_j$ can be calculated through a sediment transport formula. Figure 5.3 (c) represents the distribution of the solid discharge of each grain-size class and, then, the distribution of the sediment transported by the flow. It can be noticed that the two grain-size distributions, in the river-bed (Figure 5.3 (a)) and (Figure 5.3 (c)) are different as reported by Armanini [6]. Consequently, the sediment fraction p_{Tj}, transported by the flow, differs from the sediment fraction p_j in the mixing layer:

$$p_{Tj} = \frac{p_j \left(Q_c\right)_j}{\sum_j p_j \left(Q_c\right)_j}. \tag{5.9}$$

The two systems of m equations, Equations (5.1) and (5.2), with the EMP model, Equations (3.8)-(3.10), can be numerically solved as reported in the Chapter 6 in order to model the river processes. The difference is that, in the non-uniform model, the solid discharge is the sum of all class contributions:

$$Q_s = \sum_{j=1}^{m} \left[p_j \left(Q_c\right)_j \right] \tag{5.10}$$

where m is the number of classes in which the curve is divided.

The two main limitations of using Einstein theory in order to calculate the solid discharge Q_s are:

- the unsteadiness is neglected and the hypothesis is based on the local equilibrium conditions;
- the hiding effects are not taken into account.

Finally, it should be noticed that, in the EMP model, the solid discharge Q_s is considered equal to $\alpha_{u^2} CQ$. Then, the Equations (5.1) and (5.10) are rewritten:

$$C_b \frac{\partial}{\partial t} \left(p_j A_\delta\right) + \frac{\partial}{\partial x} \left(\alpha_{u^2} C_j Q\right) + C_b \bar{p}_j \frac{\partial}{\partial t} \left(A_b - A_\delta\right) = 0 \qquad j = 1...m, \tag{5.11}$$

$$C = \sum_{j=1}^{m} \left[p_j \left(C_c\right)_j \right] \tag{5.12}$$

where $(C_c)_j$ is the sediment transport capacity calculated through a closure formula reported in the Section 1.3 under the hypothesis of sediment availability and uniform diameter equal to d_j. Consequently, the total amount of solid

discharge CQ is a function of all the solid concentration C_j for each grain size class in which the grain size distribution curve is divided.

5.2 The Moments Approach

In literature, a novel approach proposed by Armanini [4] is also derived by writing the sediment transport capacity as a function of the mean diameter of the sediment mixture, expanding in series and substituting in the continuity equations for each sediment class, Equations (5.1) and (5.2). Herein an analytical derivation of the moments equations is proposed in order to have a procedure suitable for all the statistical moments.

5.2.1 An Analytical Procedure for the Derivation of the Moments Equations

Grain-size density and distribution are continuous concepts, Section 5.1.1, where the random variable is the diameter d, Figure (5.4). Consequently, the solid discharge Q_s or, equivalently, the sediment concentration C, depends on the grain size distribution $p\left(t, x, \phi, \mu, \sigma^2\right)$ where the average μ, the variance σ^2 and all the statistical moments considered can change in time t and space x. The objective of this formulation is the reduction of the number of unknowns from the number of classes in which the distribution curve is discretized, Section (5.1.2), to the number of statistical moments necessary to describe the shape of the distribution curve. Firstly, in the conservation equation for the solid phase (EMP model)

$$C_b \frac{\partial A_b}{\partial t} + \frac{\partial Q_s}{\partial x} = 0, \tag{5.13}$$

the sediment discharge Q_s should be expressed in function of the statistical moments. In agreement with the Einstein theory, the solid discharge Q_s is the integral over the grain-size interval $[0, +\infty)$ of the product between the grain size distribution curve p and the sediment capacity Q_c:

$$Q_s\left(t, x\right) = \int_0^{+\infty} p\left(t, x, \phi, \mu, \sigma^2\right) Q_c\left(\phi\right) d\phi, \tag{5.14}$$

where, in this section, ϕ is a dummy variable denoting the diameter d in order to avoid possible misunderstanding in the notations of the integral and Q_c is the capacity discharge calculated as all the sediment is distributed with diameter ϕ. In this way, the product between the distribution curve and the transport capacity for each class, $p\left(t, x, \phi, \mu, \sigma^2\right) Q_c\left(\phi\right)$, represents the solid discharge of

each sediment diameter ϕ. The integral of the function $p\left(t, x, \phi, \mu, \sigma^2\right) Q_c\left(\phi\right)$ gives the solid discharge Q_s, Figure (5.4).

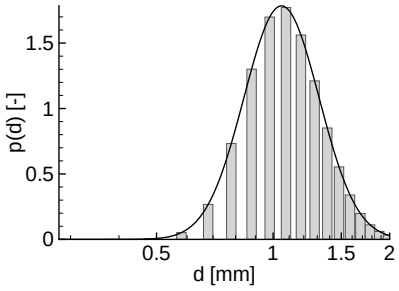

(a) Distribution of the grain-size of the sediment in the mixing layer

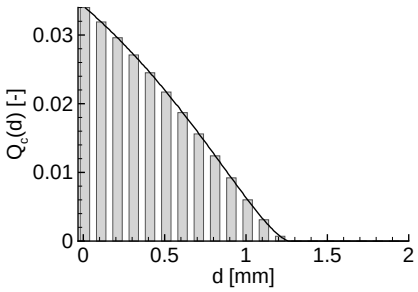

(b) Sediment transport capacity calculated through a transport formula

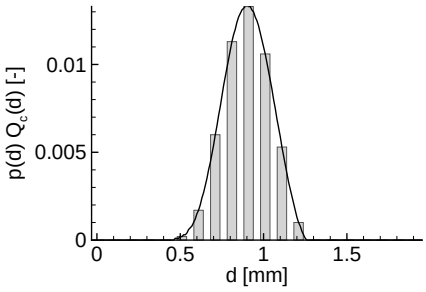

(c) Solid concentration for each class of sediment that is equal to the product between the availability factor p and the transport capacity Q_c

Figure 5.4: *Sediment distribution curve.*

In order to calculate the integral Equation 5.14, firstly, the discharge of the sediment class capacity $Q_c\left(\phi\right)$ is expanded in Taylor series around the mean value μ. In particular the distribution p is assumed to be dependent only on the average μ and the variance σ, for this reason the Taylor expansion is considered until second-order partial derivatives:

$$Q_c\left(\phi\right) = Q_c\left(\mu\right) + \left.\frac{\partial Q_c}{\partial \phi}\right|_{\phi=\mu} \left(\phi - \mu\right) + \left.\frac{\partial^2 Q_c}{\partial \phi^2}\right|_{\phi=\mu} \frac{\left(\phi - \mu\right)^2}{2} + o\left(\phi^3\right). \quad (5.15)$$

Secondly, the equation (5.15) is multiplied by p and integrated over $[0, +\infty)$ to

obtain the total discharge Q_s:

$$Q_s = \int_0^{=+\infty} pQ_c(\mu)\, d\phi + \int_0^{+\infty} p\phi \left.\frac{\partial Q_c}{\partial \phi}\right|_{\phi=\mu} d\phi + \tag{5.16}$$
$$- \int_0^{+\infty} p \left.\frac{\partial Q_c}{\partial \phi}\right|_{\phi=\mu} \mu d\phi + \int_0^{+\infty} p \left.\frac{\partial^2 Q_c}{\partial \phi^2}\right|_{\phi=\mu} \frac{(\phi-\mu)^2}{2} d\phi + o\left(\phi^3\right).$$

where p is still dependent on the statistical moments μ and σ. By remembering that $\int_0^{+\infty} p(\phi)\, d\phi = 1$, the following expression works out:

$$Q_s = Q_c(\mu) + \frac{1}{2} \left.\frac{\partial^2 Q_c}{\partial \phi^2}\right|_{\phi=\mu} \sigma^2 + o\left(\phi^3\right), \tag{5.17}$$

where μ is the mean diameter and $\sigma^2 = \int_0^{+\infty} p(\phi-\mu)^2\, d\phi$ represents the variance of the grain size distribution curve.

The statical moments can now be used for describing the shape of the distribution, Figure (5.4 a). In particular, time variations of the function p causes temporal changes of the statical moments. In order to calculate the temporal derivatives of the statistical moments:

$$\mu = \int_0^{+\infty} \phi p d\phi, \tag{5.18}$$

$$\sigma^2 = \int_0^{+\infty} p(\phi-\mu)^2\, d\phi, \tag{5.19}$$

$$n - moment = \int_0^{+\infty} p(\phi-\mu)^n\, d\phi, \tag{5.20}$$

the conservation equations of the sediment for each grain size class, Equations (5.1) and (5.2), are multiplied by ϕ^n where n is the $n-$statistical moment and integrated :

$$\int_0^{+\infty} \left[\phi^n C_b \frac{\partial}{\partial t}(pA_\delta) + \phi^n \frac{\partial}{\partial x}(pQ_c) + \phi^n C_b \bar{p} \frac{\partial}{\partial t}(A_b - A_\delta)\right] d\phi = 0, \tag{5.21}$$

$$\int_0^{+\infty} \left[\phi^n C_b \frac{\partial}{\partial t} \left[p^{subst} \left(A_b - A_\delta \right) \right] - \phi^n C_b \bar{p} \frac{\partial}{\partial t} \left(A_b - A_\delta \right) \right] d\phi = 0. \tag{5.22}$$

Here, only the mean and the variance are considered but the procedure can be extended to the other moments. If n is equal to one, the Equations (5.21) and (5.22) become:

$$\int_0^{+\infty} \left[\phi C_b \frac{\partial}{\partial t} \left(p A_\delta \right) + \phi \frac{\partial}{\partial x} \left(p Q_c \right) + \phi C_b \bar{p} \frac{\partial}{\partial t} \left(A_b - A_\delta \right) \right] d\phi = 0, \tag{5.23}$$

$$\int_0^{+\infty} \left[\phi C_b \frac{\partial}{\partial t} \left[p^{subst} \left(A_b - A_\delta \right) \right] - \phi C_b \bar{p} \frac{\partial}{\partial t} \left(A_b - A_\delta \right) \right] d\phi = 0. \tag{5.24}$$

By remembering that the diameter ϕ is an independent variable and

$$\int_0^{+\infty} \phi \frac{\partial p}{\partial t} d\phi = \int_0^{+\infty} \frac{\partial}{\partial t} \left(p\phi \right) d\phi = \frac{\partial \mu}{\partial t}, \tag{5.25}$$

the first and the last term of the Equation (5.23) becomes:

$$\int_0^{+\infty} \phi C_b p \frac{\partial A_\delta}{\partial t} d\phi = C_b \mu \frac{\partial A_\delta}{\partial t}, \tag{5.26}$$

$$\int_0^{+\infty} \phi C_b \bar{p} \frac{\partial}{\partial t} \left(A_b - A_\delta \right) d\phi = C_b \bar{\mu} \frac{\partial}{\partial t} \left(A_b - A_\delta \right). \tag{5.27}$$

where $\bar{\mu} = \int_{\phi=0}^{+\infty} \bar{p} \phi d\phi$ is equal to the mean diameter of the substrate μ^{subst} in the case of bed degradations and to μ in the case of bed aggradations. The second term of the Equation (5.23) represents the flux of sediment that determines the variation of the mean value:

$$\int_0^{+\infty} \phi \frac{\partial}{\partial x} \left(p Q_c \right) d\phi = \int_0^{+\infty} \frac{\partial}{\partial x} \left(\phi p Q_c \right) d\phi = \frac{\partial F_\mu}{\partial x}, \tag{5.28}$$

with $F_\mu = \int_0^{+\infty} \phi p Q_c d\phi$. It can be expressed in function of the statistical moments

by expanding the term $Q_c\phi$ in Taylor series around the mean diameter μ:

$$\phi Q_c(\phi) = \mu Q_c(\mu) + \left[Q_c(=\mu) + \mu \left.\frac{\partial Q_c}{\partial \phi}\right|_{\phi=\mu} \right](\phi-\mu) + \\ + \frac{1}{2}\left(2 \left.\frac{\partial Q_c}{\partial \phi}\right|_{\phi=\mu} + \mu \left.\frac{\partial^2 Q_c}{\partial \phi^2}\right|_{\phi=\mu} \right)(\phi-\mu)^2 + o\left(\phi^3\right). \tag{5.29}$$

After integration over the interval $[0,+\infty)$ of the previous equation, the flux F_μ is:

$$F_\mu = \mu Q_c(\mu) + \left(\left.\frac{\partial Q_c}{\partial \phi}\right|_{\phi=\mu} + \frac{\mu}{2} \left.\frac{\partial^2 Q_c}{\partial \phi^2}\right|_{\phi=\mu} \right)\sigma^2. \tag{5.30}$$

The Equations (5.23) and (5.24) become:

$$C_b \frac{\partial}{\partial t}(\mu A_\delta) + \frac{\partial F_\mu}{\partial x} + C_b \bar{\mu} \frac{\partial}{\partial t}(A_b - A_\delta) = 0, \tag{5.31}$$

$$C_b \frac{\partial}{\partial t}\left[\mu^{subst}(A_b - A_\delta)\right] - C_b \bar{\mu} \frac{\partial}{\partial t}(A_b - A_\delta) = 0, \tag{5.32}$$

where $\mu^{subst} = \int_0^{+\infty} p^{subst}(\phi)\, d\phi$.

To describe the evolution of the sediment distribution curve, it can be also necessary to analyze the time variation of the variance σ^2. Similarly to the procedure for the average μ, the Equations (5.21) and (5.22)are written for $n = 2$:

$$\int_0^{+\infty} \phi^2 C_b \frac{\partial}{\partial t}(pA_\delta) + \phi^2 \frac{\partial}{\partial x}(pQ_c) + \phi^2 C_b \bar{p} \frac{\partial}{\partial t}(A_b - A_\delta)\, d\phi = 0, \tag{5.33}$$

$$\int_0^{+\infty} \phi^2 C_b \frac{\partial}{\partial t}\left[p^{subst}(A_b - A_\delta)\right] - \phi^2 C_b \bar{p} \frac{\partial}{\partial t}(A_b - A_\delta)\, d\phi = 0. \tag{5.34}$$

By remembering the definition of the variance σ^2,

$$\int_0^{+\infty} p\phi^2 = \mu^2 + \sigma^2, \tag{5.35}$$

the Equations (5.33) and (5.34) become:

$$C_b \frac{\partial}{\partial t}\left[\left(\mu^2 + \sigma^2\right) A_\delta\right] + \frac{\partial F_{\sigma^2}}{\partial x} + C_b\left(\bar{\mu}^2 + \bar{\sigma}^2\right) \frac{\partial}{\partial t}(A_b - A_\delta) = 0 \tag{5.36}$$

$$C_b \frac{\partial}{\partial t}\left[\left(\mu^{subst2} + \sigma^{subst2}\right)(A_b - A_\delta)\right] - C_b\left(\bar{\mu}^2 + \bar{\sigma}^2\right) \frac{\partial}{\partial t}(A_b - A_\delta) = 0, \tag{5.37}$$

with

$$F_{\sigma^2} = \int_0^{+\infty} \left(pQ_c\phi^2\right) d\phi. \tag{5.38}$$

Herein, $\bar{\sigma}^2$ denotes the variance of the distribution for the sediment in the substrate $\left(\sigma^{subst}\right)^2$ in the case of bed degradations and to σ^2 in the case of bed aggradations. Similarly to Equations (5.29) and (5.30), the term $Q_c\left(\phi\right)\phi^2$ is expanded in series with respect to the mean diameter μ and becomes:

$$Q_c\left(\phi\right)\phi^2 = Q_c\left(\mu\right)\mu + \frac{\partial}{\partial\phi}\left(Q_c\phi^2\right)\Big|_{\phi=\mu}\left(\phi-\mu\right) + \frac{\partial^2}{\partial\phi^2}\left(Q_c\phi^2\right)\Big|_{\phi=\mu}\frac{\left(\phi-\mu\right)^2}{2}. \tag{5.39}$$

This equation is rearranged to get:

$$\begin{aligned} Q_c\phi^2 = {} & Q_c\left(\phi=\mu\right)\mu + 2\mu Q_c\left(\mu\right)\left(\phi-\mu\right) + \mu\,\frac{\partial Q_c}{\partial\phi}\Big|_{\phi=\mu}\left(\phi-\mu\right) + \\ & + \left(2Q_c\left(\mu\right) + 4\mu\,\frac{\partial Q_c}{\partial\phi}\Big|_{\phi=\mu} + \phi^2\,\frac{\partial^2 Q_c}{\partial\phi^2}\Big|_{\phi=\mu}\right)\frac{\left(\phi-\mu\right)^2}{2}, \end{aligned} \tag{5.40}$$

with

$$\frac{\partial^2}{\partial\phi^2}\left(Q_c\phi^2\right) = 4\phi\frac{\partial Q_c}{\partial\phi} + \phi^2\frac{\partial^2 Q_c}{\partial\phi^2} + 2Q_c. \tag{5.41}$$

The Equation 5.40 is then integrated over the interval $[0,+\infty)$ and the flux F_{σ^2} derived:

$$F_{\sigma^2} = Q_c\left(\mu\right)\mu + \frac{1}{2}\left(2Q_c\left(\mu\right) + 4\mu\,\frac{\partial Q_c}{\partial\phi}\Big|_{\phi=\mu} + \mu\,\frac{\partial^2 Q_c}{\partial\phi^2}\Big|_{\phi=\mu}\right)\sigma^2. \tag{5.42}$$

The final system for the sediment transport in the case of non–uniform sediment is:

$$C_b\frac{\partial A_b}{\partial t} + \frac{\partial Q_s}{\partial x} = 0, \tag{5.43}$$

$$C_b\frac{\partial}{\partial t}\left(\mu A_\delta\right) + \frac{\partial F_\mu}{\partial x} + C_b\bar{\mu}\frac{\partial}{\partial t}\left(A_b - A_\delta\right) = 0, \tag{5.44}$$

$$C_b\frac{\partial}{\partial t}\left[\left(\mu^2+\sigma^2\right)A_\delta\right] + \frac{\partial F_{\sigma^2}}{\partial x} + C_b\left(\bar{\mu}^2+\bar{\sigma}^2\right)\frac{\partial}{\partial t}\left(A_b - A_\delta\right) = 0, \tag{5.45}$$

$$C_b\frac{\partial}{\partial t}\left[\mu^{subst}\left(A_b - A_\delta\right)\right] - C_b\bar{\mu}\frac{\partial}{\partial t}\left(A_b - A_\delta\right) = 0, \tag{5.46}$$

$$C_b\frac{\partial}{\partial t}\left[\left(\mu^{subst2}+\sigma^{subst2}\right)\left(A_b - A_\delta\right)\right] - C_b\left(\bar{\mu}^2+\bar{\sigma}^2\right)\frac{\partial}{\partial t}\left(A_b - A_\delta\right) = 0. \tag{5.47}$$

where the unknowns are the bed area A_b, the mean diameter μ and the variance σ^2 and all the other variables are expressed, by replacing the dummy variable ϕ with the diameter d, in terms of the mean and the variance as:

$$Q_s = Q_c\left(d=\mu\right) + \frac{1}{2}\left.\frac{\partial^2 Q_c}{\partial d^2}\right|_{d=\mu}\sigma^2 + o\left(d^3\right), \tag{5.48}$$

$$F_\mu = \mu Q_c\left(d=\mu\right) + \left(\left.\frac{\partial Q_c}{\partial d}\right|_{d=\mu} + \frac{\mu}{2}\left.\frac{\partial^2 Q_c}{\partial d^2}\right|_{d=\mu}\right)\sigma^2, \tag{5.49}$$

$$\begin{aligned} F_{\sigma^2} &= Q_c\left(d=\mu\right)\mu + \\ &+\frac{1}{2}\left(2Q_c\left(d=\mu\right) + 4\mu\left.\frac{\partial Q_c}{\partial d}\right|_{d=\mu} + \mu\left.\frac{\partial^2 Q_c}{\partial d^2}\right|_{d=\mu}\right)\sigma^2. \end{aligned} \tag{5.50}$$

This procedure can be extended to the other statistical moments in order to better describe the time evolution of the grain-size distribution of the sediment.

Besides, the same approach can be applied to the concentration C instead of expanding in series the discharge Q_s:

$$C = C_c\left(d=\mu\right) + \frac{1}{2}\left.\frac{\partial^2 C_c}{\partial d^2}\right|_{d=\mu}\sigma^2 + o\left(d^3\right), \tag{5.51}$$

Equivalently, the fluxes are redefined as:

$$F_\mu = \left[\mu C_c\left(d=\mu\right) + \left(\left.\frac{\partial C_c}{\partial d}\right|_{d=\mu} + \frac{\mu}{2}\left.\frac{\partial^2 C_c}{\partial d^2}\right|_{d=\mu}\right)\sigma^2\right]Q, \tag{5.52}$$

$$\begin{aligned} F_{\sigma^2} &= \left[C_c\left(d=\mu\right)\mu + \right. \\ &\left.+\frac{1}{2}\left(2C_c\left(d=\mu\right) + 4\mu\left.\frac{\partial C_c}{\partial d}\right|_{d=\mu} + \mu\left.\frac{\partial^2 C_c}{\partial d^2}\right|_{d=\mu}\right)\sigma^2\right]Q. \end{aligned} \tag{5.53}$$

5.2.2 Sediment Transport Formulas with respect to the Statistical Moments

The next step is to express the sediment transport capacity formulas and its derivatives with respect to the diameter d in function of the statistical moments. In fact, this general result is in agreement with the system obtained by Armanini [3] where the discharge is calculated through a monomial formula. In this case, the transport capacity is:

$$Q_c\left(d\right) = mU^k d^{-l}. \tag{5.54}$$

and, consequently:

$$C_c(d) = \frac{mU^{k-1}d^{-l}}{A}. \tag{5.55}$$

The derivatives with respect to the diameter d are:

$$\left.\frac{\partial C_c}{\partial d}\right|_{d=\mu} = -C_c(\mu)\frac{l}{\mu}, \tag{5.56}$$

$$\left.\frac{\partial^2 C_c}{\partial d^2}\right|_{d=\mu} = \frac{l(l+1)}{\mu}C_c(\mu). \tag{5.57}$$

By substitution of Equations (5.56) and (5.57) into Equation 5.48, the following expression for the sediment discharge Q_s is obtained:

$$C = C_c(\mu)(1 + c_2\frac{\sigma^2}{\mu^2})Q, \tag{5.58}$$

where

$$c_2 = \frac{l(l+1)}{2}. \tag{5.59}$$

Secondly, the flux F_μ is calculated:

$$F_\mu = \mu C_c(\mu)\left(1 + c_1\frac{\sigma^2}{\mu^2}\right)Q, \tag{5.60}$$

where

$$c_1 = \left(\frac{l(l-1)}{2}\right). \tag{5.61}$$

Finally, the flux F_{σ^2}, can be derived as:

$$F_{\sigma^2} = \mu C_c\left(1 + c_3\frac{\sigma^2}{\mu^2}\right)Q, \tag{5.62}$$

with

$$c_3 = \left(\frac{l\left(2 - 3l - l^2\right)}{2}\right). \tag{5.63}$$

A similar procedure can be developed for the empirical relations such as Meyer-Peter and Müller. As reported in Section 1.3 , the relation can be rewritten in function of the diameter d as:

$$C_c = Fr^2\frac{8}{\Delta_s}\left(\frac{g}{k_s^2 R_h^{1/3}} - \frac{g\Delta_s d}{U^2}\theta_c\right)^{3/2}. \tag{5.64}$$

Under the hypotheses of k_s constant with respect to μ, the derivatives of C_c are:

$$\frac{\partial C_c}{\partial d} = -12\frac{g}{U^2}\theta_c Fr^2 \left(\frac{g}{k_s^2 R_h^{1/3}} - \frac{g\Delta_s d}{U^2}\theta_c\right)^{1/2}, \tag{5.65}$$

and

$$\frac{\partial^2 C_c}{\partial d^2} = 6\frac{g^2}{U^4}\theta_c^2 Fr^2 \Delta_s \left(\frac{g}{k_s^2 R_h^{1/3}} - \frac{g\Delta_s d}{U^2}\theta_c\right)^{-1/2}. \tag{5.66}$$

The advantages of using this formulation is the reduction of the number of unknowns from $2m$, with m number of classes in which the sediment distribution curve is divided, to twice the number of statistical moments considered, for example the mean μ and the variance σ. In this work the equations for the statistical moments, Equations (5.43)-(5.46), are implemented in a simplified model, where the hydrodynamic is considered quasi-steady, in order to find a reference solution. Instead, the bed material fraction approach is implemented by extending the scheme proposed in Section 3 to the non-uniform sediment transport.

5.3 A Simplified Solution for the Evolution of the River-Bed and the Grain-Size Distribution

A simplified solution of the EMP hydrodynamic and morphodynamic system with non-uniform grain-size distribution is herein reported. A similar solutions was proposed by Ribberink [42]. Starting from the solution proposed in Section 2.2, Equation (2.53), in the case of EMP model ($\epsilon = 0$), a simplified equation for the bed evolution is derived. It should be noticed that C depend also from the mean diameter μ, if the variance is assumed constant, Equation (5.51). By considering the non-dimensional analysis of Section 2.2 and the dependency of C from the mean μ, the derivative of C with respect to space is:

$$\frac{\partial C}{\partial x} = \frac{\partial C}{\partial z_b}\frac{\partial z_b}{\partial x} + \frac{\partial C}{\partial \mu}\frac{\partial \mu}{\partial x}, \tag{5.67}$$

and the simplified equation for the bed evolution becomes:

$$\frac{\partial z_b}{\partial \tau} + \bar{Q}C_z\frac{\partial z_b}{\partial x} + \bar{Q}C_\mu\frac{\partial \mu}{\partial x} = 0. \tag{5.68}$$

where C_μ and C_z are respectively the derivatives of C with respect to μ and z_b.

Secondly, the Equation (5.46) is scaled under the following assumptions:

- rectangular channel with constant width,

- thickness δ of the mixing layer constant in time
- variance σ constant in time.

The scale factors are:

$$\mu = \mu_0 \mu^*, \tag{5.69}$$

$$\delta = h_0 \delta^*, \tag{5.70}$$

$$F_\mu = C_0 U_0 h_0 \mu_0 F_\mu^*, \tag{5.71}$$

where C_0, U_0, h_0, μ_0 denotes the values of the variable for the base stationary flow. The non-dimensional equation for the temporal derivatives of the mean diameter is then:

$$\frac{\partial \mu^*}{\partial \tau^*} = -\frac{1}{\delta^*}\frac{\partial F_\mu^*}{\partial x^*} - \frac{\bar{\mu}^*}{\delta^*}\frac{\partial z_b^*}{\partial \tau^*}. \tag{5.72}$$

where F_μ^* is a function of μ and z_b. Then:

$$\frac{\partial F_\mu^*}{\partial x^*} = \frac{\partial F_\mu^*}{\partial \mu^*}\frac{\partial \mu^*}{\partial x^*} + \frac{\partial F_\mu^*}{\partial z_b^*}\frac{\partial z_b^*}{\partial x^*} \tag{5.73}$$

Equation (5.72) and the simplified equation for the bed evolution, Equation (5.68), constitute a system of two equations where the unknowns are bed level z_b and the mean diameter μ under the assumption of substrate infinite and μ^{subst} constant in time. The system can solved numerically by the method of characteristics.

Chapter 6

Extension of the Numerical Scheme to the Non-Uniform Sediment Transport

The two methods proposed in the Chapter 3 are extended to the non-uniform transport calculation. The solution procedure still remains the same, but the concentration C is calculated through the Equation (5.12) and the availabilities factors p_j^{subst} and p_j are updated.

6.1 Equations of the Model

Under the assumption of EMP model, the set of equations to be solved is:

$$\frac{\partial \eta}{\partial t} + \frac{\partial Q}{\partial x} = 0 \tag{6.1}$$

$$\frac{\partial Q}{\partial t} + \frac{\partial F}{\partial x} + gA\frac{\partial \eta}{\partial x} + \alpha Q = 0 \tag{6.2}$$

$$C_b\frac{\partial A_b}{\partial t} + \frac{\partial (CQ)}{\partial x} = 0, \tag{6.3}$$

$$\frac{\partial}{\partial t}(p_j A_\delta) + \frac{\partial}{\partial x}(\alpha_{u^2} C_j Q) + p_j^*\frac{\partial}{\partial t}(A_s - A_\delta) = 0 \qquad j = 1...m, \tag{6.4}$$

$$\frac{\partial}{\partial t}\left[p_j^{subst}(A_s - A_\delta)\right] = p_j^*\frac{\partial}{\partial t}(A_s - A_\delta) \qquad j = 1...m, \tag{6.5}$$

with

$$F = \frac{\alpha_{u^2} Q^2}{A}, \tag{6.6}$$

$$\alpha = \gamma + \frac{\partial U}{\partial x}, \tag{6.7}$$

$$C = \sum_{j=1}^{m} \left[p_j \left(C_c \right)_j \right]. \tag{6.8}$$

The unknowns of the system are the water free surface elevation η, the discharge of the mixture Q, the area A_b, the sediment concentration C, the m fractions of sediment in the mixing layer p_j and in the substrate p_j^{subst}. All the other terms are expressed in function of the unknowns.

The discretization of the Equations (6.1)-(6.3) has been already explained in the Chapter 3. Instead the equations of mass conservation for each grain-size class, under the hypothesis of A_δ constant in time, is herein discretized.

6.2 Continuity Equations for Each Sediment Class

The computational grid still remains the same propose in the Chapter 3 for the discrimination of Equations (6.1)-(6.3). The integer nodes are x_i and the half integer nodes are $x_{i+1/2} = (x_i + x_{i+1})/2$. The availability factors are defined at the integer nodes i, while at the nodes $i+1/2$ they are computed by an upwind-weighted interpolation. The equation (6.5) is integrated over the control volume i defined by nodes $i - 1/2$ and $i + 1/2$.

$$\int_{i-1/2}^{i+1/2} \left(C_b A_\delta \frac{\partial p_j}{\partial t} dx + \frac{\partial \left(Q_s \right)_j}{\partial x} + C_b p_j^* \frac{\partial A_s}{\partial t} \right) dx \qquad j = 1...m. \tag{6.9}$$

where j denotes the grain-size class. The first term of the previous equation is discretized by a forward-in-time finite difference method:

$$\left[V_\delta \frac{\partial p_j}{\partial t} \right]_i \simeq \frac{\left(p_j \right)_i^{n+1} V_\delta - \left(p_j \right)_i^n V_\delta}{\Delta t}, \tag{6.10}$$

while, the second term, the gradient of solid discharge, is discretized in space by a centred finite difference and in time by a semi-implicit time-averaging:

$$\begin{gathered} \left(\Delta Q_s \right)_{i,j}^{n+\theta} \simeq \left(Q_s \right)_{i+1/2,j}^{n+\theta} - \left(Q_s \right)_{i-1/2,j}^{n+\theta} \simeq \\ \vartheta \left[p_{i+1/2,j}^n \left(C_c \right)_{i+1/2,j}^n Q_{i+1/2}^{n+1} - p_{i-1/2,j}^n \left(C_c \right)_{i-1/2,j}^n Q_{i-1/2}^{n+1} \right] + \\ + \left(1 - \vartheta \right) \left[p_{i+1/2,j}^n \left(C_c \right)_{i+1/2,j}^n Q_{i+1/2}^n - p_{i-1/2,j}^n \left(C_c \right)_{i-1/2,j}^n Q_{i-1/2}^n \right], \end{gathered} \tag{6.11}$$

where ϑ is the time-averaging parameter and $p_{i+1/2,j}$ is computed by an upwind-weighted interpolation. In the last term of Equation (6.9) the fraction $\left(p^* \right)_j$ is

explicit:

$$\left[(p^*)_j \frac{\partial V_s}{\partial t}\right]_i \simeq (p^*)_{i,j}^n \frac{(\Delta V_s)_i^{n+1}}{\Delta t}. \tag{6.12}$$

where $\frac{(\Delta V_s)_i}{\Delta t}$ is calculated through the Equation (6.3).

The final system is:

$$\begin{aligned} C_b \frac{p_{i,j}^{n+1} V_\delta - p_{i,j}^n V_\delta}{\Delta t} + \vartheta \left[p_{i+1/2,j}^n \left(C_c\right)_{i+1/2,j}^n Q_{i+1/2}^{n+1}\right. \\ \left. - p_{i-1/2,j}^n \left(C_c\right)_{i-1/2,j}^n Q_{i-1/2}^{n+1}\right] + + (1-\vartheta) \left[p_{i+1/2,j}^n \left(C_c\right)_{i+1/2,j}^n Q_{i+1/2}^n\right. \\ \left. - p_{i-1/2,j}^n \left(C_c\right)_{i-1/2,j}^n Q_{i-1/2}^n\right] + C_b p_{i,j}^n \frac{(\Delta V_s)_i^{n+1}}{\Delta t} = 0 \qquad j = 1...m. \end{aligned} \tag{6.13}$$

By rearranging the previous equation, the availability factor $p_{i,j}^{n+1}$ in the mixing layer becomes:

$$\begin{aligned} p_{i,j}^{n+1} = p_{i,j}^n - \frac{\vartheta \Delta t}{C_b V_\delta} \left[p_{i+1/2,j}^n \left(C_c\right)_{i+1/2,j}^n Q_{i+1/2}^{n+1}\right. \\ \left. - p_{i-1/2,j}^n \left(C_c\right)_{i-1/2,j}^n Q_{i-1/2}^{n+1}\right] - \frac{(1-\vartheta)\,\Delta t}{C_b V_\delta} \left[p_{i+1/2,j}^n \left(C_c\right)_{i+1/2,j}^n Q_{i+1/2}^n\right. \\ \left. - p_{i-1/2,j}^n \left(C_c\right)_{i-1/2,j}^n Q_{i-1/2}^n\right] - (p^*)_{i,j}^n \frac{(\Delta V_s)_i^{n+1}}{V_\delta} \qquad j = 1...m, \end{aligned} \tag{6.14}$$

where $(p^*)_{i,j}^n$ is equal to $p_{i,j}^n$ in the case of bed aggradation and to $\left(p^{subst}\right)_{i,j}^n$ for bed degradation.

Similarly, to update the gradation p_j^{subst} in the substrate, the Equation (6.5) is integrated over the control volume i:

$$\int_{i-1/2}^{i+1/2} \frac{\partial}{\partial t}\left(p_j^{subst} A_s\right) = \int_{i-1/2}^{i+1/2} p_j^* \frac{\partial A_s}{\partial t} \qquad j = 1...m, \tag{6.15}$$

and discretized in time by a forward finite difference method:

$$\left(p_j^{subst}\right)_i^{n+1} = \frac{(p^*)_{i,j}^n \left(\Delta V_s\right)_i^{n+1} + \left(p^{subst}\right)_{i,j}^n \left(V_s\right)_i^n}{\left(V_s\right)_i^{n+1}} \qquad j = 1...m. \tag{6.16}$$

The value of $(p^*)_{i,j}^n$ depends on the sediment process:

$$\left(p^{subst}\right)_{i,j}^{n+1} = \begin{cases} \dfrac{p_{i,j}^n \left(\Delta V_s\right)_i^{n+1} + \left(p^{subst}\right)_{i,j}^n \left(V_s\right)_i^n}{\left(V_s\right)_i^{n+1}} & \text{if } (p^*)_{i,j}^n = p_{i,j}^n \\ \left(p^{subst}\right)_{i,j}^{n+1} & \text{if } p_j^* = p_j \end{cases} \tag{6.17}$$

Finally, in order to preserve the physical meaning of the positivity of $(p_j)_i^{n+1}$,

the size fraction has to be guaranteed:

$$\Delta t < C_b \frac{p_{i,j}^n V_\delta - (p^*)_{i,j}^n (\Delta V_s)_i^{n+1}}{(\Delta Q_s)_{i,j}^{n+\theta}} \qquad j = 1...m.$$

6.3 Extension of the Solution Procedure

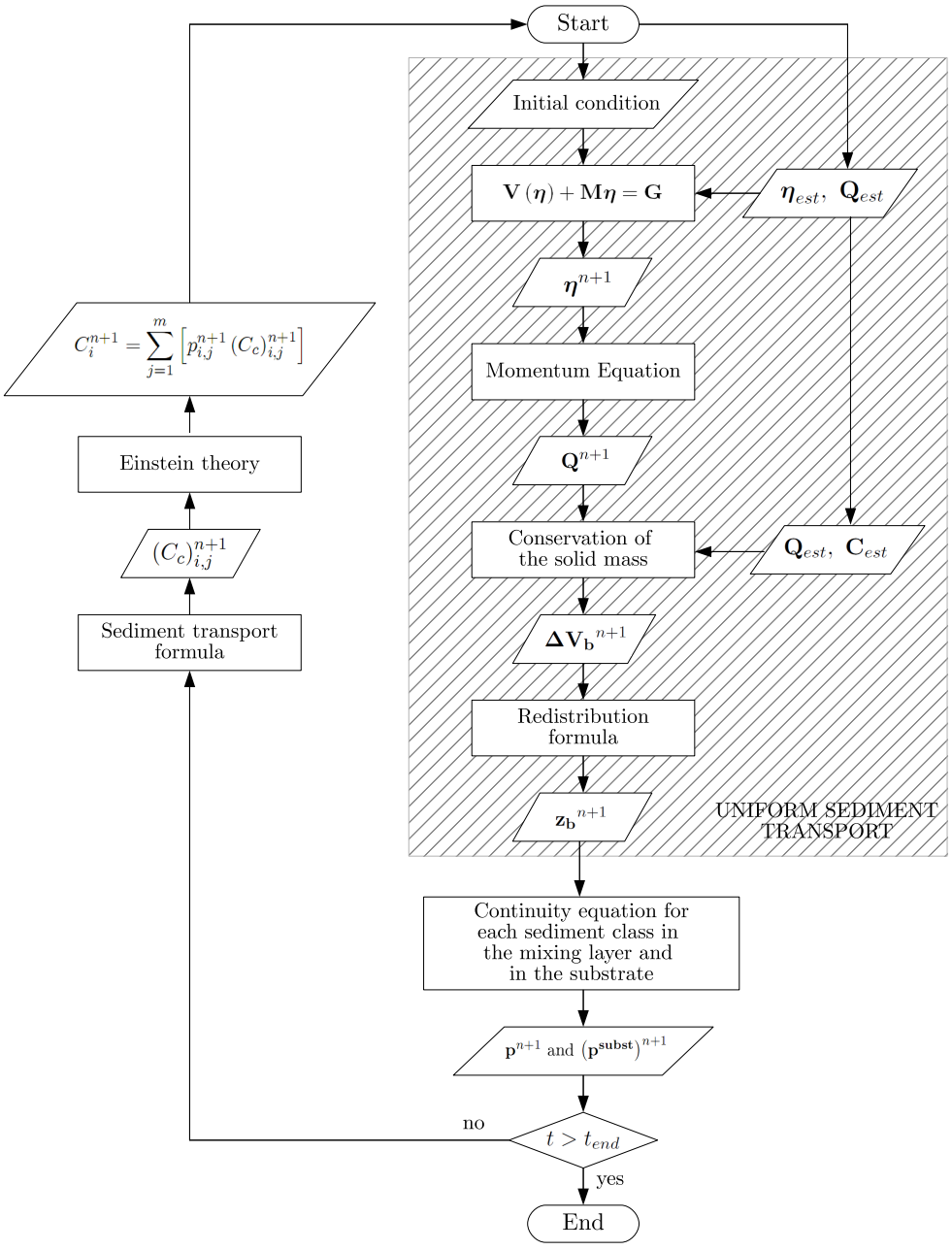

Figure 6.1: *Solution procedure for the non uniform model*

The initial and boundary conditions still remain the same explained in Chapter 3. The only difference is that, if no values of the initial concentration $\mathbf{C^0}$ are known, they are calculated thorough Equation (6.8) in function of the availability factor $p^0_{i,j}$ where i denotes the section and j the grain size class. As in the uniform case, the free surface elevation $\boldsymbol{\eta}^{n+1}$, the discharge $\mathbf{Q}^{n+1}$, the variation of the bed volume $\boldsymbol{\Delta V_b}^{n+1}$ are calculated. Then, the matrix $\mathbf{p}^{n+1}$ of the unknowns $p_{i,j}$ is calculated thorough Equation (6.14), while the matrix $\left(\mathbf{p^{subst}}\right)^{n+1}$ of the unknowns $p^{subst}_{i,j}$ is updated through Equation (6.16) as shown in Figure 6.1. The vector $\mathbf{C}^{n+1}$ of the concentration values at the time $n+1$ is calculated through Equation (5.12) where the sediment capacity $(C_c)^{n+1}_{i,j}$ is computed by means of a sediment transport formula, i.e. Meyer-Peter and Müller or a monomial formula:

$$C_i^{n+1} = \sum_{j=1}^{m} \left[p_{i,j}^{n+1} \left(C_c\right)_{i,j}^{n+1} \right]. \tag{6.18}$$

Chapter 7

Test Cases

The analytical solution found by solving the system of two equations for the unknowns bed mean diameter and bed elevation, Chapter 5, is compared with numerical results of the EMP scheme in case of non-uniform sediment. Secondly, a case test for a non prismatic channel is presented. Finally experimental data are compared with the numerical results of the scheme.

7.1 Propagation of a Small Perturbation

The first case consists in a rectangular channel with a small, but finite, perturbation of the bed level at the center of the domain. The analytical solution in Section 5.3 was found under the assumption of small amplitude of the perturbation, or bed form, so that the variation of the surface elevation becomes trivial. Moreover, the discharge is considered constant over the whole domain, thus, the solution can be used only for problems with a small migration rate of the bed form compared to the mean velocity of the fluid. Under the previous assumptions is possible to use the equations for the mean diameter μ and the bed level z_b evolution derived in Section 5.3 with the hypothesis of infinite substrate. The numerical solutions of these equations, Equations (5.68)-(5.72), are computed by means of the method of characteristics. The closure formula is [42]:

$$C_c = \frac{kU^{n-1}}{A} d_j^{-l} \tag{7.1}$$

with n equal to 5.66 and l to 0.908. The channel is frictionless and is discretized with cells of size 0.05 m. The bed concentration C_b is equal to 0.6. The mixing layer thickness is 0.3 mm. The boundary conditions are imposed by assuming a discharge value of 0.138 $m^3 s^{-1}$ and water elevation 0.8 m respectively for the upstream and the downstream boundary. The initial bed level, Figure 7.1 (a),

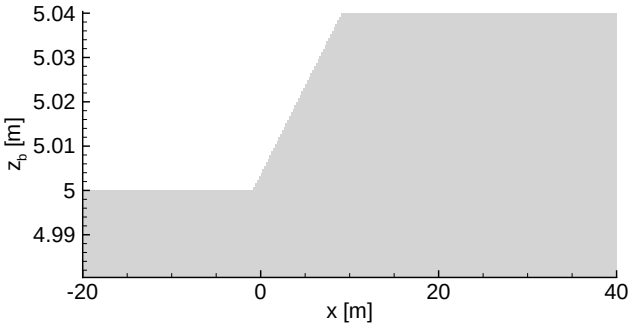

(a) Bed level

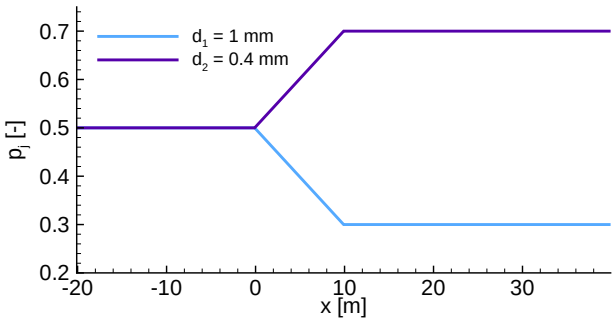

(b) Availability factors in the mixing layer along the longitudinal coordinate

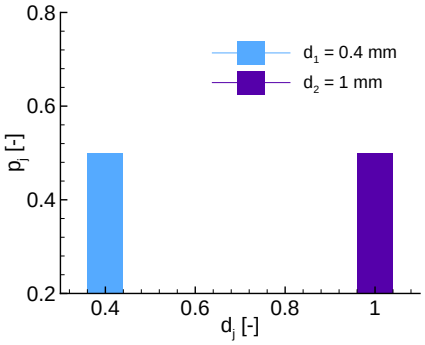

(c) Grain size distribution in the first section of the mixing layer

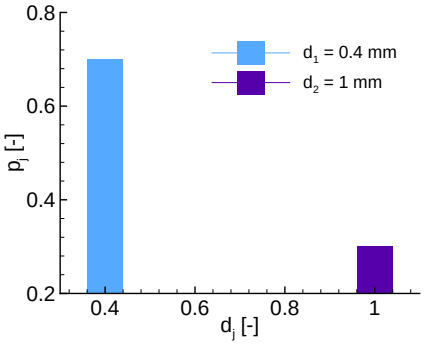

(d) Grain size distribution in the last section of the mixing layer

Figure 7.1: *Initial conditions.*

is:

$$z_b\left(x,0\right)=\begin{cases} z_b=5\ m & \text{if } x<0\ m \\ z_b=5\ m+0.004\ x & \text{if } 0\ m<x<10\ m \\ z_b=5.04\ m & \text{if } x>10\ m \end{cases}$$

Two classes of sediment are considered with the diameter d_j of 0.4 mm and 1 mm, Figure 7.1 (c) and (d) . The fraction p_1 changes from 0.5 to 0.3 in 10 m, while the fraction p_2 changes from to 0.5 to 0.7, Figure 7.1 (a). The system of Equations (5.68) and (5.72) is solved numerically and the solutions are compared with numerical results of the full system of Equations (6.1)-(6.5) as shown in Figure 7.2. The scheme proposed in Chapter 6 calculates the two sediment fractions p_1^{n+1} and p_2^{n+1}, the average μ is calculated starting from these two values and compared with the average μ calculated from Equation (5.72).

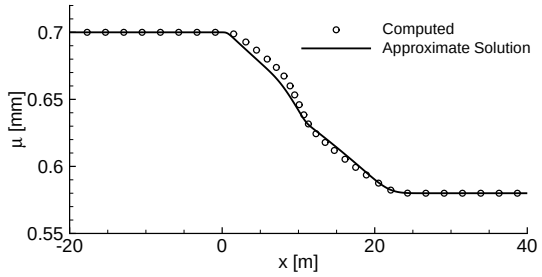

(a) Mean diameter

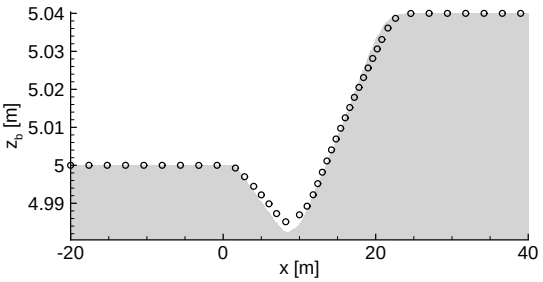

(b) Bed level

Figure 7.2: *Comparison between the simplified solution and the EMP model with non-uniform sediment.*

7.2 Non Prismatic Channel

The second test consists in a no prismatic channel of 1000 m, as shown in Figure 7.3, with roughness coefficient constant ($k_s = 20\ m^{1/3}s^{-1}$). The sediment is distributed in two classes, Figure 7.4 (b) and (c), and the mixing layer thickness is set to 0.03 m. The total discharge at the upstream boundary is set equal to 175.412 m^3s^{-1} and the free surface elevation is 4 m at the downstream boundary. In Figure 7.4 the initial conditions and the numerical results for the bed elevation and the availability factors of the two classes are reported. The

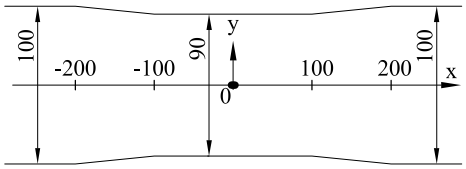

Figure 7.3: *Channel geometry*

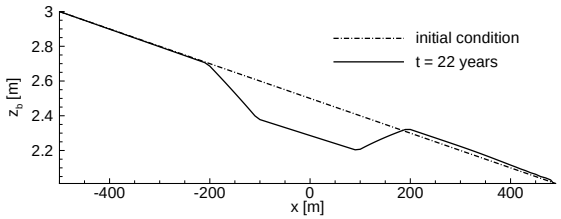

(a) Bed level

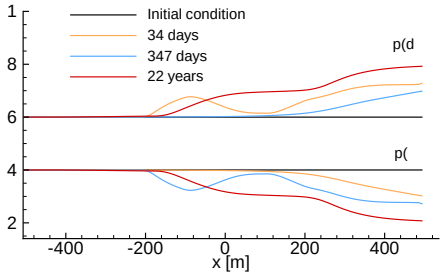

(b) Grain-size fraction in the mixing layer

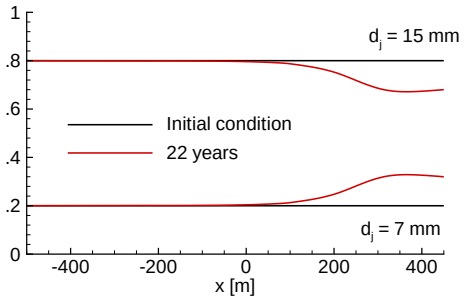

(c) Grain-size fraction in the substrate

Figure 7.4: *Time evolution of the bed level and the sediment fractions in a non prismatic channel.*

results show that the finer sediment of the substrate increases in correspondence to the channel enlargement, Figure 7.4 (c), while the availability factors of the

mixing layer evolve to the upstream boundary condition ($p_1 = 0.4$ and $p_2 = 0.6$) Figure 7.4 (b).

7.3 Effects on the Numerical Results of the Thickness of the Mixing Layer

A trapezoidal channel is considered. The wall slopes is 33.7° , while the Chézy friction coefficient is set equal to 20 $m^{1/2}s^{-1}$. The channel is 30 m wide and 1000 m long. The initial discharge Q is 50 m^3s^{-1} and the water depth is 1 m. The inlet and outlet conditions are reported in Table 7.1. Besides, in order to

time $[h]$	Q $[m^3s^{-1}]$	h $[m]$
0	150	0.85
100	300	1.5
200	150	0.85
∞	150	0.85

Table 7.1: *Upstream and downstream boundary conditions.*

have a degradation process, the solid concentration at the upstream boundary is imposed and the sediment fractions transported by the flow change during the simulation as shown in Table 7.2. The sediment transport formula is the Meyer-Peter Müller formula. The channel is discretized with 101 cells ($\Delta x = 10\ m$) and

time $[h]$	p_{T1} $[-]$	p_{T2} $[-]$	p_{T3} $[-]$	p_{T4} $[-]$	C $[-]$
0	0.02	0.12	0.24	0.62	$4\ 10^{-4}$
100	0.02	0.16	0.36	0.46	$5\ 10^{-3}$
200	0.02	0.12	0.24	0.62	$4\ 10^{-4}$
∞	0.02	0.12	0.24	0.62	$4\ 10^{-4}$

Table 7.2: *Boundary conditions on the grain size distribution.*

the maximum Courant number based on the celerity is 7.1, while the Courant number C_{vel} is set equal to 1.2. The sensitivity of the calculated bed elevation z_b to the mixing layer thickness is analyzed by changing the value of mixing layer thickness from twice to three times the initial d_{90}, Figure 7.5.

Consequently, the thickness of the mixing layer influences also the time variation of the grain-size distribution curve. In Figure 7.6 the grain size distribution at $x = 200\ m$ is calculated at time $t = 1000\ h$ with the two different values of δ. As observed by Wu [52], the influence of the mixing layer thickness is large during degradation processes. Usually the thickness δ is set to twice the d_{90},

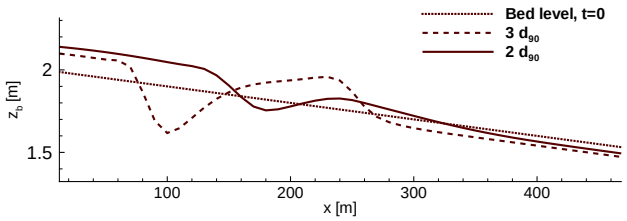

(a) Bed evolution

Figure 7.5: *Bed level calculated with different thickness δ of the mixing layer at time* 1000 h.

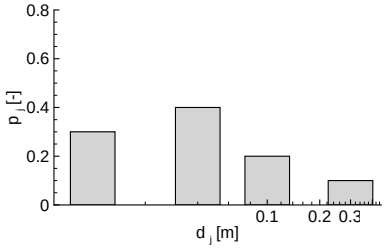

(a) *Initialcondition*

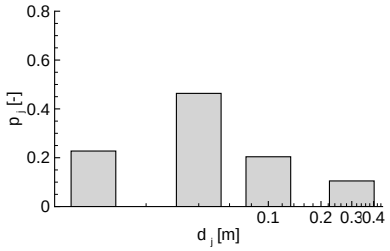

(b) $t = 1000\ h$, $\delta = 2\ d_{90}$

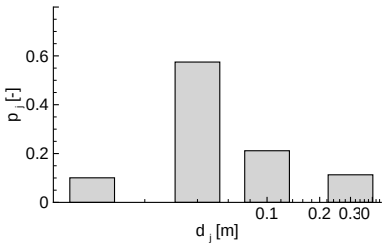

(c) $t = 1000\ h$, $\delta = 3\ d_{90}$

Figure 7.6: *Grain-size distribution at the* 21^{th} *section* ($x = 200\ m$).

but, if it increases, the bed profiles changes. The thickness is consequently important to calculate the bed profile and size distribution in the mixing layer (Figure 7.7).

7.4 Comparison with Experimental Data

Finally, numerical results of the EMP model with non-uniform sediment are compared with the experimental data obtained by Ribberink [42]. In the experiment performed by Ribberink [42], the variations in average grain size of the transported material and the material in the transport layer are large. Con-

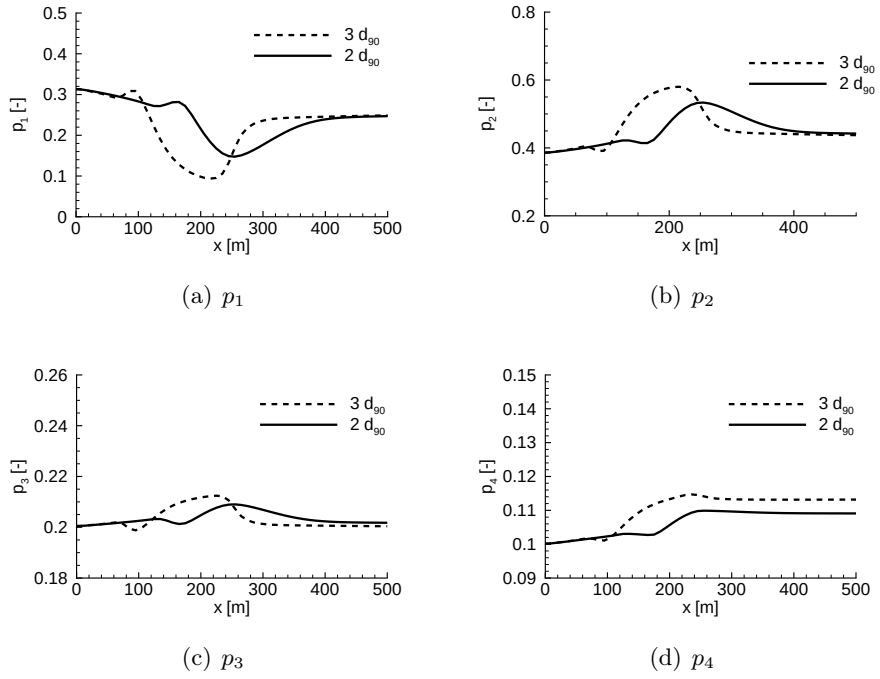

(a) p_1 (b) p_2

(c) p_3 (d) p_4

Figure 7.7: *Sediment fraction p_j calculated with different thickness δ of the mixing layer at time* 1000 *h.*

sequently, the application of a morphological model for non-uniform sediment is required. A change in the mixture composition is imposed by changing the fraction of the transported material at the upstream boundary of the flume. During this test the composition of the mixing layer was measured. For the numerical simulation, the experiment E8 and E9 described by Ribberink [42] are considered. As shown in Section 5.1.2, the fraction of sediment transported by the flow p_{Tj} is different then the fraction of sediment p_j in the mixing layer:

$$p_{Tj} = \frac{p_j C_c(d_j)}{\sum_j p_j C_c d_j}. \tag{7.2}$$

with $d_1 = 0.78\ mm$ and $d_2 = 1.29\ mm$. The fraction p_{1T} of transported sediment at the upper boundary decreases linearly from 0.5 to 0 during 30 hours. The water discharge at the upper boundary and the water depth at downstream are constant in time. The value necessary for the simulation are reported in Table 7.3. The numerical results of the EMP model with non-uniform sediment are compared with the experimental data obtained by Ribberink [42] and the results of his model, Figure 7.8. The wave proceeds in the downstream direction. The EMP model seems to better explain the time evolution of the fraction p_1

Exp	Q $[m^3 s^{-1}]$	h $[m]$	i $[-]$	p_1 $[-]$	p_{T1} $[-]$	Q_s $m^{1/2} s^{-1}$	χ
8	0.02410282	16.7	1.65	0.43	0.50	$2.82\ 10^{-6}$	35.2
9	0.0241027	15.4	2.01	0	0	$2.70\ 10^{-6}$	37.0

Table 7.3: *Upstream boundary conditions.*

with respect to the model proposed by Ribberink [42].

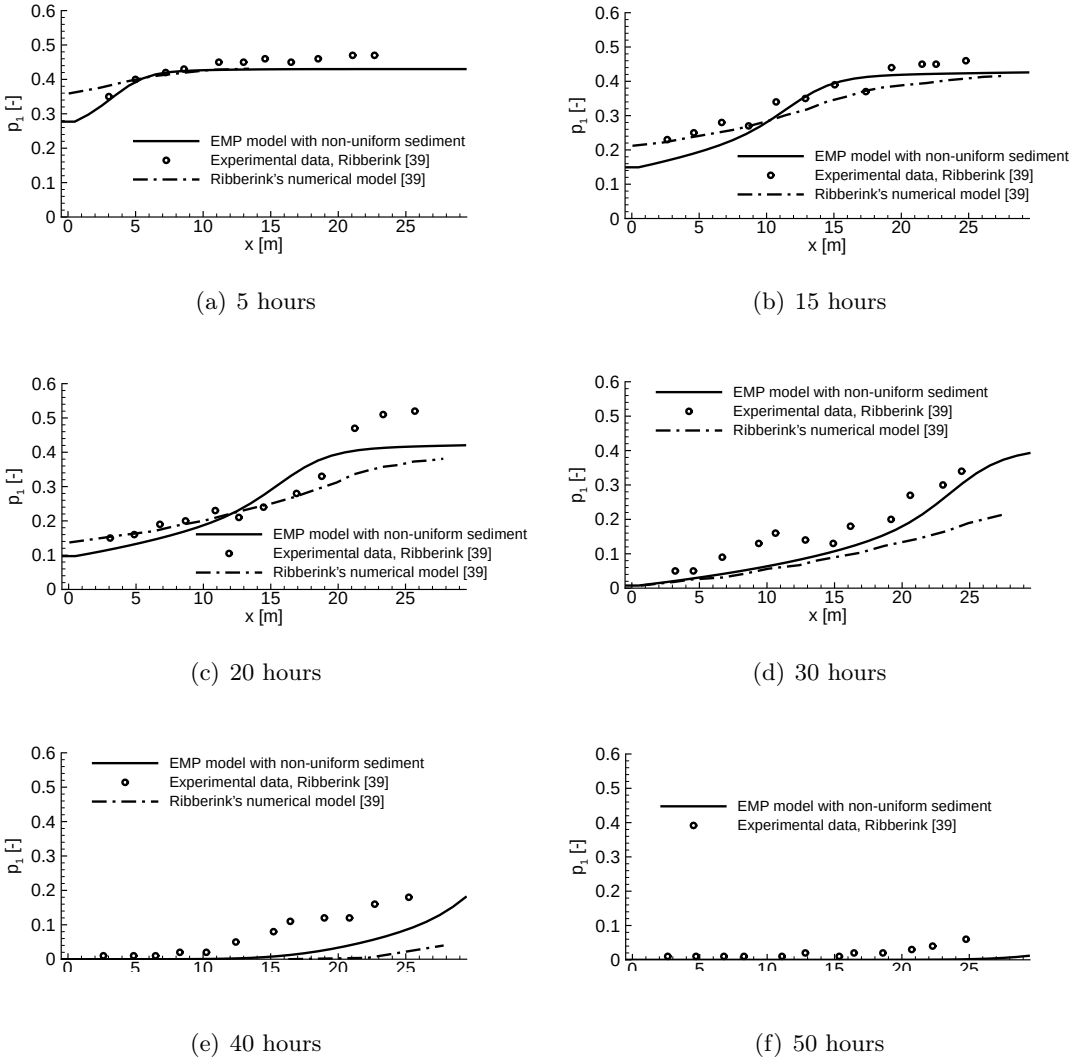

(a) 5 hours

(b) 15 hours

(c) 20 hours

(d) 30 hours

(e) 40 hours

(f) 50 hours

Figure 7.8: *Evolution of the transport layer composition p_1.*

7.5 Conclusions

Numerical results were compared with the developed analytical solution. Besides, a test case in a no prismatic channel is presented. Secondly, a degradation test in a trapezoidal channel with four sediment classes is considered in order to observe the sensitivity of the model to the mixing layer thickness. This parameter seems to have a great influence on the solution in the case of scouring processes as already observed by Wu [52] and can be a limit for the application of the model. Nevertheless, the model was applied to the experiment performed by Ribberink [42] and the results show a better agreement with the measured data with respect to the numerical model proposed by the same author. In conclusion, the model results suitable to study the non-uniform sediment transport in channel with low concentration (EMP model) but the limit of a formulation based on the mixing layer should be considered.

Conclusions

A detailed analysis of the most widely used models for mobile bed river dynamics was carried out in the idealized framework of one dimensional flow in a channel with rectangular cross section. More specifically, quasi two-phase model (QTP) and essentially mono-phase (EMP) approaches were compared showing that several partly mono-phase formulations are inconsistent with a rigorous scaling analysis. A consistent simplified model was derived, EMP model, and its range of validity pointed out. The EMP model, in fact, results suitable for low sediment concentration values. A limit value C_{QTP} of applicability for the essentially mono-phase model is analytically derived and confirmed by numerical results. The limit of concentration C_{QTP} highlighted in this work is 6.5‰. For larger concentration values, the numerical solutions of the QTP model differ from the ETP model.

Secondly, starting from the quasi two-phase model, a simplified equation for the bed evolution was derived in the case of quasi-steady free surface and mixture flows. The solution of the simplified equation can be computed very accurately by the method of characteristics and provides a useful benchmark for numerical methods. This simplified problem allows to compare the performance of different numerical approaches in a more physically relevant context.

Besides, an highly efficient and accurate semi-Lagrangian numerical method for the quasi two-phase mobile bed system is proposed, based on the numerical scheme proposed by Rosatti et al. [45] for the fixed bed case. Also an upwind Eulerian discretization is developed with the advantage that the solution procedure remains the same for the two schemes. The semi-Lagrangian method is linearly unconditionally stable and allows to employ much longer time-steps than standard explicit discretization. This property is extremely important for realistic applications to morphodynamic problems, where numerical simulations of very long time intervals are necessary to study the long term impact of erosion and deposition processes. The quality of the numerical solutions obtained by the proposed method is assessed by several numerical experiments presented in Section 4 and also by employing the newly introduced benchmark problem.

Numerical results show that, with the proposed numerical method, the quasi two-phase models can be used without any loss in efficiency with respect to the essentially mono-phase or fixed bed case. Since the model is suitable for arbitrary shapes of the cross section, the next step will be the validations of the model provisions for realistic problem in natural rivers against real measured data.

In the second part, a model based on the division of the grain size distribution curve in a discrete number of classes was implemented by extending the EMP model and test cases studied. Besides, an analytical derivation of the approach proposed by Armanini [4] was carried out. This approach is based on studying the time evolution of the statistical moments that describe the grain-size distribution curve. The reduction of the number of unknowns is one of the advantages of the statistical moments approach proposed by Armanini [4]. In fact, in this formulation, the number of variable is reduced to the number of statistical moments, while, in the standard approaches, it is equal to the number of classes in which the grain-size distribution curve is divided. An analytical solution was developed under the assumption that the amplitude of bed perturbations is so small that the variation of the surface elevation can be ignored. Under the previous hypothesis, it is possible to derive a system of two equations for the bed level and the mean diameter of the grain-size distribution curve. This system is numerically solved by the method of characteristics and constitutes a benchmark problem in order to verify the implemented method for non-uniform sediment transport in rivers.

Finally, several numerical tests are proposed. The limit of this model is the sensitivity to the mixing layer thickness above all in degradation processes. Nevertheless, this formulation is the most suitable for numerical schemes of unsteady flow. Besides the numerical results were compared with experimental data and a good agreement with the measured data is obtained. The future development of this second part is, firstly, the application to a real problem in order to describe the dynamics of solid transport for sediment mixture and to better predict morphological changes. Secondly, it should be possible to reduce the computational cost of the scheme by discretizing the equations based on the statistical moments in the model for unsteady flow.

Bibliography

[1] J.D. Abad, G.C. Buscaglia, and M. H. Garcia. 2D stream hydrodynamic, sediment transport and bed morphology model for engineering applications. *Hydrological Processes*, 22:1443–1459, 2007.

[2] E. Aldrighetti and P. Zanolli. A high resolution scheme for flow in open channels with arbitrary cross-section. *International Journal of Numerical Methods in Fluids*, 47:817–824, 2005.

[3] A. Armanini. Variation of bed and sediment load mean diameters due to erosion deposition processes. *Dynamics of gravel-bed rivers*, pages 351–358, 1992.

[4] A. Armanini. Non-uniform sediment transport: dynamic of the active layer. *J. Hydraulic Research*, 33:611–622, 1995.

[5] A. Armanini. *Principi di idraulica fluviale.* Editoriale Bios, Cosenza, 1999.

[6] A. Armanini. L'idraulica dei sistemi naturali. In *Atti del XXVII convegno nazionale di idraulica e costruzioni idrauliche.*, pages 37–58, 2000.

[7] A. Armanini. La modellazione idraulica dei fluidi bifasici solido e liquido. In Walter Farina Editore, editor, *Atti del XXXII convegno nazionale di idraulica e costruzioni idrauliche.*, pages 133–161, 2010.

[8] A. Armanini and G. Di Silvio. A one-dimensional model for the transport of a sediment mixture in non-equilibrium conditions. *J. Hydraulic Research*, 26(3), 1988.

[9] A. Armanini, L. Fraccarollo, and G. Rosatti. Two-dimensional simulation of debris flows in erodible channels. *Computer & Geosciences*, 35:993–1006, 2009.

[10] D. Azbel and P. Kemp-Pritchard. *The two-phase flows in chemical engineering.* Cambridge University Press, 1981.

[11] W.R. Brownlie. Compilation of alluvional channel data: laboratory and field. Technical Report KH-R-43B, Californian Institute of Technology, 1981.

[12] G. W. Brunner. *HEC-RAS River Analysis System: Hydraulic Reference Manual*. US Army corps of engineers hydrologic engineering center, 609 Second Street Davis, CA 95616-4687, 2008.

[13] Z. Cao, R. Day, and S. Egashira. Coupled and decoupled numerical modeling of flow and morphological evolution in alluvial rivers. *J. Hydraulic Engineering*, 128(3):306–321, 2002.

[14] Z. Cao, G. Pender, and P. Carling. Shallow water hydrodynamic models for hyperconcentrated sediment-laden ?oods over erodible bed. *Advances in Water Resources*, 29(4):546–557, 2006.

[15] V. Casulli. Semi-implicit finite difference methods for the two dimensional shallow water equations. *Journal of Computational Physics*, 86:56–74, 1990.

[16] V. Casulli and E. Cattani. Stability, accuracy and efficiency of a semi-implicit method for three-dimensional shallow water flow. *Computers and Mathematics with Applications*, 27(4):99–112, 1994.

[17] V. Casulli and G. Stelling. Numerical simulation of 3d quasi-hydrostatic, free-surface flows. *J. Hydraulic Engineering*, 124:678Ű686, 1998.

[18] T. Cheng, V. Casulli, and J. W. Gartner. Tidal, residual, intertidal mudflat (trim) model and its applications to san francisco bay, california. *Estuarine, Coastal and Shelf Science*, 36:235Ű280, 1993.

[19] ASCE Task Committee. River width adjustment. *J. Hydraulic Engineering*, 124(9):881–917, 1998.

[20] Y. C. Cosso. *‚stensione di un modello monodimensionale di evoluzione morfologica a casi di evoluzione differenziata del fondo all'interno della sezione*. PhD thesis, Università degli studi di Trento, 2005-2006.

[21] Y. Cui, G.Parker, T.E.Lisle, J.E. Pizzuto, and A.M. Dodd. More on the evolution of bed material waves in alluvial rivers. *Earth Surface Processes and Landforms*, 30:107–114, 2005.

[22] M. de Vries. Considerations about non-steady bed-load transport in open channels. *Proc. XI IAHR Congr.*, pages 3.8.1–3.8.8, 1965.

[23] B.M. Duc, T. Wenka, and W. Rodi. Numerical modeling of bed deformation in laboratory channels. *J. Hydraulic Research*, 130:894–904, 2004.

[24] H.A. Einstein. The Bed-Load Function for Sediment Trasnsportation in Open Channel Flow. *Technical Bulletin No. 1026, Dept. of Agriculture, Washington D.C.*, 1950.

[25] M. Falcone and R. Ferretti. Convergence analysis for a class of semi-lagragian advection schemes. *SIAM Journal of Numerical Analysis*, 35: 909–940, 1998.

[26] L. Fraccarollo and G. Rosatti. Lateral bed load experiments in a flume with strong initial trasversal slope, in sub- and supercritical conditions. *Water resources research*, 45, 2009.

[27] A.J. Grass. Sediment transport by waves and current. Technical Report FL29, SERC London Centre for Marine Technology, 1981.

[28] M. Hirano. Studies on variation and equilibrium state of a river bed composed of non-uniform material. *Trans. of JSCE*, 4:128–129, 1971.

[29] J. Hudson and P.K. Sweby. Formulations for numerically approximating hyperbolic systems governing sediment transport. *Journal of Scientific Computing*, 19:225–252, 2003.

[30] J. Hudson, J. Damgaard, N Dodd, T. Chesher, and A. Cooper. Numerical approaches for 1d morphodynamic modelling. *Coastal Engineering*, 52: 691–707, 2005.

[31] A. A. Kassem and M. H. Chaudry. Comparison of coupled and semicoupled numerical models for alluvial channels. *J. Hydraulic Engineering*, 124(8): 794–802, 1998.

[32] A. A. Kassem and M. H. Chaudry. Numerical modeling of bed evolution in channel bends. *J. Hydraulic Engineering*, 128(5):507–514, 2002.

[33] N. L. Komarova and S. J. M. H. Hulscher. Linear instability mechanisms for sand wave formation. *Journal of Fluid Mechanics*, 413:219–246, 2000.

[34] H. Lee and H. Hsieh. Numerical simulations of scour and deposition in a channel network. *International Journal of Sediment Research*, 18:32–49, 2003.

[35] R. J. Leveque. *Finite Volume Methods for Hyperbolic Problems*. Cambridge University Press, Cambridge, UK, 2002.

[36] X. Liu, B.J. Landry, and M.H. García. Two-dimensional scour simulations based on coupled model of shallow water equations and sediment transport on unstructured meshes. *Coastal Engineering*, 55:800–810, 2007.

[37] D.A. Lyn and M. Altinakar. St. Venant–Exner equations for near-critical and transcritical flows. *J. Hydraulic Engineering*, 128(6):579–587, 2002.

[38] A. Mangeney-Castelnau, J.P. Vilotte, B. Perthame M.O. Bristeau, F. Bouchut, and S. Yerneni C. Simeoni. Numerical modeling of avalanches based on saint venant equations using a kinetic scheme. *Journal of Geophysical Research*, 108(11):1–118, 2003.

[39] C. Meruane, A. Tamburino, and O. Roche. On the role of the ambient fluid on gravitational granular flow dynamics. *Journal of Fluid Mechanics*, pages 381–404, 2010.

[40] E. Meyer-Peter and R. Müller. Formulas for bed-load transport. *Proc. 2nd Meeting IAHSR, Stockholm, Sweden*, pages 1–26, 1948.

[41] P. H. Morris and D. J. Williams. Relative celerities of mobile bed flows with finite solid concentrations. *J. Hydraulic Engineering*, 122(6):311–315, 1996.

[42] J. S. Ribberink. Mathematical modelling of one-dimensional morphological changes in rivers with non-uniform sediment. Communications on hydraulic and geotechnical engineering of the Faculty of Civil Engineering 87-2, Delft University of Technology, 1987.

[43] G. Rosatti and L. Fraccarollo. A well-balanced approach for flows over mobile-bed with high sediment-transport. *Journal of Computational Physics*, 220(1):312–338, 2006.

[44] G. Rosatti, L. Bonaventura, and D. Cesari. Semi-implicit, semi-Lagrangian environmental modelling on cartesian grids with cut cells. *Journal of Computational Physics*, 204:353–377, 2005.

[45] G. Rosatti, L. Bonaventura, A. Deponti, and G. Garegnani. An accurate and effcient semi-implicit method for section-averaged free-surface flow modelling. *International Journal of Numerical Methods in Fluids*, 2009.

[46] R.M. Iverson R.P. Denlinger. Flow of variably fluidized granular masses across three-dimensional terrain: 2. numerical predictions and experimental tests. *Journal of Geophysical Research*, 106(B1):533–566, 2001.

[47] J. Sieben. A theoretical analysis of discontinuous flows with mobile bed. *J. Hydraulic Research*, 37(2):199–212, 1999.

[48] G. Simpson and S. Castellfort. Coupled model of surface water flow, sediment transport and morphological evolution. *Computer & Science*, 32(10): 1006–1014, 2006.

[49] J. P. Soni, R. J. Garde, and K. G Raju. Aggradation in streams due to overloading. *Journal of Hydraulic division, American Society Civi Engineering*, 106(1):117–132, 1980.

[50] G.S. Stelling and A. Verwey. Numerical flood simulation. *Encyclopedia of Hydrological Sciences*.

[51] P.A. Tassi, S. Rheberge, C.A. Vionnet, and O. Bokhove. A Discontinuous Galerkin finite element model for river bed evolution under shallow flows. *Computer Methods in Applied Mechanics and Engineering*, 197:2930–2947, 2008.

[52] W. Wu. *Computational river dynamics*. Taylor, Francis Balkema, P.O.Box 447,2300 AK Leiden, The Netherlands, 2007.

[53] W. Wu and D. Vieira. One Dimensional Channel Network Model. *Technical Report NCCHE-TR-2002-1, National Center for Computational Hydroscience and Engineering, University of Mississippi*, 2002.

[54] W. Wu and S. S. Y. Wang. One-dimensional explicit finite-volume model for sediment transport with transient flows over movable beds. *J. Hydraulic Research*, 46(1):87–98, 2008.

[55] W. Wu, A. Molinas, and P.Y. Julien. Bed-materials load computations for non-uniform sediments. *J. Hydraulic Engineering*, 130(10):1002–1012, 2004.

[56] W. Wu, D. A. Vieira, and S.Y.W. Sam. One-dimensional numerical model for non uniform sediment transport under unsteady flows in channel networks. *J. Hydraulic Engineering*, 9(1):914–923, 2004.

[57] M.S. Yalin. *Mechanics of Sediment Transport*. Pergamon Press, 1972.

[58] C. T. Yang. Gstars computer models and sedimentation control in surface water system. In *The 3^{rd} International Conference on Water Resources and Arid Environments*, 2008.